# Microgrid White Paper

2026.06

# Table of Contents

# 1 Overview of Microgrids

## 1. 1 Current Status of Microgrid Development Globally and in China

Against the macro-level backdrop of the global energy system transitioning toward decarbonization, decentralization, and digitalization, the microgrid, as an advanced energy architecture capable of achieving local self-balancing of energy supply and demand and flexible interaction with the bulk power grid, is moving beyond the demonstration stage toward large-scale commercial deployment at an unprecedented pace. Microgrids are not only critical infrastructure for responding to extreme climate events and improving grid resilience, but also a core solution for integrating distributed renewable energy resources (DERs) and mitigating grid capacity pressure caused by artificial intelligence (AI) data centers, AIDCs, and electrified transportation.

### 1.1.1 Market Size and Installed Capacity Overview

The global microgrid market is currently in a strategic window characterized by intensive capital inflows and rapid capacity expansion. Based on multiple authoritative market research sources, the global microgrid market was valued between USD 43.19 billion and USD 52 billion in 2024 and is expected to expand strongly at a compound annual growth rate (CAGR) of 16.5% to 18% from 2025 to 2030, with the market size projected to exceed USD 140.3 billion or more by 2030. The underlying logic behind this exponential growth lies in the sharp increase in renewable energy penetration and the substantial decline in the cost of core energy storage components. For example, since 2010, the cost of lithium-ion batteries has fallen by more than 80%, enabling the economics of long-duration, high-reliability microgrids to become increasingly evident. In terms of installed capacity, global renewable energy is entering a period of historic expansion. It is forecast that between 2025 and 2030, approximately 4600 GW of renewable energy capacity will be added worldwide, equivalent to the combined existing installed capacity of China, the European Union, and Japan. In 2024 alone, global installed renewable power generation capacity increased by 741 GW, reaching a record high, with deployments of solar photovoltaic (PV) and battery energy storage systems reaching record levels. Distributed PV, including residential, commercial, industrial, and off-grid projects, accounted for 42% of global PV capacity additions, providing a solid generation foundation for the broad deployment of microgrids.

In terms of regional distribution, North America currently dominates the global market, accounting for approximately 35.8% of revenue in 2025. The United States and Canada have significant first-mover advantages in grid resilience investment, defense against extreme weather such as severe cold and wildfires, and microgrid retrofits for military bases and critical healthcare infrastructure. However, the Asia-Pacific region is widely recognized as the fastest-growing future engine. Its large population base, rapid industrialization, and urgent demand for electrification in remote areas and islands create fertile conditions for explosive microgrid growth.

As the absolute core of the Asia-Pacific region, China's microgrid market demonstrates exceptionally high growth and large scale, exceeding the global average. Data indicate that China's microgrid market generated approximately USD 9.585 billion in revenue in 2025, accounting for nearly 10% of the global total, and is expected to reach USD 47.046 billion by 2033, with a CAGR of 22.5% from 2026 to 2033. Behind this remarkable growth is China's leading position in new energy installed capacity. By the end of 2024, China's total installed power generation capacity reached 3349 GW, of which zero-

emission capacity, including wind power, PV, nuclear power, and hydropower, accounted for 57% (1693 GW). In 2024 alone, China added 277.57 GW of utility-scale PV capacity, more than twice the capacity added by the United States over the same period. China's ultra-large projects currently under construction and planning, such as the 100 GW "PV Great Wall" project in the Kubuqi Desert of Inner Mongolia, are not only reshaping the centralized energy landscape but also providing an excellent testbed and absorption environment for intelligent microgrid technologies. In specific market segments, combined heat and power (CHP) systems are currently the highest-revenue and fastest-growing generation segment in China's microgrid market, while grid-connected microgrids and hardware systems account for the largest market shares by microgrid type.

| Indicator Dimension | Global Market Data and Forecasts | China Market Data and Forecasts |
|---|---|---|
| **Base-Year Market Size** | USD 43.19 billion - USD 52 billion (2024 base) | USD 9.585 billion (2025 base) |
| **Forecast-Period Market Size** | USD 140.3 billion (by 2030) | USD 47.046 billion (by 2033) |
| **Compound Annual Growth Rate (CAGR)** | 16.5% - 18% (2025-2030) | 22.5% (2026-2033) |
| **New Renewable Energy Capacity** | 4600 GW added from 2025 to 2030 | 277.57 GW of PV added in 2024 alone |
| **Main Segments** | Hardware (largest share), off-grid (fastest growth) | CHP (largest revenue source and fastest growth) |

### 1.1.2 List of Relevant Policies and Environments Worldwide

The development of microgrids worldwide is not only a technological race, but also a direct reflection of national macro-energy strategies and policy systems. Because of differences in resource endowments, historical grid structures, and regulatory philosophies, regional markets have developed differentiated policy-driven pathways.

China: Industrial green microgrids and zero-carbon demonstration parks guided by top-level design
The Chinese government has fully incorporated microgrids into the national top-level planning for building a new power system. The National Development and Reform Commission and the National Energy Administration have jointly issued multiple guidance documents requiring coordinated optimization of interprovincial and interregional transmission corridors and local distribution network planning, gradual improvement of institutional mechanisms for the integrated development of small microgrids and large power grids, and the establishment of a grid-forming technology standards system. Directly driven by industrial decarbonization, a guidance document jointly issued by five ministries, including the Ministry of Industry and Information Technology, in early 2026 explicitly requires new renewable energy projects built by industrial enterprises and industrial parks to ensure that at least 60% of their electricity is consumed locally or in nearby areas on an annual basis. This mandatory "local consumption" threshold has directly triggered market demand for industrial-scale microgrids. By the end of 2024, more than 450 integrated "source-grid-load-storage" industrial park projects had been launched nationwide, with a total installed capacity exceeding 100 GW. In terms of specific demonstration projects, Jiangsu Province is at the forefront nationally. For example, Lianyungang Port has built China's first zero-carbon port intelligent

microgrid, integrating 5.2 MW of distributed PV, 5 MW of new energy storage, electric battery-swapping heavy trucks, and all-electric tugboats, saving more than RMB 3 million in electricity costs per year through multi-energy complementarity. In addition, Suqian has commissioned the largest user-side intelligent microgrid project in East China, comprising 5.15 MW of PV, 20 MWh of energy storage, and six wind turbines, and equipped with V2G bidirectional charging piles and 600 kW liquid-cooled ultra-fast charging equipment. At the same time, State Grid Jiaxing Power Supply Company has also made key progress in developing digital-twin distribution network architectures and standards for multi-state microgrid cluster control.

Southeast Asia: Dual-track development of transnational interconnection strategies and island electrification Southeast Asia is one of the core engines of global energy demand growth and is expected to contribute more than 25% of global energy demand growth by 2035. However, the region's high dependence on fossil fuel imports and its complex geography, such as the archipelagic terrain of Indonesia and the Philippines, make microgrids a lifeline for the energy transition. According to the International Energy Agency (IEA), to support regional grid expansion and integrate more variable renewable energy, annual investment in power networks, including microgrids and regional interconnection facilities, must double to USD 22 billion by 2035 under the stated policies scenario. The policy environment for microgrids in Southeast Asia places strong emphasis on interconnection mechanisms, such as large-scale resource optimization through the ASEAN Power Grid initiative, while vigorously promoting off-grid microgrids based on PV, battery energy storage, and demand-side response mechanisms for remote islands, with the long-term goal of reducing dependence on diesel generation and saving operating costs.

South America: Resource-endowment-driven growth and the rise of the utility-scale energy storage market South America's microgrid market is rising rapidly under the dual drivers of remote mining operations, islanded power supply, and abundant new energy resources. Brazil is the leader in South America's energy transition, currently with 30 GW of onshore wind capacity, while its extensive coastline offers offshore wind development potential of up to 1228 GW. Brazil's policy orientation is gradually upgrading isolated remote microgrid systems, such as SIGFI systems under the "Luz para Todos" PV program, into complex microgrid clusters deeply integrated with green hydrogen production and large-scale energy storage. On the other hand, Chile has enabled the bankability of energy storage projects through excellent regulatory and market incentive adjustments, making it the leader in utility-scale battery energy storage systems (BESS) in Latin America. Major power generation companies such as Engie, Enel, and AES Andes have deployed BESS at scale, including Engie's 139 MW Coya system, providing a mature policy model for large microgrids participating in grid ancillary services and capacity markets.

Middle East: National vision endorsement and ultra-large green hydrogen islanded microgrids The Middle East, especially Saudi Arabia, is using its substantial sovereign capital and national vision programs, such as Saudi Vision 2030, to fundamentally reshape its energy structure. Saudi Arabia has set an ambitious target of achieving 50% clean-energy electricity by 2030 through 130 GW of renewable energy capacity, including 58.7 GW of solar and 40 GW of wind. This top-down policy environment has given rise to the world's largest and most advanced microgrid system: the NEOM green hydrogen project. Jointly advanced by ACWA Power, Air Products, and NEOM, the project completed an USD 8.4 billion financing close in 2023. This gigawatt-scale microgrid, fully isolated from the main grid, integrates 4 GW of wind and solar capacity and is expected to be fully completed and commissioned in 2026, producing 600 tonnes of green ammonia per day through electrolyzers for the global market. To support such large-scale off-grid operation, the NEOM project uses highly sophisticated HOMER software for techno-economic optimization analysis. Studies show that in this geographic region, an integrated architecture combining PV, wind turbines, battery energy storage, electrolyzers, and fuel cells (PV/WT/BSS/Elec/FC), although having a net

present cost (NPC) of USD 2.3 million and an LCOE of USD 0.106/kWh, provides optimal system supply reliability.

Europe: Legal empowerment of citizen energy communities and the Clean Energy Package Europe is at the regulatory frontier of global microgrid policymaking, with the EU Clean Energy Package (CEP) as its core hallmark. Unlike other regions driven by industry or utilities, European policy places strong emphasis on energy "democratization" and "decentralization." Through the Internal Electricity Market Directive (IEMD), the EU established the legal status of citizen energy communities (CECs), and through the recast Renewable Energy Directive (RED II), it introduced renewable energy communities (RECs). This legal framework allows consumers to become "prosumers" and legally conduct peer-to-peer (P2P) energy trading and sharing within communities using open-source platforms. Nordic countries such as Denmark and Sweden substantially increased the self-consumption share of distributed generation through early national support programs and tax reduction policies, with Denmark's potential self-generated electricity reaching 3636 GWh. However, implementation at the national level still faces obstacles. Non-core EU members such as Norway still lack a specific legal definition of energy communities, while existing data privacy laws, consumer protection laws, and platform liability risks also hinder seamless operation of the distributed P2P microgrid market to some extent.

Africa: Filling the electrification gap and optimizing microgrid regulatory mechanisms Across the African continent, microgrids are regarded as the most essential means of leapfrogging traditional centralized grid construction and achieving universal electrification. In recent years, several countries, including Nigeria, Kenya, South Africa, and Zambia, have significantly improved their microgrid regulatory frameworks, as measured by RGI, RSI, and ROI indicators. The Economic Community of West African States (ECOWAS) is promoting the development of community microgrids through regional electricity markets (REM) and renewable energy auction mechanisms. According to the Africa MG Developers Association (AMDA), by 2030, Africa is planning more than 6116 new microgrid sites, including 3501 in Nigeria and 404 in Zambia, and is expected to attract USD 2.2 billion in financing, approximately 50% of which will rely on concessional or grant financing, with the aim of connecting 14 million people to electricity. In this process, hybrid microgrids, combining solar, diesel, and energy storage, already account for more than 88% of new sites, fundamentally changing the previous reliance on diesel generation alone. However, the report also notes that despite gradual improvements in written regulations, there is often a major implementation gap between formal rules and actual execution, making the combination of technical assistance and commercial financing particularly important.

## 1.2 Key Challenges in Microgrid Development

Despite the significant macro-level vision and technical potential, for microgrids to transition from isolated demonstrations to seamless integration with large power grids, they still face three major challenges: economic models, underlying physical characteristics, and complex system management.

### 1.2.1 The Growing Pains of Reshaping Economics and Business Models

Microgrid projects are inherently asset-intensive investments, and high initial capital expenditure (CAPEX) has long been the largest barrier to project implementation. To alleviate customers' financial pressure, business models are undergoing a profound paradigm shift from traditional customer-owned purchase models to Microgrid-as-a-Service (MaaS) and power purchase agreement (PPA) models. Under these innovative models, third-party energy developers are responsible for building, owning, and operating the microgrid, while users do not bear upfront capital investment and instead pay fixed monthly capacity and energy fees under long-term contracts. This model not only helps customers avoid equipment depreciation and technology iteration risks, but also provides long-term electricity price certainty. For

example, Direct Relief adopted a third-party PPA model when deploying medical-grade solar microgrids, ensuring that it could focus on its core life-saving mission rather than energy management.

### 1.2.2 Grid Technical Security Bottlenecks Caused by Inverter-Based Resources (IBRs)

When the penetration of distributed energy resources in a microgrid, such as PV, wind power, and battery energy storage, exceeds a certain critical threshold, the fundamental physical characteristics of the entire power system undergo a qualitative transformation: from a mechanical-inertia grid dominated by synchronous machines to a network driven by power electronic equipment, namely inverter-based resources (IBRs). This transition creates extremely difficult protection and control crises.

The first issue is the comprehensive failure of relay protection coordination. Traditional power system relay protection devices, such as overcurrent protection and distance protection, are designed based on the short-circuit characteristics of synchronous generators (SGs). During faults, conventional synchronous machines can provide large short-circuit currents up to 5 to 10 times their rated current, driving protection devices to trip rapidly. However, because inverters are constrained by the very limited thermal withstand capability of their internal semiconductor switching devices, they strictly limit short-circuit current to between 1.1 and 1.5 times rated current during faults through current-limiting control. As a result, overcurrent relays inside the microgrid may suffer from insufficient sensitivity or serious failure to operate because they cannot obtain adequate fault signatures.

An even more severe issue is the disordering of distance protection. Because inverter control strategies during transient faults, especially negative-sequence current injection, are highly complex, IBRs can produce time-varying negative-sequence currents whose frequency is inconsistent with the grid voltage frequency. This current frequency deviation causes the apparent impedance calculated by protection relays to oscillate sharply, with the impedance phasor continuously rotating relative to the voltage phasor. This behavior directly undermines the security and reliability of protection devices, causing Zone 1 of distance protection to potentially overreach or Zone 2 to underreach. For high-penetration IBR networks, microgrids must thoroughly reconstruct traditional protection-setting principles by adopting adaptive protection algorithms with dynamic topology awareness, or even real-time short-circuit feature extraction systems based on electromagnetic transient (EMT) models and deep learning.

The second issue is the lack of system inertia and extreme frequency fluctuations. During off-grid or islanded operation, a microgrid loses the strong voltage and frequency support of the main grid. Grid-following (GFL) inverters that traditionally rely on phase-locked loops (PLLs) to track grid phase are highly prone to control-loop interaction resonance under low short-circuit ratio, weak grid conditions. Even small load disturbances may cause a very high rate of change of frequency (ROCOF), triggering system-level collapse. Addressing these bottlenecks requires the industry to fully evolve toward grid-forming (GFM) technologies with virtual inertia.

### 1.2.3 Management and Dispatch Coordination under Complex Multi-Objective Architectures

Because larger-scale microgrids typically aggregate heterogeneous energy carriers such as cooling, heating, electricity, and gas, as well as stochastic wind and solar output, their energy management systems (EMSs) face extremely high computational requirements for massive data throughput and multi-objective optimization. Modern microgrid dispatch must not only satisfy basic power balance, but also optimize total benefits over the entire life cycle, including operation and maintenance costs, fuel costs,

penalties for curtailed solar and wind generation, penalties for energy shortages, carbon emissions management costs, and electricity market arbitrage.

At the control hierarchy level, the industry currently widely adopts hierarchical control architectures, including primary, secondary, and tertiary control, to address dispatch requirements over different time scales. To eliminate data silos among different hardware vendors, microgrids are widely adopting the IEC 61850 international communication standard. As a cornerstone of substation automation and distributed energy resource integration, IEC 61850 uses an object-oriented modeling mechanism, implements millisecond-level trip signals and protection interlocking trips among nodes through the GOOSE (Generic Object Oriented Substation Event) protocol, and uses MMS (Manufacturing Message Specification) services for upper-level monitoring data transmission. Although IEC 61850-based distributed control can improve flexibility and reliability, achieving both ultra-low communication latency and very high cybersecurity in cluster networks containing thousands of nodes remains a major challenge.

## 1.3. Future Technological Innovation and Development Trends

In response to the economic constraints, protection failures, communication, and dispatch challenges described above, microgrid systems are undergoing a deep technological transformation spanning digital software and core hardware media.

### 1.3.1 Intelligent and Digital System Upgrades

AI empowerment, or the comprehensive penetration of artificial intelligence, has moved beyond the theoretical modeling stage and become the "central brain" of microgrid energy management systems. Given the limitations of traditional mathematical programming in handling high-dimensional nonlinear uncertainty, such as output forecasting under extreme weather, machine learning (ML), deep learning (DL), and reinforcement learning (RL) are being deeply integrated into microgrid controllers. AI applications in microgrids are reflected in multiple dimensions: first, highly accurate load and renewable power forecasting, reducing reserve capacity redundancy caused by stochastic fluctuations; second, multi-source coordinated dispatch, enabling optimal Markov strategies involving energy storage charging and discharging and gas turbine start-stop decisions to be formulated rapidly at the microsecond level; and third, fault diagnosis and predictive maintenance. For example, AI predictive maintenance projects based on Arduino hardware platforms combined with Internet of Things (IoT) sensor data show that when AI models identify component degradation or potential fault anomalies, relay control can automatically execute load adjustments, achieving true millisecond-level preventive closed-loop response and thereby minimizing unplanned grid downtime. In addition, for data anomaly detection, artificial neural networks (ANNs) have a frequency error of only 7.62%, significantly outperforming traditional K-means algorithms and adaptive neuro-fuzzy inference systems (ANFIS).

Deployment of edge computing architectures with the exponential growth of microgrid device density, transmitting all control data to a centralized cloud for processing not only creates unacceptable communication latency, but also exposes major cybersecurity vulnerabilities. The introduction of edge computing moves AI analytics and decision-making logic down to edge devices such as smart meters, inverters, and local controllers. This cloud-edge architecture allows global optimization to be performed periodically in the cloud, while real-time dispatch and millisecond-level frequency/voltage control are executed instantaneously by local controllers. Numerous industry pilots have confirmed that edge AI not only greatly reduces upstream data network congestion, but also supports reliable execution of high-level demand-side response and high-frequency V2G dispatch.

### 1.3.2 Evolution of Operating Forms: Clustering and Prosumer Integration through Virtual Power Plants

From islands to networks: multi-microgrid clusters Traditional standalone microgrids are rapidly evolving into geographically proximate and physically interconnected multi-microgrid clusters (MMGs). When multiple microgrids are interconnected, the system exhibits strong internal complementarity. For example, the daytime demand peak of a commercial building microgrid can be effectively offset by the nighttime load of a residential microgrid. In the islanded multi-microgrid cluster (IMMG) mode, through a two-stage stochastic mixed-integer linear programming EMS and a blockchain-based peer-to-peer (P2P) distributed energy trading architecture, neighboring microgrids can automatically bid, exchange surplus electricity, and share spinning reserve capacity without centralized intervention. This structure not only minimizes total operating costs while maintaining frequency security constraints, but also addresses local voltage violations and harmonic pollution in distribution networks.

New model of prosumer integration: deep coupling with Virtual Power Plant (VPP 2.0) Microgrids are no longer limited to traditional physical boundaries, but instead participate deeply in broader electricity markets as high-quality, dispatchable flexible asset portfolios. Virtual power plant (VPP) technology uses the Internet of Things and communication protocols, such as OpenADR, to aggregate hundreds or thousands of dispersed microgrids, distributed PV systems, energy storage assets, and electric vehicle charging networks into a large, dispatchable "cloud power plant."

### 1.3.3 Hardware Technology Innovation: Long-Duration Energy Storage and Bidirectional V2G Interaction

Integration of long-duration energy storage (LDES) The lithium-ion batteries that currently dominate the market are constrained by material costs and safety, and their economic discharge duration is generally limited to 2 to 4 hours, making it difficult to meet the inter-day or seasonal peak-shaving and valley-filling requirements of microgrids under severe weather or consecutive days without sunlight. Therefore, breakthroughs in long-duration energy storage (LDES) are regarded as the final piece of the puzzle for microgrids to fully replace fossil fuels. Between 2024 and 2025, non-lithium LDES technology pathways achieved breakthrough commercialization progress. Relevant studies show that compared with the single objective of decarbonizing the overall grid, microgrid end users have more stringent requirements for extreme resilience and islanded operation capability, and LDES is the only pathway to cost-optimal 100% zero-carbon resilient microgrids.

Grid integration of vehicle-to-grid (V2G) interaction as tens of millions of new energy vehicles enter service, the aggregate battery capacity of electric vehicles (EVs) will become an enormous energy reservoir. V2G technology allows electric vehicles not only to absorb electricity from microgrids as loads, but also to inject surplus battery energy back into the grid during peak periods. It is forecast that by 2030, EV batteries in Europe could provide up to 114 TWh of bidirectional flexible storage potential for the system. V2G has now moved from concept to substantive large-scale pilots. In Norway, Oslo Gardermoen Airport conducted a large-scale V2G dispatch pilot using thousands of long-parked passenger battery electric vehicles, verifying the feasibility of converting dormant assets into distributed grid storage nodes. In Europe, Renault's Mobilize service program in France, the Netherlands, Germany, and the United Kingdom is currently the fastest-moving and most commercially complete project. Business model: the program packages vehicles with native V2G support, dedicated bidirectional AC chargers, and exclusive energy contracts. Backend algorithms automatically charge during low-price periods and discharge to the grid during peak-price periods. [1] As smart meters and bidirectional charging infrastructure become widespread, mobile EV fleets aggregated and dispatched through edge computing will completely reshape the reserve capacity architecture of microgrids.

## 1.4 In-Depth Analysis of Power, Safety, and EU NC RfG 2.0

To address the severe impacts of large-scale grid connection of inverter-based resources (IBRs) on power system frequency and voltage stability, the European Union has comprehensively revised the Network Code Requirements for Generators 2.0 (NC RfG 2.0). This code is among the world's most stringent and advanced grid-connection technical frameworks, and it not only defines the security baseline for Europe's transmission grid, but also profoundly shapes the R&D direction and technical access thresholds for core microgrid control equipment worldwide, such as PCS inverters and battery management systems.

### 1.4.1 Overview of NC RfG 2.0 and the Core Shift toward Grid-Forming (GFM)

The most disruptive change in NC RfG 2.0 is the introduction, for the first time at the regulatory level, of grid-forming capability (GFC) requirements. In the past, microgrid inverters mostly followed grid-following control logic, relying on PLLs to follow the frequency and phase of the bulk power grid. However, once the main grid failed or disappeared, the microgrid was highly vulnerable to collapse. NC RfG 2.0 explicitly requires future non-synchronous generation and energy storage modules to have grid-forming technologies capable of actively establishing internal system voltage magnitude and frequency while providing synthetic inertia and system strength, namely short-circuit current, to the system. The second-stage technical report released by the dedicated technical group (TG GFC) established by the European Network of Transmission System Operators for Electricity (ENTSO-E) clearly endorses the position that in a Europe dominated by non-synchronous generation, grid-forming capability is no longer optional but essential for maintaining stable operation of the Continental European synchronous grid. In addition, the code pays particular attention to the threat of forced oscillations (FO) caused by power electronic equipment. For onshore and offshore wind power and PV park projects, namely Type C and Type D, ACER and ENTSO-E, based on recommendations from the TG FO group, have established strict oscillation suppression thresholds in Article 21(3) and Article 26(2), respectively, to prevent high-frequency resonance within microgrids from propagating to the bulk transmission grid. Notably, NC RfG 2.0 fully aligns the positioning of energy storage equipment by stipulating that power storage modules, including V2G bidirectional electric vehicle charging stations, will be subject to the same technical constraints as generating units, thereby eliminating legal ambiguity around grid-connected microgrid energy storage.

### 1.4.2 List of Main Requirements and Comparison of Tiered Thresholds

To balance grid security requirements with equipment manufacturers' retrofit costs, especially for technologies facing large-scale deployment barriers such as micro combined heat and power (Micro-CHP), NC RfG 2.0 implements refined tiered management across four types, A, B, C, and D, according to the connection voltage level and maximum capacity (MW) of generating units and energy storage modules:

While this tiered system strives to avoid stifling foundational innovation, offering greater flexibility for Type A equipment, it firmly requires backbone support nodes, namely Types B/C/D, to assume security responsibilities for grid stability. This EU model is profoundly reshaping the global R&D roadmap for microgrid equipment.

## 1.5 Summary

In summary, global microgrids are undergoing a historic transformation from a marginal backup role for regional outage response into an energy hub supporting energy decarbonization, transportation electrification, and the explosive growth of the AI digital economy. Their development can be summarized by the following core conclusions:

1. Deepening resonance between markets and policy: from China's mandatory local consumption threshold for industrial parks to Europe's consumer-empowering citizen energy communities, from Saudi Arabia's extreme green hydrogen island at NEOM to thousands of planned microgrids filling Africa's electrification gap, global policy is removing market barriers with unprecedented force. Over the next decade, large-scale capital inflows will be directly guided by these policy orientations and cross-regional interconnection strategies.
2. Higher-dimensional competition in commercial value: the economics of microgrid assets have fully moved beyond a simple equipment price-differential model. Whether developers can use AI-based edge computing systems to precisely balance physical battery degradation against highly profitable ancillary service market revenues, such as bidding gains in the MISO frequency regulation market, and flexibly use VPP architectures to interact with the bulk grid at millisecond time scales will be the key determinant of their survival under the Microgrid-as-a-Service (MaaS) business model.
3. Rigorous reshaping of safety standards: the failure of traditional relay protection and the loss of inertia caused by high shares of inverter-based resources (IBRs) connected to the grid represent a critical industry-wide risk. The grid-forming (GFM) technical standards mandated by EU NC RfG 2.0 mark the end of the grid-following control paradigm. Combined with long-duration iron-air energy storage (LDES) that can overcome multi-day periods without wind or sunlight, and mature IEC 61850 communication standards, future multi-microgrid clusters will become highly intelligent systems capable of self-protection, self-healing, and strong support for the bulk power grid.

# 2. Microgrid Control Strategies and EMS

## 2.1 In-Depth View of Microgrid Fundamentals and Architectural Systems

### 2.1.1 Definition, Core Physical Components, and Topological Ecosystem of Microgrids

A microgrid is rigorously defined as a relatively small but highly functional local power system that deeply integrates multiple types of distributed generation (DG), battery energy storage systems (BESS), diverse loads, and intelligent monitoring centers through advanced power electronics and control theory. Its core design concept is to consume renewable energy locally, thereby greatly reducing electrical losses and infrastructure investment associated with long-distance transmission.

At the physical component level, distributed generation mainly includes photovoltaic (PV) arrays and wind turbine generators. These sources are characterized by strong intermittency and variability, with output highly dependent on meteorological conditions such as solar irradiance and wind speed. To smooth source-side power fluctuations, the energy storage system (BESS) becomes an indispensable energy-buffering hub in the microgrid. Energy storage can not only absorb surplus electricity caused by sudden increases in PV or wind output, but also provide instantaneous active power support when renewable generation drops sharply or load increases suddenly. The monitoring center, through a distributed sensor network and data acquisition modules, forms the "nervous system" of the microgrid and is responsible for round-the-clock equipment status monitoring, data aggregation, and issuance of upper-level dispatch instructions.

From the perspective of topological ecosystems, modern microgrids mainly take the form of AC microgrids, DC microgrids, and hybrid AC/DC architectures. Taking a highly typical industrial PV-storage-diesel microgrid as an example, it often adopts a DC-coupled or hybrid-coupled architecture. In this

architecture, the PV array and battery energy storage system usually share a common DC bus, while rigid AC loads with very high-power quality requirements and diesel generators as the final backup are connected on the AC bus side. The advantage of this multi-energy complementary topology is that it can achieve very high renewable energy penetration. When solar irradiance is sufficient, the system prioritizes PV generation, reducing diesel generator output or even shutting it down completely to save high fossil fuel costs. When nighttime, extreme weather, or load peaks occur, the energy storage system and diesel generator coordinate rapidly, maintaining DC bus voltage constancy and AC-side frequency stability through complementary output.

## 2.2 Analysis of Operating Modes and the Fundamental Mechanism of Seamless Grid-Connected/Islanded Transition

Microgrids have two basic operating modes: grid-connected mode and islanded/off-grid mode. In grid-connected mode, the microgrid voltage and frequency are clamped by the upstream bulk power grid with effectively infinite capacity. The microgrid primarily serves as a supplement to the main grid, carrying out controlled active and reactive power exchange and helping smooth the main grid load curve. At this stage, inverters within the microgrid typically do not participate in voltage and frequency formation. In off-grid mode, due to external grid faults or planned disconnection, the microgrid must rely on internal grid-forming (GFM) inverters or dominant generation equipment to independently establish and maintain system voltage magnitude and frequency stability.

The transition from grid-connected state to islanded state, and from islanded state back to the bulk grid, is known as the grid-connected/islanded transition. Traditional direct switching methods often cause severe voltage oscillations and large closing inrush currents at the instant of mode transition due to mismatches in phase angle and voltage magnitude. This may not only damage fragile power electronic devices, but also cause short-duration power interruptions to sensitive loads in the system. Therefore, achieving seamless grid-connected/islanded transition is one of the core challenges in microgrid control theory.

Detailed transient mechanism studies show that the core of seamless transition lies in state following and phase pre-synchronization control strategies. During the transition from islanded to grid-connected mode, the microgrid must first capture the restored state of the bulk grid. At this point, the microgrid control center uses a phase-locked loop (PLL) to monitor voltage signals on both sides of the point of common coupling (PCC) circuit breaker in real time. After the bulk grid voltage returns to normal, the controller introduces a phase pre-synchronization module that gradually aligns the islanded voltage phase on the microgrid side with the bulk grid phase by fine-tuning the frequency output of the internal grid-forming inverter, until strict phase-angle synchronization is achieved. Only when the phase and magnitude of the voltages on both sides of the grid-connection switch are detected to be fully equal and stable will the system issue a closing command. At the instant of closing, the V/f controller that previously established voltage uses an internal state-following algorithm to smoothly transition its output and follow the output of the new P/Q controller, thereby eliminating closing inrush current caused by abrupt changes in state variables and allowing the bulk grid to take over and lead controllable loads into stable grid-connected operation.

## 2.3 Underlying Control Strategies: Multidimensional Coordination between the Execution Layer and Controllers

Primary control, or zero-level control, forms the physical foundation for stable microgrid operation. It directly determines the transient stability boundary of the system, power quality under parallel operation of multiple sources, and power-sharing strategies among large numbers of distributed generators.

### 2.3.1 Islanding Detection Mechanisms and Grid-Connection Requirements for Inverters

During grid-connected operation, microgrids must have sensitive islanding detection capability. When the external bulk grid experiences an outage due to a fault, if the microgrid continues blindly feeding power into the bulk grid, it can cause serious safety incidents and interfere with relay protection actions in the main grid. To address such issues, IEEE 1547-2018 sets highly stringent requirements for the voltage and frequency ride-through capability of distributed energy resources (DERs).

Under the new standards framework, the underlying microgrid controller cannot immediately trip as in the past when detecting minor disturbances. Instead, the microgrid is required to withstand voltage or frequency fluctuations within a certain time window. Controllers are divided into three progressive reliability categories according to equipment performance: Category I, II, and III:

| IEEE 1547-2018 Ride-Through Category | Description of Design Objectives and Technical Requirements | Applicable Control Capability Indicators |
|---|---|---|
| **Category I (Basic Performance)** | Meets the most basic reliability requirements of the bulk power grid. Applicable to distributed generators based on earlier technologies. | Has limited voltage/frequency ride-through capability; low-frequency response is optional; rate of change of frequency (ROCOF) withstand capability must reach 0.5 Hz/s. |
| **Category II (Coordinated Compatibility)** | Fully coordinated with the stability/reliability requirements of all bulk power systems, such as NERC standards. Avoids unnecessary equipment tripping over a broader disturbance range. | Must have full-frequency response capability under high/low-frequency conditions; rate of change of frequency (ROCOF) withstand capability must reach 2.0 Hz/s; supports dynamic voltage support and voltage phase-angle jump ride-through. |
| **Category III (Highest Robustness)** | Designed for high-penetration DER scenarios and compatible with the extreme reliability and power quality requirements of all distribution networks and the main grid. | Requires the highest levels of low-voltage ride-through (LVRT), frequency modulation, inertia response, and extreme ROCOF withstand capability. |

Under this framework, the microgrid islanding detection and off-grid transition strategy must be deeply coupled with the above ride-through mechanisms. Only when the detected voltage sag, frequency deviation, or voltage phase-angle jump persists beyond the maximum clearing time specified by IEEE 1547-2018 will the system determine that a true islanding event has occurred, decisively open the PCC switch, and initiate switching of the underlying control strategy.

### 2.3.2 Basic Control Modes for Distributed Generation: PQ and V/f Control Mechanisms

The core control logic of underlying inverters within a microgrid differs fundamentally under different operating modes. The two main basic control modes are PQ control and V/f control.

PQ control (constant power control): This is typically deployed in microgrids under grid-connected mode, or in units operating as grid-following (GFL) inverters under islanded mode. Its core objective is to achieve fully decoupled control of output active power (P) and reactive power (Q), so that the inverter strictly follows power reference commands issued by the upper-level EMS. In mathematical modeling of three-phase grid-connected inverters, the Park Transformation is commonly used to convert the three-phase stationary coordinate system into a two-phase rotating coordinate system. In this coordinate system, the mathematical expressions for instantaneous active power and reactive power are as follows:

$$P = 1.5(v_{od}i_{od} + v_{oq}i_{oq})$$

If the grid voltage vector is aligned with the d-axis through a phase-locked loop (PLL), that is, *v_oq = 0*, then active power is controlled only by the d-axis current *i_od*, while reactive power is controlled only by the q-axis current *i_oq*. The PQ control strategy adopts a nested closed-loop structure: the outer loop is the power control loop, and the inner loop is the current control loop. The system eliminates errors through multiple sets of decoupled proportional-integral (PI) controllers. The generation of the reference voltage signal usually follows the following matrix equation:

$$\begin{bmatrix} V_{do} \\ V_{qo} \end{bmatrix} = \begin{bmatrix} -K_{p3} & -\omega L_f \\ \omega L_f & -K_{p3} \end{bmatrix} \begin{bmatrix} i_d \\ i_q \end{bmatrix} + \begin{bmatrix} K_{p3} & 0 \\ 0 & K_{p3} \end{bmatrix} \begin{bmatrix} i_{dr} \\ i_{qr} \end{bmatrix}$$

To effectively reduce steady-state errors and dynamic overshoot in active and reactive power under abrupt load changes, advanced control techniques have begun to introduce heuristic algorithms such as adaptive population extremum optimization (APEO). These methods perform multivariable automatic tuning of the six key PI parameters in the above equations, such as *K_p3*, thereby achieving an optimal balance between response speed and robustness.

V/f control (constant-voltage/constant-frequency control): When a microgrid enters islanded mode because of a main-grid outage, the system loses external stiff voltage support. At this point, at least one large-capacity inverter equipped with an energy storage system, or a synchronous generator, must switch to V/f control mode and act as a grid-forming (GFM) source. The core task of V/f control is to establish and maintain the rated voltage amplitude and rated frequency of the local grid. This control also uses a dual closed-loop architecture: the outer loop is a voltage loop that ensures steady-state accuracy of the output AC voltage, while the inner loop is a current loop that limits the peak inverter output current and accelerates the dynamic response. During this period, the remaining PQ-controlled inverters in the microgrid continue controlled power output using the voltage and frequency established by the V/f source as their reference.

### 2.3.3 Droop Control and Advanced Power Quality Regulation

In islanded microgrids without centralized high-bandwidth communication, achieving balanced power sharing among multiple parallel inverters is a highly challenging physical problem. Droop control, inspired by the grid-connected operating characteristics of conventional synchronous generators, provides an elegant communication-free solution to this problem.

The basic principle of classical droop control is to achieve automatic load sharing by intentionally introducing an inverse relationship between output active power and frequency (P-f droop), and between reactive power and voltage amplitude (Q-V droop). When the total active-power demand of the microgrid increases, each inverter increases its active-power output; according to the P-f curve, the inverter

autonomously reduces its output frequency. After a brief period of physical self-balancing, all parallel units converge to the same steady-state frequency point and share the total load in proportion to their droop coefficients, which are typically inversely proportional to rated capacity.

However, conventional droop control exhibits serious limitations in modern microgrids. First, it is highly susceptible to impedance mismatch among microgrid branches. Such impedance mismatch can produce large reactive-power circulating currents among parallel inverters, severely reducing power-supply efficiency and system stability. Second, when facing large numbers of nonlinear loads, such as switched-mode power supplies, rectifiers, and charging piles, conventional droop control cannot effectively allocate the harmonic currents generated by nonlinear loads. To address this power-quality challenge, the industry has introduced an advanced control loop based on virtual output impedance. By adding virtual resistance or reactance voltage-drop terms to the original droop control algorithm, the inverter can reshape its equivalent output impedance without changing the physical hardware. This not only suppresses circulating distortion power caused by line differences, but also enables accurate sharing of high-order harmonic currents among devices, thereby substantially reducing system voltage deviations and realizing closed-loop management of microgrid frequency fluctuation damping and harmonic mitigation.

### 2.3.4 Advanced Reconstruction Technology for Virtual Synchronous Generators (VSGs)

As renewable-energy penetration in power systems approaches its practical limits, large numbers of grid-connected devices interfaced through power electronics have deprived the system of the large mechanical rotational inertia traditionally provided by rotating machines. The sharp reduction in system inertia causes microgrids to exhibit highly fragile and rapid frequency fluctuations even under minor disturbances. To restore the disturbance-resistance capability of microgrids, the virtual synchronous generator (VSG) concept has emerged as a leading form of grid-forming control.

The essence of VSG control is to embed the classical synchronous-generator rotor swing equation as the core algorithm in the inverter microprocessor, thereby forcing a static power-electronic converter to exhibit electromagnetic and mechanical inertial responses at its external terminals that are consistent with those of a rotating machine. Its core mathematical model is expressed as follows:

$$J \frac{d\omega}{dt} = T_m - T_e - D(\omega - \omega_{ref})$$

In this rotor swing equation:

- J (virtual rotational inertia): represents the system's resistance to changes in rotational speed. When a short-circuit fault or abrupt load change causes power imbalance in the grid, the virtual rotor releases or absorbs equivalent "kinetic energy" according to the equation, thereby greatly reducing the maximum rate of change of frequency (RoCoF) during a frequency drop and raising the frequency nadir.
- D (virtual damping): this term emulates the electrical characteristics of damping windings in conventional synchronous machines and is usually represented as damping power proportional to the slip frequency relative to the infinite-bus angular frequency, *P_d = D(ω_bus - ω_m)*. Because mechanical friction damping is extremely small and can be neglected, electrical damping is the key factor that suppresses power oscillations and accelerates the return to steady state after a major disturbance in a microgrid.

In deeper theoretical proofs of control stability, researchers have used Lyapunov transient energy functions to conduct rigorous mathematical derivations for VSG systems. To ensure continuous energy

dissipation during transient oscillations, the derivative of the energy function must be negative. In VSG control schemes with variable rotational inertia, the derivative of the Lyapunov function contains the core damping term *-Dω^2*. This term forces the system state variables to converge rapidly in the time domain, fundamentally ensuring the asymptotic stability of the local grid. In addition, to match the instantaneous high-power throughput required when a VSG emulates flywheel inertia, practical engineering systems often directly couple the classical resistor-capacitor (RC) model of a supercapacitor (SC) with the VSG controller, thereby compensating for the physical limitations of ordinary lithium batteries in millisecond-scale transient power output.

### 2.3.5 Fast Response Control and Extreme-System Black Start Procedure

Low-level microgrid control must provide extreme fault tolerance and rapid intervention. In addition to reverse-power prevention through control algorithms, which prevents surplus PV power at low-load periods from backfeeding into the upstream substation and causing protection misoperation, the most technically challenging process is black start.

Black start refers to the complex process by which, after a catastrophic total outage of a microgrid or even its wider-area host grid, the system autonomously and sequentially re-establishes voltage and frequency using limited internal generation and energy storage under conditions with no external grid support, and then gradually restores supply to critical loads. This process depends heavily on low-level hardware execution capability and must also comply with stringent international standards for microgrid protection and dynamic control, such as IEC TS 62898-3-1.

The advanced technical specification and detailed timing sequence for microgrid black start typically follow the logic below:

1. Micro-source energy storage health and capacity assessment: During black-start initialization, the system must traverse all available micro-sources, such as BESS units with black-start capability. The evaluation criteria are stringent: the total storage capacity of each candidate micro-source is extracted, and a preset capacity threshold is calculated, typically requiring the remaining SOC to be between 40% and 60% of total capacity. Only when the capacity margin is nonnegative is the energy storage unit determined to be qualified as the leading black-start source, thereby generating a "black-start sequence" sorted by capacity.
2. Grid-forming source startup and bus-voltage establishment: According to the black-start sequence, the highest-ranked GFM inverter or high-speed diesel generator is started to energize the de-energized main bus for the first time. The key criterion for determining whether bus voltage has been successfully established is that the frequency deviation of the bus output voltage must be strictly limited within *\pm 1\% ω_0* of the nominal value, and the amplitude deviation must not exceed *\pm 10\% U_0*. If this criterion is not met, the system forcibly disconnects the newly started micro-source, declares the restoration attempt failed, and re-enters the initialization safety sequence.
3. Activation of frequency and voltage regulation algorithms and connection of subordinate micro-sources: Once the backbone bus voltage is confirmed to be stably established, the controller immediately activates the upper-level frequency and voltage regulation algorithms. At this stage, the microgrid is extremely fragile, and the leading source must provide robust support. The system then sequentially checks the algorithm modes of other renewable generation units in the subsequent black-start sequence, such as PV inverters. If they do not have frequency and voltage regulation capability, they are forced to connect in grid-following (GFL) mode with zero-power or low-power commands, avoiding reverse impact on the fragile bus.

4. Load power matching and stepwise restoration: After the micro-source system has been reconstructed, the process enters the load-restoration stage. Before load connection (SOC-101 soft transition), the controller must calculate the current remaining output power of the microgrid in real time and strictly compare it with the instantaneous power and startup inrush demand of the load to be connected. Only when the system power margin is substantially greater than the load demand will the corresponding circuit breaker close, allowing safe load connection and completing the entire black-start cycle.

## 2.4 Core Architecture and Optimization Coordination of the Microgrid Energy Management System (EMS - Management Layer)

If low-level control is regarded as the "limbs" and "cerebellum" of a microgrid, ensuring reflex-like rapid response and survivability, then the microgrid energy management system (EMS) is its indispensable "brain." The EMS operates on longer time scales, from minutes to hours or day-ahead planning, and focuses primarily on aggregating multisource information, assessing equipment health, forecasting massive time-series datasets, and solving a complex global optimization problem that seeks both economic and environmental objectives under multiple constraints.

### 2.4.1 Real-Time Monitoring, Data Acquisition (SCADA), and High-Precision Energy Storage SOC Estimation

The data foundation of the EMS is built on a powerful supervisory control and data acquisition (SCADA) system. Through a distributed sensor matrix, the SCADA system continuously aggregates telemetry and teleindication data from converters, circuit breakers, weather stations, and meters. Among the massive volume of sensing data, monitoring the state of charge (SOC) of the battery energy storage system (BESS) is the most central endogenous variable and one of the most difficult to measure directly.

Accurate battery SOC estimation is not only a safety boundary for preventing severe overcharge or critical overdischarge, but also the computational basis for global active-power optimization and dispatch by the EMS. Conventional SOC estimation methods mainly rely on ampere-hour integration, extended Kalman filtering (EKF), or basic neural networks (NNs). However, when faced with the complex internal electrochemical nonlinearities of power batteries and frequent shallow charge-discharge cycles during peak shaving and valley filling in microgrids, these algorithms often exhibit serious weaknesses such as model divergence and accumulated error.

Advanced academic research and industrial practice have introduced the unscented Kalman particle filter (UKPF) algorithm for high-dimensional state-space reconstruction. Empirical analysis based on multi-algorithm comparison clearly shows that the UKPF algorithm provides outstanding accuracy and robustness in characterizing the SOC of microgrid power batteries.

| Power Battery SOC Estimation Algorithm | Average Error (%) | Maximum Error (%) | Convergence Speed Characteristics | Overall Algorithm Performance Evaluation |
|---|---|---|---|---|
| **Extended Kalman Filter (EKF)** | Relatively high | Relatively large | Relatively fast | Prone to divergence in highly nonlinear regions, with significant long-term accumulated error. |

| Power Battery SOC Estimation Algorithm | Average Error (%) | Maximum Error (%) | Convergence Speed Characteristics | Overall Algorithm Performance Evaluation |
|---|---|---|---|---|
| **Basic Neural Network (NN)** | Relatively high | < 5.0% | Slow | Highly dependent on the coverage of training-data samples, with weak generalization capability. |
| **Unscented Kalman Particle Filter (UKPF)** | **1.35%** | **< 2.5%** | **Extremely fast** | Fastest convergence, extremely low error, and the best stability under highly nonlinear energy storage charge-discharge conditions. |

Enabled by high-precision algorithms such as UKPF, the EMS can obtain high-fidelity SOC data in real time with errors controlled within 2.5%. This high-precision state input is seamlessly connected to the optimization engine, allowing the controller to make precise use of every unit of capacity redundancy in the energy storage system and greatly expand the safe dispatch boundary of the microgrid.

### 2.4.2 High-Dimensional Power Forecasting: The Deep Learning Transformation of PV, Wind, and Load Forecasting

In microgrid day-ahead scheduling and intra-day rolling strategies, the ability to accurately anticipate future changes in "source" and "load" directly determines dispatch performance. Because wind and PV generation are highly stochastic and end-user electricity consumption behavior is highly discrete, building high-precision power forecasting models has become a leading challenge for microgrid EMS.

With the rapid development of deep learning, time-series forecasting has undergone a fundamental paradigm shift. In early deep-learning applications, long short-term memory artificial neural networks (LSTM, Long Short-Term Memory) were widely deployed. Using their unique gating mechanisms, including input, forget, and output gates, LSTMs can very effectively capture short-term dependencies in time series. Empirical studies show that, in short-term forecasting scenarios with a 24- to 48-hour forecast horizon, LSTM models deliver highly stable accuracy. However, when a microgrid EMS requires longer-horizon forecasting and planning, such as meteorological evolution and load-cycle inference beyond 48 hours, LSTMs are constrained by their recursive structure and face severe gradient-vanishing issues and reduced capability in capturing long-range dependencies.

At this point, Transformer architectures centered on self-attention have emerged as a powerful alternative. Transformers completely eliminate the constraints of sequential recursive processing and can compute global correlation weights between any two time points in time-series data in parallel. This architecture demonstrates substantially stronger data-mining capability than LSTM in long-horizon forecasting tasks beyond 48 hours.

To combine the strengths of both approaches and address the highly complex physical boundaries of microgrids, cross-architecture hybrid deep learning models, such as LSTM-Informer or ANN-LSTM-Transformer, have been proposed and deployed in practice. This multilayer hybrid network enables refined functional coordination:

1. ANN layer: responsible for processing highly heterogeneous static covariate inputs, such as geographic location and baseline electrical-infrastructure capacity parameters;
2. LSTM layer: responsible for highly sensitive extraction of local sequence disturbances caused by abrupt meteorological changes within short time windows, such as cloud shading of PV panels;

3. Transformer layer: captures long-range dependencies across the entire forecasting horizon, such as the cumulative air-conditioning load effect caused by consecutive extreme high-temperature days. Multidimensional data validation shows that this hybrid framework comprehensively outperforms conventional single-model architectures in forecasting accuracy, model scalability, and robustness to extreme fluctuations in electricity consumption behavior, providing the microgrid EMS with day-ahead planning priors that closely approximate real conditions.

### 2.4.3 Algorithmic Innovation in Economic Dispatch Optimization and Multi-Energy Complementarity

Peak shaving and valley filling based on time-of-use (TOU) tariffs, together with global coordinated optimization of multi-energy complementary microgrids such as PV-storage-diesel systems, constitute the central mathematical problem for a microgrid EMS. In operations research, this problem is abstracted as a typical high-dimensional, nonlinear, mixed-integer programming problem. Its objective function seeks not only to minimize total operating cost, including fuel consumption, equipment depreciation, and grid-interaction electricity charges, but often also to minimize greenhouse-gas emissions.

In selecting solvers for such complex optimal dispatch problems, conventional methods have shown clear divergence and evolution:

| Optimization Algorithm Class | Core Mechanism and Computational Characteristics | Limitations and Challenges in Industrial Applications |
|---|---|---|
| **Mixed-Integer Linear Programming (MILP)** | Uses the simplex method or interior-point method to conduct deterministic search within a strictly linear constraint space, ensuring that the global optimum can be found. | Cannot directly handle nonlinear charge-discharge efficiency curves of energy storage systems. If the physical model is oversimplified or energy storage efficiency losses are ignored, severe constraint-violation faults may occur when dispatch commands are issued in practice. |
| **Particle Swarm Optimization (PSO)** | A heuristic algorithm that simulates flock foraging behavior. Through iterative velocity and position equations, it performs multipoint parallel exploration and is well suited to highly nonlinear objectives and complex physical constraints. | When facing the high-dimensional solution space of a microgrid, especially with stringent penalty functions to avoid constraint violations, optimization particles can easily fall into local minima, causing optimization failure. |

To overcome these technical bottlenecks, academia and advanced industry have developed MILP-PSO collaborative optimization algorithms. This strategy combines the strengths of both methods: in the initial stage of computation, the system first uses a large-scale dimension-reduced and linearized MILP model to perform a macroscopic sweep, rapidly locating the broad feasible region that contains the global optimum. This high-quality solution-space boundary is then injected into the PSO algorithm as initial points. Within this tightly bounded initial region, PSO carries out deep nonlinear fine-tuning optimization while retaining all real nonlinear constraints, such as battery lifetime degradation models and diesel-generator fuel-consumption curves. This collaborative algorithm not only avoids the tendency of standalone PSO to become trapped in local optima, but also effectively mitigates the risk of dispatch failure caused by neglecting physical details when using MILP alone.

### 2.4.4 Reserve Capacity Management and Extreme Reliability Constraints

While the EMS performs economic dispatch, it must never compromise system safety and resilience. Reserve capacity management is the lifeline that maintains survivability in microgrids, especially those supplying military bases or remote islands.

During day-ahead dispatch planning, the EMS must introduce strict reliability constraints and an expected unserved energy cost (EUAC) objective function. This means that the EMS must not overdischarge the energy storage system merely to exploit time-of-use price spreads. The system must calculate, in real time, the lower-confidence-bound output of PV or wind power over the next 24 hours and combine it with the expected duration of islanded faults under worst-case conditions, forcing a portion of diesel-generator or energy storage battery-cluster capacity to be locked as mandatory reserve capacity that is not allowed to participate in routine economic arbitrage. Only in this way, when the main grid suffers an unexpected catastrophic outage, can the low-level black-start process and GFM inverters of the microgrid have sufficient underlying energy resources to support the absolutely safe operation of critical loads, such as life-support systems and core communication base stations, throughout the entire islanded period.

# 3 Microgrids and Application Scenarios

## 3.1 What Is a Weak Grid

A weak grid refers to a grid environment in which the ratio of grid short-circuit capacity to the rated capacity of connected equipment, namely the short-circuit ratio (SCR), is low. According to internationally accepted criteria, SCR<2 defines a weak grid, while SCR<1.2 indicates an extremely weak grid. The short-circuit ratio is calculated as:

$$\mathrm{SCR} = \frac{S_{sc}}{S_n} = \frac{\text{grid short-circuit capacity}}{\text{rated capacity of connected equipment}}$$

The core characteristics of a weak grid include voltage fluctuations caused by high grid impedance, poor frequency stability caused by low system inertia, and limited renewable-energy hosting capacity due to insufficient grid short-circuit capacity. Typical scenarios include distribution networks in remote areas, island microgrids, rural feeder ends, and regions with large-scale renewable-energy integration. In these scenarios, voltage fluctuations may reach ±12%, and frequency deviations may reach ±2Hz, seriously threatening the stable operation of grid-connected equipment.

## 3.2 Weak-Grid Problems and PCS-Based Solutions

### 3.2.1 Main Weak-Grid Problems

| Problem Type | Specific Manifestation | Severity |
| --- | --- | --- |
| Control Stability Problem | Reduced current-loop bandwidth (from 1kHz to 200Hz), risk of phase-locked loop (PLL) loss of lock | High |

| Problem Type | Specific Manifestation | Severity |
|---|---|---|
| Harmonic Amplification Problem | Grid impedance and inverter filters form LC resonance (300Hz-2kHz), and the 11th harmonic may be amplified to 8.3% | Medium-high |
| Power Output Limitation | Active derating is required, such as operation at 80% of rated power | Medium |
| Voltage Ride-Through Difficulty | When SCR<1.2, more stringent fault ride-through curves must be satisfied | Medium |

### 3.2.2 Mainstream PCS Solutions

#### 1. Control Strategy Optimization

PCS energy storage converters require control strategies adapted to weak grids:

- VSG control (virtual synchronous generator): By emulating the rotor swing equation of a synchronous generator and introducing virtual inertia and damping, VSG control effectively suppresses rapid frequency and voltage fluctuations and is particularly suitable for weak-grid scenarios with high renewable-energy penetration.
- PQ/VF/droop control combination: PQ control is used in grid-connected operation to achieve accurate power dispatch; VF control is used in off-grid operation to maintain voltage and frequency stability; and droop control is enabled during multi-unit parallel operation to achieve communication-free power sharing.

#### 2. Hardware Topology Improvements

- Wide-SCR adaptive design: supports an SCR=1.0~∞ range to meet the operating requirements of extremely weak grids
- Enhanced filtering capability: uses LCL filters with active damping control, or LLC plus hybrid-filter topologies, to suppress resonance
- High/low voltage ride-through (HVRT/LVRT): satisfies the stringent requirement that grid-connected operation be maintained for 150ms even when voltage drops to 0% under SCR<1.2

#### 3. System-Level Protection Strategies

- Active impedance scanning: periodically injects small-signal disturbances to update the grid impedance model in real time
- Q-V droop coefficient configuration: sets reactive-power regulation at 5% for every 1% voltage change to provide voltage support

### 3.2.3 Weak Grids and VSG

#### 1. Technical Principles of VSG

Virtual synchronous generator (VSG) technology embeds the mathematical model of a synchronous generator into the inverter control algorithm, enabling a static power-electronic device to emulate the operating characteristics of a rotating machine. Core technical elements include:

**1. Rotor Swing Equation Emulation**

By emulating the rotor swing equation of a synchronous generator, VSG realizes active power-frequency droop characteristics and reactive power-voltage droop characteristics:

$$J\frac{d\omega}{dt} = T_m - T_e - D(\omega - \omega_0)$$

where *J* is the virtual inertia, *D* is the damping coefficient, *T_m* is the mechanical torque, and *T_e* is the electromagnetic torque.

**2. Active Support Capability**

- Inertia support: rapidly responds during the initial stage of frequency variation, smoothing both the amplitude and rate of frequency change
- Primary frequency regulation: generates frequency-regulation commands based on frequency deviation and rate of change, providing frequency support similar to that of synchronous units
- Active voltage regulation: maintains point-of-common-coupling voltage stability through reactive power-voltage droop control

**3. Weak-Grid Adaptive Parameter Design**

For weak-grid scenarios, the design principles for key VSG parameters are:

| Parameter | Typical Value Range | Design Principle |
|---|---|---|
| Virtual inertia *J* | 0.5~2.0 kg·m² | Larger inertia makes frequency changes smoother, but excessive inertia must be avoided because it can cause power oscillations |
| Damping coefficient *D* | 50~200 N·m·s/rad | Larger damping improves system stability but reduces response speed |
| Primary frequency-regulation coefficient *K_f* | 2%~5% | Determined according to grid frequency-regulation requirements |

### 3.2.4 Application Value of VSG in Weak Grids

In an online case involving a 100MW PV plant project (SCR=0.9), after enabling VSG mode and configuring a Q-V droop coefficient of 5%, voltage fluctuations were reduced from ± 12% to ± 3%, eliminating frequent disconnection problems. VSG technology shifts renewable-energy generation from "passive regulation" to "active support" and has become an effective pathway for addressing the challenges of "dual-high" power systems, namely high shares of renewable energy and high shares of power-electronic equipment.

## 3.1.4 Weak Grids and Islanding Detection

**1. Overview of the Islanding Effect**

The islanding effect refers to the formation of an independently operating electrical island when distributed generation systems, such as PV and energy storage, continue supplying local loads after grid interruption caused by faults or outages. Islanded operation may introduce safety risks, including hazards to maintenance personnel, power-quality problems such as uncontrolled voltage and frequency, and risks of equipment damage.

## 2. Classification of Islanding Detection Methods

### a. Passive Detection Methods

Passive methods determine islanding conditions by monitoring abnormal changes in grid parameters, without actively injecting disturbances into the grid:

| Detection Method | Principle | Advantages | Limitations |
|---|---|---|---|
| Over/Undervoltage Protection (OVP/UVP) | Monitors whether the point-of-common-coupling voltage exceeds thresholds, typically ±10% | Simple implementation, no harmonic injection | Has a nondetection zone and fails under load matching |
| Over/Underfrequency Protection (OFP/UFP) | Monitors whether frequency exceeds thresholds, typically ±0.5Hz | Fast response | Also has a nondetection zone |
| Voltage Harmonic Detection | Monitors changes in harmonic content | Sensitive to load changes | Strong interference from background grid harmonics |
| Rate of Change of Frequency (ROCOF) | Monitors whether df/dt exceeds the threshold | Relatively fast detection | Nonlinear loads may cause misoperation |

### b. Active Detection Methods

Active methods determine islanding conditions by injecting small disturbances into the grid and monitoring the grid response:

| Detection Method | Principle | Key Parameters | Applicable Scenario |
|---|---|---|---|
| Active Frequency Drift (AFD) | The inverter output current frequency is shifted; under normal grid conditions the frequency is locked, while under islanding the frequency shift accumulates | Disturbance magnitude within ±5% | Single-inverter systems |
| Active Frequency Drift with Positive Feedback (AFDPF) | The larger the frequency deviation, the larger the injected disturbance | Dynamic adjustment of feedback coefficient k | Parallel multi-inverter systems |
| Slip-Mode Frequency Shift (SMS) | Achieves frequency shifting through phase shifting | Initial phase-angle setting | Loads with quality factor Qf<2.5 |
| Active Current Disturbance Method | Injects specific harmonic currents and monitors impedance changes | Disturbance current amplitude | Weak-grid scenarios |

| Detection Method | Principle | Key Parameters | Applicable Scenario |
|---|---|---|---|
| Impedance Detection Method | Injects high-frequency signals to measure grid impedance | Injection frequency selection | Complex grid conditions |

**c. Hybrid Detection Methods**

For weak-grid scenarios, a hybrid scheme combining passive and active methods is recommended:

- Passive layer: uses voltage unbalance and ROCOF methods for rapid preliminary screening
- Active layer: uses reactive-power disturbance or adaptive slip-mode frequency shift for confirmation
- Trigger logic: the active method is started only after the passive method detects an abnormality, reducing the impact on power quality

**d. Key Technical Points for Islanding Detection in Weak Grids**

- Anti-interference design: weak grids exhibit large voltage fluctuations, so reasonable detection thresholds and delays must be configured to avoid misoperation
- Multi-unit coordination: when multiple inverters operate in parallel, disturbance strategies must be unified to avoid mutual cancellation
- Coordination with fault ride-through: islanding detection must be coordinated with high/low voltage ride-through functions to prevent false detection during faults

## 3.1.5 Common Hardware-Related Issues in Off-Grid BESS

As core equipment in weak-grid and islanded scenarios, off-grid battery energy storage systems (BESSs) depend directly on hardware reliability for safe system operation. The following summarizes major hardware problems and solutions based on engineering practice.

**I. Common Battery System Problems**

| No. | Problem Type | Specific Manifestation | Severity | Mainstream Solutions |
|---|---|---|---|---|
| 1 | Battery Thermal Runaway | Abnormal rise in internal battery temperature triggers a chain reaction and may cause fire | Extremely high | ① Deploy off-gas detection systems (warning 6 minutes and 11 seconds earlier than smoke detection); ② link with automatic shutdown; ③ configure thermal management systems (liquid cooling/air cooling); ④ provide redundant temperature sensors |
| 2 | Overcharge/Overdischarge Fault | BMS failure causes batteries to operate outside the safe voltage range | High | ① Multilevel BMS protection (software + hardware); ② independent overcharge/overdischarge protection circuits; ③ fuses/circuit breakers; ④ periodic capacity calibration |
| 3 | Battery Balancing Failure | Excessive voltage differences among cells cause some cells to | Medium | ① Active balancing circuits (energy-transfer type); ② passive balancing resistors; ③ periodic balancing maintenance; ④ replacement of abnormal cells |

| No. | Problem Type | Specific Manifestation | Severity | Mainstream Solutions |
|---|---|---|---|---|
| | | overcharge or overdischarge | | |
| 4 | Battery Aging and Degradation | Capacity loss, increased internal resistance, and shortened cycle life | Medium | ① Real-time SOH (state of health) monitoring; ② intelligent charge-discharge strategy; ③ optimized temperature control; ④ second-life utilization assessment |

**II. Battery Management System (BMS) Hardware Problems**

| . | Problem Type | Specific Manifestation | Severity | Mainstream Solutions |
|---|---|---|---|---|
| 1 | Sampling Abnormality | Voltage/current/temperature sampling values drift or fail | High | ① Multi-channel redundant sampling; ② periodic calibration; ③ cross-validation algorithms; ④ isolation of faulty sampling channels |
| 2 | Communication Fault | Communication interruption or data errors between BMS and PCS/EMS | Medium-high | ① Dual communication redundancy (CAN+RS485); ② communication timeout detection; ③ breakpoint resume mechanism; ④ local caching |
| 3 | Balancing Circuit Fault | Balancing resistor open circuit or MOSFET short circuit | Medium | ① Balancing circuit self-test; ② balancing-current monitoring; ③ isolation of faulty balancing channels; ④ periodic balancing-function testing |
| 4 | High-Voltage Control Failure | Main positive/main negative relay adhesion or failure to open | High | ① Relay status monitoring (auxiliary contacts); ② adhesion detection algorithm; ③ dual-relay series configuration; ④ emergency-stop button hardware cutoff |

**III. Energy Storage Power Conversion System (PCS) Hardware Problems**

| No. | Problem Type | Specific Manifestation | Severity | Mainstream Solutions |
|---|---|---|---|---|
| 1 | DC-Side Arc Fault | Loose DC connections or poor contact produce high-temperature arcs | Extremely high | ① DC arc detection (time-domain + frequency-domain algorithms); ② intelligent terminal temperature detection; ③ AFCI arc-fault protection; ④ periodic tightening inspection of connection points |
| 2 | Power Device Overheating | Excessive junction temperature of IGBTs/MOSFETs causes protection action or damage | Medium-high | ① Multi-point temperature sensor monitoring; ② intelligent air-cooling/liquid-cooling control; ③ derating operation strategy; ④ power-device redundancy design |
| 3 | DC Bus Overvoltage | Battery-side voltage exceeds the allowable PCS range | Medium | ① DC-side overvoltage protection (hardware + software); ② tiered battery-pack voltage |

| No. | Problem Type | Specific Manifestation | Severity | Mainstream Solutions |
|---|---|---|---|---|
| | | | | management; ③ overvoltage discharge circuit; ④ battery-pack switch disconnection protection |
| 4 | Grid-Connected/ Off-Grid Transition Fault | Grid-connected/islanded transition failure or excessive transition time | Medium | ① STS static transfer switch; ② synchronous phase-locking control; ③ seamless transition algorithm; ④ transition-failure protection logic |

**IV. Electrical Connection and Protection Hardware Problems**

| No. | Problem Type | Specific Manifestation | Severity | Mainstream Solutions |
|---|---|---|---|---|
| 1 | DC Fuse/Circuit Breaker Fault | Nuisance fuse blowing or circuit-breaker failure to trip | Medium-high | ① Optimized fuse selection (rated current 1.25~1.5 times); ② circuit-breaker status monitoring; ③ coordinated graded protection; ④ periodic fuse replacement |
| 2 | Insulation Fault | Insulation resistance from DC positive/negative poles to ground is below 50kΩ | High | ① Real-time insulation resistance monitoring; ② insulation-fault location; ③ ground-fault protection; ④ periodic insulation testing |
| 3 | Ground Fault | Abnormal grounding on the AC or DC side | Medium-high | ① Grounding resistance monitoring; ② ground-fault protection; ③ equipotential bonding; ④ periodic grounding-system inspection |
| 4 | Contactor Fault | Contactor contact erosion or coil fault | Medium | ① Contactor status monitoring (auxiliary contacts); ② contact-wear detection; ③ redundant contactor configuration; ④ periodic maintenance and replacement |

**V. Auxiliary System Hardware Problems**

| No. | Problem Type | Specific Manifestation | Severity | Mainstream Solutions |
|---|---|---|---|---|
| 1 | Thermal Management System Fault | Liquid-cooling pump fault, air-cooling fan fault, or valve defect | Medium-high | ① Redundant thermal management equipment; ② temperature-linked control; ③ fault transfer logic; ④ periodic maintenance and cleaning |
| 2 | Fire Protection System Fault | Fire-extinguishing system defect or detector failure | High | ① Multiple detector types (smoke + temperature + off-gas); ② automatic fire-extinguishing system; ③ periodic fire-protection system testing; ④ linkage with BMS |

| No. | Problem Type | Specific Manifestation | Severity | Mainstream Solutions |
|---|---|---|---|---|
| 3 | Monitoring System Fault | Data acquisition unit fault or communication interruption | Medium | ① Redundant monitoring equipment; ② local data caching; ③ remote monitoring backup; ④ fault alarm mechanism |

## 3.1.6 Core Hardware-Related Technical Issues in Off-Grid BESS

In the practical deployment and high-intensity operation of microgrids and off-grid battery energy storage systems (BESSs), the underlying hardware architecture of the power conversion system (PCS) directly determines the system's ability to handle complex loads, suppress harmonic interference, and transition seamlessly between grid-connected and off-grid states. With increasing distributed-energy penetration and widespread integration of high shares of nonlinear loads, off-grid systems face numerous severe hardware-level challenges. This section provides an in-depth analysis of the electrical mechanisms and control-theory implications of common hardware problems in off-grid BESS operation, and systematically demonstrates the necessity and technical landscape of an integrated three-phase four-leg converter solution based on silicon carbide (SiC) wide-bandgap devices for contemporary industrial applications.

### 3.1.6.1 Loss of Grid Neutral Support and Grounding Safety Challenges in Off-Grid Operation

In conventional grid-connected operation, the distribution transformer of the public grid, typically using a grounded wye winding or a Delta-Wye configuration, provides robust grid neutral support and a low-impedance grounding loop for the entire power system. However, when a microgrid or BESS switches to off-grid (islanded) mode because of an external fault or command, if the energy storage converter side lacks an effective neutral-point construction mechanism and grounding management protocol, the system immediately faces severe neutral-point drift and complex grounding safety (N-PE bonding) challenges.

The core physical mechanism behind the lack of physical neutral support in off-grid operation is that the system loses the stiff reference point that constrains the neutral potential of the three-phase voltage vectors. When single-phase loads or three-phase unbalanced loads operate, asymmetric load impedances prevent zero-sequence current from returning through a low-impedance path. This not only causes severe phase-voltage imbalance, with the lightly loaded phase voltage rising sharply and the heavily loaded phase voltage falling sharply, but more seriously creates a floating neutral problem in off-grid operation. When the system is disconnected from the grid, if the microgrid does not implement reliable dynamic connection between the neutral conductor (N) and protective earth (PE), equipment metal enclosures may become energized because of N-conductor potential drift and parasitic-capacitance coupling. In commercial and industrial (C&I) applications, such as data centers, hospitals, or high-precision production lines, as well as in mobile microgrids such as RVs and shipboard power systems, this creates an unacceptable electric-shock hazard. This potential instability can also cause residual-current devices (RCDs or ELCBs) to lose their reference and either misoperate or fail to operate, and may generate destructive common-mode voltage stress in complex distribution networks, accelerating cable insulation aging and even causing fire.

In contemporary industrial-grade solutions, logic control for off-grid N-PE grounding bonding is an extremely precise safety protocol. The generally accepted industrial safety principle requires that any islanded electrical network must have one and only one neutral-to-earth (N-PE) bonding point. This is intended to avoid parallel ground-fault paths and stray circulating ground currents, thereby preventing excessive touch current on metal structures. Modern advanced BESS architectures have moved away from simple static hard wiring and instead integrate dynamically controlled grounding relays or contactors inside the PCS or intelligent static transfer switch (STS) module. Their automatic operating logic is highly adaptive: in grid-connected mode, when the system detects external grid voltage, the converter must immediately open its internal N-PE relay and assign grounding responsibility to the upstream grid transformer; if a direct N-PE short exists on the microgrid load side at this time, it will cause circulating-current conflict from multipoint grounding and introduce reverse-power backfeed risk. In off-grid mode without an external generator, the converter closes the internal N-PE relay, and the PCS actively establishes the local grounded neutral point, ensuring that leakage-protection devices can accurately detect unbalanced leakage current. When the system operates together with a backup diesel generator, the converter must determine the grounding attributes of the generator through communication or electrical detection. If the generator already has internal N-PE bonding, the PCS actively opens its own bonding to avoid conflict; if the generator is designed with a floating ground, the PCS maintains its own bonding in the active state.

To establish this neutral point on the converter side, early solutions typically connected a bulky isolation transformer in series at the inverter output and relied on its winding structure to absorb zero-sequence current and forcibly clamp the neutral-point potential. However, such physical transformers significantly increase system volume, life-cycle cost, and core component iron and copper losses. Therefore, introducing native three-phase four-wire converter technology in transformerless topologies has become a key hardware foundation for eliminating dependence on physical isolation transformers and improving system energy density.

### 3.1.6.2 Comparison of Three-Phase Four-Wire PCS Architectures: Differences Between Three-Leg Split-Capacitor and Four-Leg Topologies

To provide a low-impedance neutral-current path and support up to 100% unbalanced loads without a transformer, the power-electronics industry has mainly developed two distinct topologies for three-phase four-wire systems: the three-phase three-leg split-capacitor topology and the three-phase four-leg topology (3-Phase 4-Leg Topology, 3P4L). These two hardware schemes differ fundamentally in their performance boundaries, conversion efficiency, and impact on the DC bus (DC-link).

As a conventional and relatively simple solution, the three-phase three-leg split-capacitor topology is characterized by direct hard connection of the grid or load neutral conductor to the physical midpoint of series capacitors on the DC bus. This connection provides a direct return path for zero-sequence current from the AC side into the DC side. However, this topology has significant physical drawbacks. The first is its extreme requirement for DC bus capacitance. Under three-phase unbalanced loads, neutral current inevitably flows into the capacitor midpoint, causing severe capacitor-voltage imbalance and low-frequency ripple, typically second-order ripple at twice the grid frequency. To limit such voltage fluctuations and prevent the inverter from entering the overmodulation region or triggering overvoltage protection, designers are forced to use large electrolytic capacitor arrays. In a detailed simulation study of a 42.5 kVA converter system, each half-bridge of the three-leg split-capacitor topology required capacitance as high as 4.1 mF (millifarads) to limit DC bus voltage variation within a safe 69V range. This directly causes a sharp decline in system power density and introduces short-life electrolytic capacitors as a reliability bottleneck. In

addition, because the neutral-point potential is directly clamped to the DC bus midpoint, common-mode voltage injection is restricted, so the system can use only conventional sinusoidal pulse-width modulation (SPWM) and completely loses the ability to use space-vector modulation (SVPWM) or third-harmonic injection PWM (THIPWM). As a result, DC bus voltage utilization is very low, and a higher total DC bus voltage, with a theoretical calculated value of up to 785V, is required to ensure undistorted peak AC phase-voltage output under heavy load.

By contrast, the three-phase four-leg topology (3P4L) represents the advanced paradigm for contemporary off-grid PCS. On the basis of the conventional three legs, this topology adds a fully independent fourth controllable half-bridge leg dedicated to controlling and providing a high-frequency digital path for neutral conductor current, thereby completely eliminating the physical connection between the neutral conductor and the DC bus capacitor midpoint. Through high-frequency modulation of common-mode voltage, the fourth leg actively cancels or absorbs zero-sequence components caused by phase-current asymmetry and substantially blocks second-order ripple energy from flowing into the DC bus. In principle, only a very small amount of nonpolar film capacitance is required to absorb transient high-frequency spike energy from semiconductor switching and maintain system stability. In the same 42.5 kVA system evaluation, the four-leg topology required only 50 μF (microfarads) of DC capacitance to strictly suppress DC bus voltage fluctuations caused by neutral-point offset within a small ±2.5V range. This means capacitor volume can be reduced by more than two orders of magnitude, producing a step change in system reliability. More importantly, the four-leg architecture gives the system four independent voltage-control degrees of freedom, enabling full support for three-dimensional space-vector PWM (3D-SVPWM) or third-harmonic injection. This increases theoretical DC bus voltage utilization by 15.47% compared with SPWM and, under the same AC output requirement, reduces the bus-voltage threshold from 785V to 620V, a reduction of 165V. This not only alleviates voltage stress on semiconductor devices, but also broadens the usable voltage window of the front-end battery energy storage system (BESS).

To more clearly quantify the overall performance of these two topologies in industrial implementation, the following table presents a comparative analysis across key dimensions:

| Performance Evaluation Dimension | Three-Phase Four-Leg Topology (3-Phase 4-Leg, 3P4L) | Three-Phase Three-Leg + Split DC Capacitor Topology (3-Leg Split-Capacitor) |
|---|---|---|
| **Neutral Conductor Electrical Connection Location** | Connected to the midpoint of an independent fourth controlled half-bridge | Physically connected directly to the DC bus capacitor midpoint |
| **DC Support Capacitance Requirement** | Extremely low (only 50 μF for a 42.5kVA system), can use all-film capacitors | Extremely high (4.1 mF per half-bridge for a 42.5kVA system), with limited lifetime |
| **Control of Second-Order Bus Voltage Fluctuation** | Extremely low fluctuation (less than ±2.5V), inherently immune to unbalance impacts | Severe imbalance (fluctuation up to ±69V), requiring large capacitance buffering |
| **Compatible Modulation Strategy** | Fully supports three-dimensional space-vector modulation (3D-SVPWM) and THIPWM | Limited to conventional sinusoidal pulse-width modulation (SPWM), with no common-mode degree of freedom |

| Performance Evaluation Dimension | Three-Phase Four-Leg Topology (3-Phase 4-Leg, 3P4L) | Three-Phase Three-Leg + Split DC Capacitor Topology (3-Leg Split-Capacitor) |
|---|---|---|
| **Lower Limit of Required DC Bus Voltage** | Lower (approximately 620V), significantly improving voltage utilization and battery compatibility | Higher (approximately 785V), leading to higher device withstand-voltage requirements |
| **Efficiency Under Extremely Unbalanced Light Load** | Slightly lower (high-frequency switching and conduction losses in the fourth leg) | Better (no additional switching loss from a fourth leg) |
| **Energy Efficiency Under Medium- to High-Load Unbalance** | Significantly better (loss reduced by approximately 15% through lower bus voltage and advanced modulation) | Poorer (dominated by capacitor loss and high-voltage stress) |

More detailed technical comparison table:

| Item | Four-Leg | Three-Leg + Balancing Bridge |
|---|---|---|
| Switching Devices | High (4 high-power half-bridge modules) | Medium (4 high-power half-bridge modules) |
| Gate Drivers | Medium (8 channels) | Medium (6+2 channels) |
| Thermal Management | High (large fourth-leg loss) | Medium (lower balancing-bridge loss) |
| Filtering | High (fourth leg plus reactor) | Medium (small balancing-bridge inductor) |
| Bus Capacitors | Medium (45uF/1000V*6*4) | High (820uF/500V*38) |
| DSP Algorithm Development | High (3D-SVPWM) | Medium-low |
| Debugging Time | Long (EMC + neutral-point regulation) | Shorter |
| Conducted Interference | High-frequency PWM switching of the fourth leg introduces additional differential-mode noise | Conducted interference mainly comes from switching noise in the main bridge legs |
| | If the neutral-point bridge leg and DC bus capacitors form a high-frequency loop, conducted EMI may be aggravated | Switching action of the balancing bridge additionally increases differential-mode noise, but the noise source is localized in the balancing bridge |
| Radiated Interference | 1,The enlarged current-loop area of the fourth leg increases high-frequency magnetic-field radiation<br>2,High-frequency neutral-point | High-frequency switching may increase local radiation, but because its power is lower (only neutral-point current is processed), the |

| Item | Four-Leg | Three-Leg + Balancing Bridge |
|---|---|---|
| | oscillation may couple through cables or heat sinks and generate electric-field radiation | overall radiation intensity is lower than that of the four-leg topology |
| Common-Mode Noise | Switching action of the fourth leg causes high-frequency neutral-point potential fluctuations, producing common-mode current through parasitic capacitance and conducting it to the grid or load | Relatively low |
| Control Algorithm | 3D-SVPWM introduces an independent zero-sequence degree of freedom through the fourth leg, enabling precise dynamic control of the neutral-point voltage; the algorithm is complex but highly flexible | The main bridge uses conventional SVPWM, while the balancing bridge regulates neutral-point potential through local closed-loop control, such as PID or sliding-mode control |
| | Supports real-time harmonic compensation, such as elimination of third harmonics, and is suitable for nonlinear-load scenarios | Supports segmented modulation: the balancing bridge is activated only when needed, such as when neutral-point offset is detected, reducing normal-state loss |
| Voltage Utilization | 100% (theoretical limit) | 95% (dependent on balancing-bridge capability) |
| Dynamic Response | Extremely fast (direct neutral-point control) | Relatively fast (requires balancing-bridge response time) |
| High-Frequency Potential | High (suitable for SiC/GaN full-bridge applications)<br>A full-SiC solution is simpler | Medium (the balancing bridge can be locally operated at high frequency) |
| Fault Tolerance | Fourth-leg faults affect the entire system | Fault-isolation design between the main bridge and balancing bridge is simpler |
| Modulation Method | 3D-SVPWM | SVPWM |
| | Injects zero-sequence voltage through the fourth leg to extend line-voltage output capability | The midpoint potential is stable and does not participate in voltage synthesis |
| Modulation Wave | $Va=M\sin(\theta)+1/6M\sin(3\theta)$ | |
| Applicable Advanced Scenarios | Stronger suppression of unbalanced current, suitable for future distributed energy resource (DER) systems | Industrialized mass production, low-cost energy storage, and suitable for low-cost retrofits. |

Although the three-leg topology may have a slight advantage in absolute conduction loss under extreme edge conditions with severe unbalance and near no-load operation because it has no fourth-leg

switching action, in most practical medium- to high-load microgrid operating conditions, the four-leg topology can reduce semiconductor-level losses by approximately 80 W, or about 15%, by lowering bus voltage and using advanced decoupling control. Considering system volume, equipment life-cycle cost, including the tradeoff between weight and long-life capacitors, and the potential of high-frequency digital control, the three-phase four-leg topology (3P4L) has become the dominant mainstream choice for managing nonlinear and unbalanced loads in off-grid energy storage systems.

### 3.1.6.3 Current Distortion Caused by Nonlinear Loads and Mitigation Strategies for High-Order Harmonics

In microgrid and off-grid islanded power supply scenarios, loads are often no longer ideal linear impedances. Instead, they include many nonlinear devices equipped with front-end rectifiers, such as high-power LED driver supplies, DC fast chargers for electric vehicles, UPS systems, and various motors using variable-frequency drives. These nonlinear loads exhibit extremely steep impedance characteristics and draw large pulsed currents over short intervals in each half-cycle, thereby producing highly distorted phase-current and neutral-conductor current waveforms. If the control system of the off-grid PCS lacks sufficient bandwidth and robustness to absorb and compensate these high-frequency harmonic currents, the node voltages of the microgrid will be severely distorted, causing the total harmonic distortion (THD) to far exceed the 8% safety limit recommended by IEC 62040-3, which can in turn lead to operational failures or even thermal collapse of sensitive equipment. To address this issue at the fundamental logic level of the control algorithm, modern four-leg PCSs commonly introduce higher-order multiple closed-loop control strategies and three-dimensional space vector modulation algorithms.

Deeply coordinated control model based on multiple proportional-resonant (PR) and repetitive control (RC) strategies. Conventional proportional-integral (PI) controllers usually operate in the synchronous rotating reference frame (dq frame), requiring complex decoupling networks to convert AC signals into DC signals for control. However, under asymmetrical abnormal grid conditions or complex multi-harmonic distortion, PI control has difficulty achieving zero steady-state-error tracking of sinusoidal AC signals in the stationary reference frame. Its gain also decays rapidly at higher frequencies, leaving it with very limited capability to suppress high-order harmonics. Therefore, the inner-loop current control and outer-loop voltage control of modern industrial converters widely adopt a composite control architecture based on the stationary reference frame (*α β γ* frame), namely “proportional multi-resonant (PMR) plus repetitive control (RC).”

The mathematical essence of a proportional-resonant (PR) controller is to use internal resonators to provide nearly infinite open-loop gain at specific AC frequencies. Its standard continuous-domain transfer-function model can be described as:

$$G_{PR}(s) = K_p + \sum_{h=1}^{n} \frac{2K_{ih}\,\omega_c\,s}{s^2 + 2\omega_c\,s + (h\omega_0)^2}$$

In this equation, *K_p* is the proportional gain that determines the transient response speed; *K_ih* is the resonant control gain for the specific *h*th harmonic; *ω_c* is the cutoff frequency that controls the resonant peak width, i.e., the damping bandwidth factor; and *ω_0* denotes the fundamental angular frequency of the grid. To adapt the model to the discrete digital execution environment of microprocessors such as DSPs, the Laplace-domain continuous model above must be converted into a Z-domain discrete transfer function using the bilinear transform, also known as the Tustin approximation. Because the Tustin transform provides the best match between continuous-time and discrete-time systems in frequency response, it ensures that within the discrete sampling period *T_s*, the compensation gain at specific odd harmonics, such as the 3rd, 5th, 7th, and higher-order harmonics, does not introduce phase deviation. In

three-phase systems, by combining positive-sequence and negative-sequence synchronous reference frames, the improved PR controller can completely eliminate interference from off-diagonal cross-coupling terms, allowing each phase to be precisely decoupled and controlled as an independent single-phase system.

However, when facing high-order broadband nonlinear distortion currents generated by equipment such as EV chargers, relying solely on several PR resonant branches at specific frequencies cannot completely eliminate harmonics. Therefore, repetitive control (RC), based on the Internal Model Principle (IMP), is introduced as a feedforward or parallel compensation link. Because any distorted signal with a period equal to the fundamental period can be regarded as the superposition of infinitely many harmonics, an RC controller is equivalent to countless resonators connected in parallel and can achieve zero steady-state-error tracking of any known integer-period disturbance. To address the dynamic response lag caused by the full fundamental-period delay in conventional RC, industry has introduced frequency-adaptive improved repetitive controllers (FA-IRC). This architecture integrates an improved internal-model filter and a finite impulse response (FIR) fractional-delay element. When the frequency of the external grid, or the off-grid islanded system, drifts, it can calculate and adjust the resonant frequency in real time to match the actual grid frequency, thereby substantially broadening the effective resonant bandwidth and ensuring that the system maintains very low THD and extremely fast transient voltage recovery under severe load steps.

Mathematical dimensionality reduction and implementation geometry of three-dimensional space vector pulse-width modulation (3D-SVPWM) in a four-leg topology. The reference voltage signals generated by the control algorithm, which contain rich compensation components, must ultimately be converted by the modulation module into insulated-gate drive signals. In a three-phase four-wire four-leg topology, four independent bridge legs, namely the three phase legs plus the neutral leg, provide *2^4 = 16* deterministic switching states. These include two zero-vector states, *V_0(0000)* and *V_15(1111)*, as well as fourteen nonzero active vectors. The two-dimensional hexagonal vector plane of a conventional three-leg PCS can no longer describe the zero-sequence voltage dimension introduced by the fourth leg. In the mathematical space of a four-leg converter, if the reference point is set as the AC neutral point, the space vector is projected and mapped into a three-dimensional dodecahedral volume formed by two cubes joined at a vertex.

To convert the continuous reference vector *s(v_α, v_β, v_γ)* in three-dimensional space into pulse-width duty ratios for the four bridge legs, the DSP must perform intensive real-time spatial-geometry computation. The core process can be summarized in three steps:

- Tetrahedron Determination: The entire dodecahedral space is geometrically partitioned into 24 non-overlapping tetrahedra. The system first uses the coordinate values of the reference vector, together with defined polarity judgment functions, such as intermediate variables calculated from polarity, and six decision boundary values, to rapidly identify the specific tetrahedron in which the target reference vector lies.
- Duty Ratios Calculation: Once the tetrahedron is identified, the three specific nonzero vertex vectors surrounding the reference vector, *V_adjx*, *V_adjy*, and *V_adjz*, together with the zero vector, are determined. Based on the volt-second balance principle, the system uses inverse-matrix operations to project the reference vector *s* onto these three adjacent basis vectors. The resulting projection scalars are the corresponding vector action times, *Proj(V_adjxs), Proj(V_adjys), Proj(V_adjzs)*. In this process, to ensure precise control of the neutral-point current, a compensation duty-ratio control equation for the zero-sequence voltage must be introduced. For example, by imposing the constraint *d_zx = -d_1x + d_3x + 2*, the zero-

sequence voltage difference $\Delta d_{zx}$ is calculated and used to regulate the dynamic output of the fourth leg.

- Switching Sequence Generation: To minimize high-frequency switching losses and reduce common-mode electromagnetic interference (EMI), after the action times are obtained, a carefully designed seven-segment or five-segment symmetric switching sequence, such as a sequence arrangement based on mirror symmetry, is adopted. This ordering ensures that only one bridge leg changes state at each switching transition and that the switching states are symmetrically distributed around the center of each PWM period.

With high-clock-frequency microprocessor architectures and this fast computational mechanism that avoids large look-up tables, advanced four-leg inverters can run the closed-loop algorithms described above, with high-order harmonic compensation capability, at very high control-loop frequencies. Test data confirm that, using this hardware and control system, an off-grid inverter can tightly control output-voltage THD at an extremely low level of 0.77% under highly nonlinear rectifier loads, while strictly maintaining phase-voltage unbalance within 1%, thereby fully overcoming the power-quality problems caused by nonlinear loads.

## 3.1.6.4 Physical impact mechanism by which oscillatory power ripple introduced on the PCS DC side under off-grid conditions affects the front-end DC-DC stage, MPPT, and battery

During off-grid microgrid operation, even if the converter output uses perfectly symmetrical three-phase four-leg hardware, severe instantaneous pulsating power at twice the grid fundamental frequency, i.e., 100Hz or 120Hz, ($p_{2\omega}$) will be generated as long as the load side of the microgrid includes single-phase high-power nonlinear loads, such as the starting of a single-phase AC motor, or severe three-phase load unbalance occurs. If the converter lacks deep system-level decoupling intervention, this destructive low-frequency pulsating energy will inevitably pass through the inverter stage and penetrate into the system DC-link, causing severe low-frequency voltage and current ripple with a sinusoidal envelope on the DC side. For a typical deeply integrated PV-storage BESS, this low-frequency ripple constitutes a dual critical threat to the physicochemical lifetime of lithium-ion batteries and the maximum power point tracking (MPPT) accuracy of the front-end PV DC-DC converter.

1. **Physical impact mechanism of low-frequency ripple on electrochemical degradation and heat accumulation in lithium-ion batteries**

From a conventional macroscopic monitoring perspective, the constant-current constant-voltage (CC-CV) charging profile applied to a BESS by the battery management system (BMS) appears stable. However, at the microscopic electrochemical level, 100Hz/120Hz low-frequency AC ripple superimposed on the DC current, with amplitudes of tens or even hundreds of amperes, forces lithium-ion batteries to undergo extremely high-frequency charge-discharge microcycles within milliseconds. Frontier experiments and failure analyses have clearly revealed three major physical and electrochemical degradation pathways induced by low-frequency ripple. First is the irreversible loss of lithium inventory (LLI). Current peaks from low-frequency pulsation cause severe local potential fluctuations at electrode interfaces, accelerating abnormal continuous growth of the solid electrolyte interphase (SEI) on the graphite anode surface and the cathode electrolyte interphase (CEI). Large amounts of active lithium ions are permanently trapped in the thickened passivation layers, accelerating absolute capacity fade. Second is structural collapse of active material, or loss of active material (LAM). Alternating high-current ripple implies extremely high rates of lithium-ion intercalation and deintercalation within the electrode lattice. This periodic imbalance accumulates large mechanical stresses inside electrode particles, eventually causing particle cracking,

transition-metal dissolution, and catastrophic lithium plating. Meanwhile, binder decomposition and electrolyte drying can sharply reduce whole-cell conductivity, known as conductivity loss (CL). Finally, low-frequency ripple introduces additional thermal effects. When the AC component flows through the ohmic and polarization resistances inside the battery, it generates Joule heat proportional to the square of the RMS ripple current (*I_rms^2 R*). In experiments involving high-current discharge superimposed with high-amplitude ripple, excessive heat generation converts more electrochemical transfer energy into thermal energy. This not only significantly reduces usable discharge capacity but also directly increases the baseline risk of battery thermal runaway. It is particularly noteworthy that physicists have recently confirmed the substantive structural changes caused by this alternating current inside batteries using ultrasonic nondestructive testing. By transmitting 5MHz longitudinal waves into pouch cells and observing second harmonic generation (SHG), researchers found a strong correlation between nonlinear acoustic parameters, which represent internal material stress and interfacial density, and battery charge-discharge cycling. This technique for detecting SoC using second harmonics indirectly confirms that second harmonics in the electromagnetic domain, such as 120Hz ripple, are likewise causing real and long-term accumulation of physical disturbances at solid-liquid interfaces inside the battery.

### 2. Interference attenuation model for the impact of 120Hz low-frequency ripple on MPPT tracking efficiency in PV DC-DC converters

For microgrid systems using a PV-storage DC-coupled architecture, the front-end PV panel DC-DC converter and the energy storage converter share the same DC bus. When unsuppressed 100Hz or 120Hz voltage ripple exists on the DC bus, this fluctuation directly modulates the output terminals of the PV array through reverse penetration, causing catastrophic losses in energy capture efficiency. From a mathematical modeling perspective, when the inverter attempts to inject steady-state AC power into the grid while encountering unbalanced loads, the current *u_I* drawn by its control algorithm from the DC capacitor will inevitably contain a large-amplitude 120Hz oscillatory component:

$$u_I = \hat{u}_I \ (1 + \sin(120 \times 2\pi \ t))$$

Because the DC-side LC low-pass filter network cannot provide infinite inductive and capacitive reactance, this large ripple fluctuation is ultimately transmitted to the PV array port, causing the actual output current *I* of the PV array to exhibit approximately 3% or higher low-frequency ripple oscillation:

$$I \approx \hat{u}_I \ (1 + 0.03 \ \sin(120 \times 2\pi \ t + \varphi))$$

Because the characteristic power-voltage (P-V) curve of a PV array exhibits a very steep nonlinear parabolic profile, even slight low-frequency jitter in terminal voltage or terminal current causes the actual operating point to swing over a wide range at high frequency on both sides of the theoretical maximum power point (MPP). Current MPPT optimization algorithms widely used in industry, such as perturb and observe (P&O) or conventional incremental conductance (Inc & Cond), are mainly based on steady-state hill-climbing models with discrete time steps. When the sampling frequency experiences aliasing or beat-frequency interference with this dynamic ripple as high as 120Hz, the optimization algorithm may infer the wrong gradient direction. As a result, the controller not only fails to lock onto the true maximum power point but instead falls into continuous misadjustment, significantly degrading overall photovoltaic conversion efficiency, i.e., MPPT efficiency. Relevant experimental quantitative data show that when 120Hz ripple caused by single-phase inverter loads exceeds the critical tolerance of the system, the energy conversion efficiency of the entire PV generation system can collapse abruptly and cannot recover by itself. Although academia has attempted to use software-based methods such as ripple correlation control (RCC) or extremum seeking control (ES) to exploit the gradient information in these ripples for passive adaptive correction, their high computational requirements and sensitivity to operating conditions make eliminating these ripples at the hardware source the most fundamental solution.

### 3. A complete hardware-based remedy: active power decoupling (APD)

To block the destructive impact of the above pulsating energy on the battery and MPPT at the source, industry has abandoned passive decoupling methods that rely solely on adding large electrolytic capacitors in volume-constrained applications, and has fully shifted toward more advanced active power decoupling (APD). In an advanced three-phase four-wire four-leg buck inverter architecture, the system contains four mutually independent DC-DC buck converters, corresponding to three phase legs and one neutral leg. When facing second-order power ripple caused by unbalanced loads, the converter uses an active feedforward algorithm to control the output voltage of each buck converter, forcing the excess double-frequency pulsating energy to be absorbed and stored in the existing AC-side filter capacitor matrix, while completely preventing it from rebounding into the DC bus. The core mathematical decoupling mechanism is highly elegant: after measuring the DC-bus feedback, the control system uses a dedicated resonant controller to generate a decoupling voltage signal *v_de* whose frequency exactly corresponds to twice the fundamental frequency:

$$v_{de} = V_{de} \sin(2\omega t + \theta_{de})$$

The system superimposes this virtual decoupling voltage equally and in phase onto the control reference voltages of the three phase legs (*v_Ca, v_Cb, v_Cc*) and the fourth neutral leg (*v_Cn*) of the four-leg inverter. Because the microgrid load ultimately experiences the line-to-neutral differential-mode voltage, namely the phase voltage *v_an = v_Ca - v_Cn*, the commonly injected decoupling voltage component *v_de* is completely cancelled in this mathematical subtraction process, i.e., the zero-sequence cancellation effect. This advanced hardware-algorithm integrated control strategy provides two decisive advantages. On the one hand, the AC supply waveform delivered to the three-phase load remains an undisturbed, perfectly symmetrical sine wave. On the other hand, the harmful double-frequency ripple energy is ingeniously isolated by the presence of the decoupling voltage and fully absorbed by the energy storage elements inside each bridge leg. With active power decoupling, the system requires no additional decoupling switching devices, compresses the required total DC capacitance to an extremely low level, greatly extends the cycle life and power density of the entire BESS, and allows the front-end PV MPPT to always operate on an exceptionally clean DC bus at maximum efficiency.

## 3.1.6.5 Third-generation power semiconductors: generational advantages of silicon carbide (SiC) MOSFETs in three-phase four-leg converters

Because three-phase four-leg converters (3P4L) involve denser semiconductor bridge legs as well as computationally complex high-frequency 3D-SVPWM modulation and multiple active decoupling algorithms, conventional hardware implementations based on silicon (Si) insulated-gate bipolar transistors (IGBTs) and their associated freewheeling diodes have reached the ceiling imposed by material physics. Accordingly, global semiconductor leaders such as Infineon have strongly recommended, based on rigorous experiments and quantitative analyses, the full application of silicon carbide (SiC) MOSFET technology in multi-leg inverters for off-grid and microgrid scenarios. This represents the irreversible ultimate evolutionary direction of modern power-electronics architectures.

**1.** Material properties drive a sharp increase in switching frequency and extreme downsizing of passive filter networks. Compared with conventional silicon, silicon carbide has three times the bandgap, three times the thermal conductivity, up to ten times the critical breakdown electric field strength, and more than twice the electron saturation drift velocity. For silicon IGBTs, which are bipolar devices, a tail current inevitably arises during turn-off because of slow minority-carrier recombination. This effect causes large

dynamic turn-off losses and therefore tightly constrains their switching frequency in high-power applications below the 10kHz to 20kHz bottleneck. However, three-phase four-leg PCSs, especially when running the aforementioned harmonic PR compensation and high-frequency active decoupling algorithms, urgently need to exceed this frequency limit. As a majority-carrier device, the SiC MOSFET not only eliminates turn-off tailing in principle, but its body diode also has extremely low reverse-recovery charge, with *Q_rr* nearly negligible, enabling very sharp high-speed commutation. Data show that under extreme high-temperature operating conditions of 150℃, the turn-on energy (*E_on*) of a 1200V-class SiC MOSFET can be reduced by an impressive 76% compared with an IGBT of the same rating. This ability to reduce dynamic losses by an order of magnitude allows SiC devices to easily break through conventional limits while maintaining very high overall system efficiency, generally above 99%, and to achieve ultra-high switching-frequency operation of hundreds of kilohertz, such as 400kHz or 500kHz, in megawatt-scale equipment. This geometric increase in switching frequency directly changes the engineering paradigm of converter hardware systems. High-frequency switching pushes the output PWM carrier ripple into a very high-frequency range far from the fundamental frequency. According to the physical relationship between the corner frequency of an LC low-pass filter and the product of inductance and capacitance, the required magnetic material for filter inductors and the volume of AC filter capacitors can be reduced by 50% or even more. This has revolutionary significance for reducing weight and cost in containerized energy storage systems and commercial and industrial rack-mounted integrated off-grid BESS solutions, where space utilization and power density are stringent requirements.

2. Substantial reduction of dead time and root-cause mitigation of native waveform distortion (THD). In any semiconductor bridge-leg structure, to prevent destructive shoot-through short circuits caused by simultaneous conduction of the upper and lower devices due to switching-command delays, the control system must forcibly insert dead time (Dead-Time, *t_d*) between complementary PWM signals. In IGBT systems, dead time usually needs to be set at the microsecond (*mu s*) level to cover the long turn-off tail. This nonlinear dead time is one of the primary root causes of inverter output-voltage fundamental drop and the introduction of substantial low-order harmonic current distortion. In the SiC MOSFET system, because the device response is extremely fast, switching delay and transition time are greatly shortened, allowing the system dead time to be safely compressed to the several-hundred-nanosecond (*ns*) level. The latest analytical models verify that reducing dead time by orders of magnitude substantially corrects the nonlinear deviation of the output phase voltage at the source. Therefore, even before complex multi-resonant compensation algorithms are enabled, the native open-loop output current THD of an all-SiC four-leg inverter already exhibits performance far superior to that of IGBT systems.

3. Revival of the two-level architecture: simplifying complexity and surpassing three-level topologies across classes. When IGBTs are used to build large 3P4L four-leg PCSs that meet strict grid-connected or off-grid harmonic requirements, such as THD strictly below 3% to 5%, engineers are often forced to abandon simple two-level topologies and adopt complex multilevel topologies, such as three-level active neutral-point-clamped (3L-ANPC) topologies or flying-capacitor multilevel schemes, or bulky multiplexed interleaved parallel techniques, to compensate for the weakness of low switching frequency and insufficient harmonic filtering. This directly doubles the number of semiconductor switching devices, sharply increases the number of gate-drive isolation transformers, and substantially raises the failure rate of the overall hardware system. However, with the high-frequency wide-band characteristics of SiC, the traditional system-architecture concept is completely overturned. Infineon’s research and quantitative simulations show that by using only the simplest and most robust conventional two-level (2-Level) three-phase four-leg topology, with four sets of SiC high-frequency half-bridge modules replacing the multilevel array that previously required eight sets of silicon superjunction or IGBT devices, efficiency and current-harmonic control performance can already match or even exceed those of complex silicon-based three-

level solutions, with output phase-current THD maintained at an excellent level below 4.83%. This architectural “revival” delivers remarkable engineering benefits for four-leg converters: the control strategy becomes simple again, the component count falls sharply by 50%, and the system MTBF (mean time between failures) is multiplied.

4. Advanced packaging and thermal management to counter high-frequency *dv/dt* parasitic effects. It is undeniable that the extremely fast high-voltage turn-on and turn-off speeds of SiC devices generate very high voltage slew rates (*dv/dt*). These can readily excite severe high-frequency resonance with parasitic stray inductance inside conventional power-module packages, producing overvoltage spikes that threaten insulation safety. This often forces designers to increase gate resistance artificially to slow switching speed, thereby wasting the efficiency advantages of SiC. To address this contradiction, modern SiC discrete modules designed specifically for compact inverters such as four-leg matrices adopt disruptive top-side cooled (TSC) packaging and high-thermal-conductivity aluminum nitride (AlN) ceramic substrates without baseplates. By moving the heat-generating interface to the top of the device for direct cooling, the electrical insulation loop and the thermal network are perfectly decoupled. This innovative three-dimensional packaging structure allows the main commutation loop in the PCB layers to be brought much closer together, reducing commutation-loop parasitic stray inductance by a full factor of three compared with conventional through-hole or bottom-cooled devices. This completely clears the parasitic-parameter barrier for the extreme high-frequency safe operation of SiC MOSFETs, ensuring that the converter can maintain peak full-power output even in harsh outdoor enclosure environments at 55℃ without any derating.

## 3.1.6.6 Comprehensive evolution path for the core hardware solution: full adoption of integrated solutions based on SiC three-phase four-leg PCS

Based on the preceding coherent theoretical derivation concerning neutral-point drift suppression, decoupling of DC low-frequency ripple to protect lithium batteries, elimination of high-order harmonics, and the performance leap enabled by wide-bandgap semiconductors, the full deployment of “three-phase four-leg” bidirectional PCS integrated energy storage cabinet solutions based on SiC high-frequency wide-bandgap devices has become a core solution for industrial microgrids over the past two years, targeting current and future microgrid and commercial and industrial energy storage applications.

The technical closed loop and core value proposition of the ultimate integrated solution are reflected in the following four strategic dimensions:

Native neutral-conductor construction and an extreme weight-reduction and safety strategy through electrical transformer elimination. Leveraging the native neutral-conductor load-support capability provided by the fourth high-frequency leg and the asymmetrical zero-sequence current return-control mechanism, this integrated solution completely eliminates the expensive, lossy, and bulky power-frequency isolation transformer network that previously had to be connected in series at the output. More importantly, in combination with an advanced microgrid control cabinet system, the solution integrates a highly reliable intelligent static transfer switch (STS module) and an automatically programmable N-PE neutral-earth bonding relay. This means that at the moment a grid outage occurs, the integrated system can seamlessly enter off-grid grid-forming mode within milliseconds while maintaining uninterrupted load supply, and can simultaneously establish a safe local system reference-ground potential by closing the grounding relay. This completely eliminates electric-shock hazards caused by floating grounds during islanded operation, prevents false RCD tripping caused by multi-point grounding, and establishes an absolutely safe protection network for precision loads in highly unstable grid regions.

Extreme protection of the full battery life cycle through active capacitive decoupling. Using the powerful control-dimensional space provided by the four-leg topology and the built-in active power decoupling technology, the system can intercept and fully absorb the large and harmful double-frequency power pulsation ($p\_2\omega$) generated by single-phase unbalanced or nonlinear loads at the hardware filter-matrix level, cutting off its reverse-injection path into the DC bus at the source. The DC-bus voltage achieves unprecedented smoothness and no longer requires massive arrays of vulnerable aluminum electrolytic capacitors. This technology not only greatly simplifies the internal cabinet structure, but more strategically, it completely prevents 100Hz/120Hz low-frequency charge-discharge microcycles from continuously causing mechanical stripping and electrochemical corrosion of the SEI interface and cathode materials inside lithium cells. In combination with frontier energy storage media such as semi-solid-state batteries, the PCS provides a bottom-level physical protection mechanism that directly enables an expected ultra-long cycle life of up to 100,000 hours or more for the entire energy storage station.

Advanced vector-space optimization and deep coordinated release in PV-storage coupled environments. By eliminating the split midpoint capacitor directly connected to the bus, the microprocessor gains complete freedom to dispatch all four bridge legs throughout the three-dimensional polyhedral space. This enables full-power operation of the 3D-SVPWM modulation algorithm and increases the DC-bus voltage utilization limit by 15%. Together with the wide high-voltage safe operating area of silicon carbide (SiC) modules, the PCS host can provide broad and flexible adaptability from low-voltage 208V to high-voltage 480V and even higher voltages. As a result, the BESS can not only be installed in outdoor standardized non-walk-in microgrid cabinets with a smaller footprint, but also achieve truly modular redundant hot-swap design, with MTTR approaching zero. In more complex hybrid AC/DC microgrids, the exceptionally clean low-frequency-ripple-free DC-bus environment enables independent PV DC-DC converters connected to the same bus to free their MPPT controllers from beat-frequency mis-tracking, ensuring that perturbation tracking performance remains at peak output without loss or attenuation.

Flexible microgrid reconfiguration and active grid-supporting grid-forming virtual synchronous characteristics. Supported by the very high switching frequency of silicon carbide and the powerful computational capability of broadband proportional-resonant plus repetitive control (PR+RC), the SiC four-leg integrated system can suppress all high-order harmonic disturbances with extremely high response speed. Even when the load side consists of harsh three-phase full-bridge high-capacity uncontrolled rectifier systems, the output supply-voltage quality, measured by THD, can reach instrument-grade precision, stably below 1%. Products represented by modular converters in the tens to hundreds of kilowatts range from companies such as NEGO, Sineng, and Sungrow, including the MR33 series and PWS1 series, have further elevated this hardware platform to the active-control level. When deeply integrated with virtual synchronous generator (VSG) algorithms and advanced grid-forming (GFM) control strategies, the integrated system is no longer merely a black-box actuator for passive charging and discharging. Instead, it evolves into a higher-order dynamic power-quality management hub with synthetic inertia, strong microgrid black start capability, and adaptive compensation for grid impedance.

In summary, the deep integration of the three-phase four-leg hardware architecture with the new materials science of silicon carbide (SiC) has moved beyond the scope of upgrading a single converter device and has formed a complete paradigm shift that comprehensively addresses the chronic hardware limitations of traditional microgrids. This integrated system, which achieves extraordinary advances simultaneously across volume, efficiency, waveform quality, grid safety, and battery lifetime, unquestionably establishes its industrial position as an indispensable core hub for global distributed off-grid energy systems over the next decade.

## 3.2 Different microgrid solutions

## 3.2.1 AC bus solution (AC-coupled microgrid solution)

**Advantages of the AC bus solution**

- Decoupled design and strong compatibility: Energy storage and PV are integrated on the AC side, and the systems remain relatively independent. This greatly facilitates retrofitting energy storage to existing standard PV plants and upgrading them into microgrids.
- Strong load-carrying and grid-forming capability: The energy storage system can serve as an independent AC main power source for microgrid grid-forming, providing stable voltage and frequency support for downstream AC loads.

**Pressure points of the AC solution**

- Sizing and load-carrying limits: The installed-capacity ratio of PV to energy storage is subject to strict constraints, such as a maximum PV-storage ratio of 1:1 or 2:1, so PV capacity cannot be expanded without limit. There are also strict requirements on load types. Nonlinear loads, unbalanced loads, and directly started motor loads must be substantially derated according to ratio to prevent inrush current from causing microgrid collapse.
- Transformer dependence: The energy storage side must be equipped with an AC isolation transformer that meets the required specifications, such as Dyn11 and 1.1 times long-term operation, increasing line losses and space occupation.

**Main module composition**

- AC generation side, including PV modules and inverters; AC energy storage side, including battery clusters and AC converters with grid-forming capability; AC parallel distribution node; AC isolation transformer; and AC electrical loads.

3.2.1.1 Interrupted-transition solution

### Interrupted-transition solution (manual/automatic interrupted grid-connected/islanded transition solution)

Interrupted transition is essentially “break-before-make” and is the most basic but also the most robust operating mode for a microgrid. Its design philosophy prioritizes grid safety over load continuity.

**1) Advantages of this solution**

- Lower cost and simple configuration: The response speed and accuracy requirements for distribution equipment are relatively low, and extremely high-precision high-speed relay protection devices are not required.
- Flexible control modes: Supports “no control” for convenient maintenance, “manual interrupted transition,” and “automatic interrupted transition,” allowing O&M personnel to determine the transition timing based on utility-grid conditions.

**2) Pressure points of this solution**

- Power supply interruption exists: During the transition between grid-connected and islanded operation, the system experiences a power outage. The outage duration includes the mechanical opening time of the grid-connected/islanded switch and the time required for the energy storage AC system to re-establish power.
- High dependence on auxiliary power: To ensure that controllers and other core equipment do not drop offline during the transition outage, the system must be additionally equipped with a UPS that provides a required backup-power duration.

**3) Main module composition**

- Energy storage system, including battery units and energy storage converter/PCS; PV inverter system; microgrid controller or data collector; distribution equipment, including a conventional grid-connected/islanded switch and loss-of-voltage detection circuit; isolation transformer; insulation monitoring device (IMD); meter at the point of common coupling; and UPS.

**4) Topology description**

- The energy storage system and PV system are coupled, i.e., paralleled, on the AC side through an isolation transformer. The microgrid system side is connected to the main grid through a conventional grid-connected/islanded switch. The system uses an independent “loss-of-voltage detection circuit” to feed grid status as a signal back to the microgrid controller, which issues commands to drive switch opening and closing and coordinates the energy storage system for grid-forming in islanded mode or grid-connected output.

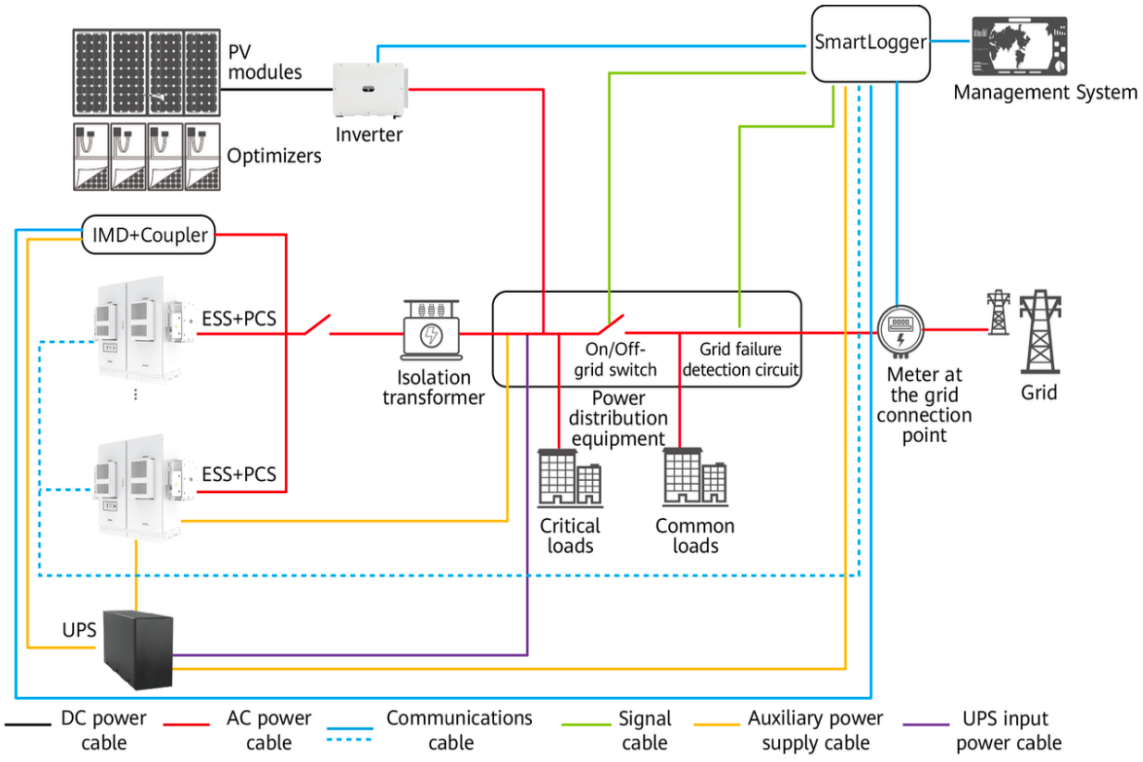


Image source: HUAWEI LUNA2000-(97KWH-200KWH) Series Commercial and Industrial Grid Forming ESS Solution User Manual (Microgrid, SmartLogger3000).pdf

In this mode, the energy storage converter (PCS) and PV inverter strictly follow grid-following (GFL) logic during grid-connected operation. That is, they operate as current sources and follow the grid voltage and frequency through a phase-locked loop (PLL).

1. **Grid-Connected operating state:**
   - The PCS operates in PQ mode, i.e., active/reactive power control, and controls current injection according to dispatch commands issued by the EMS, such as peak shaving and valley filling.
   - The PCC circuit breaker is closed.
2. **Fault detection and tripping (Fault & Trip):**
   - When abnormal grid voltage (ANSI 27/59) or abnormal frequency (ANSI 81) is detected, the anti-islanding protection logic is triggered.
   - A device similar to the Woodward LS-6 XT P1 grid-connected/islanded controller, or a relay protection device, immediately opens the PCC intelligent circuit breaker.
   - The PCS and PV inverter stop output, and the system enters a blackout state. At this point, the microgrid bus is de-energized.
3. **Off-grid black start (Black Start):**
   - The controller monitors the PCC status to confirm that it is open and checks that residual bus voltage has decayed to a safe threshold.
   - The controller sends an "islanded mode" command to the PCS, and the PCS control law switches from current-source operation to voltage-source operation (V/f control).

   The PCS establishes voltage and frequency references, such as 400V/50Hz. After detecting a stable voltage, the PV inverter reconnects and resumes generation.

**5) Applicable scenarios**

- Mainly applicable to commercial and industrial parks where grid capacity is insufficient, capacity expansion is difficult, and power curtailment occurs during peak demand periods, provided that the loads in the park are not sensitive to short-duration outages or interruptions.

---

## AC seamless solution (seamless grid-connected/islanded transition solution)

**1) Advantages of this solution**

- High power-supply continuity: Enables very fast grid-connected/islanded transitions, for example with transition time as low as approximately 150ms under full-time VSG mode, ensuring uninterrupted power supply to loads.
- Comprehensive automation and protection mechanisms: Can coordinate with high-speed relay protection devices to acquire voltage and frequency in real time. When the grid becomes abnormal, it can rapidly trigger unplanned seamless disconnection to islanded operation to protect microgrid loads.

**2) Pressure points of this solution**

- Stringent hardware performance requirements: Dedicated relay protection devices must be installed. Grid outage detection time must be <40ms, and highly accurate synchronism-check closing control must be supported, with phase-angle difference ≤2° and magnitude difference <5%.
- PV inverters are grid-following, making it difficult to ensure uninterrupted operation during the transition, especially across products from different brands.
- There are many conflicts among PV inverter transition, relay protection, and STS+PCS transition.
- There are too many constraints on using PV to supply energy storage, and many black-start issues arise.
- Auxiliary power such as UPS is required.
- Overall efficiency is lower than that of the DC solution.

**3) Main module composition**

- Grid-forming energy storage system, PV inverter system, microgrid controller, isolation transformer, insulation monitoring device (IMD), high-speed grid-connected/islanded switch STS, and high-precision relay protection device. In some scenarios, an automatic transfer switch (ATS) and backup diesel generator may be integrated as needed.

**4) Topology description**

- Energy storage and PV are likewise coupled on the AC side through an isolation transformer. The difference is that the microgrid and the main grid are controlled through a relay protection device. The relay protection device directly samples the voltages on both sides of the switch in real time through potential transformers (PTs), independently performs high-speed opening and closing control, and interfaces with the microgrid controller through communication protocols such as Modbus to achieve coordinated seamless transition at the underlying hardware level.

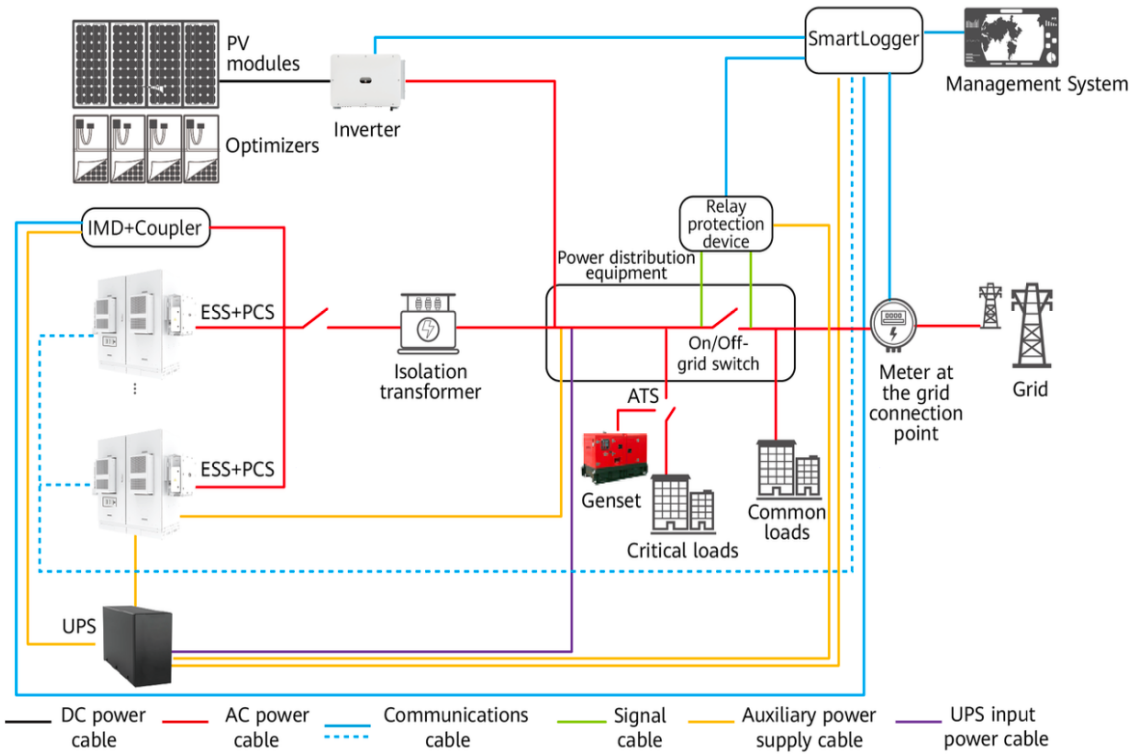

Image source: HUAWEI LUNA2000-(97KWH-200KWH) Series Commercial and Industrial Grid Forming ESS Solution User Manual (Microgrid, SmartLogger3000).pdf

**5) Applicable scenarios**

- Also applicable to commercial and industrial parks facing power curtailment and insufficient grid capacity, but especially suited to applications with critical loads, such as key production lines, precision instruments, and data servers, where power interruption is strictly prohibited or would cause severe economic losses.

## 3.2.2 DC bus solution

**From the perspective of system benefits:**

- Because the number of system components is reduced, future system hardware costs will decrease significantly. At present, DC/DC converters are temporarily less cost-effective because of scale limitations.
- Reduces multiple "DC-AC-DC" power conversion stages and associated energy losses, improving efficiency by about 5%.
- Overall engineering copper usage is reduced by 30% to 40%.
- Full-load duration is optimized.
- The system changes from rigid to flexible, making it better able to cope with fluctuations inside and outside the microgrid.

**Compared with AC-coupled solutions, DC-coupled technology can better achieve the following:**

- PV can always charge the battery and still operate well under low-light conditions, making it suitable for rainy Southeast Asia and low-irradiance Northern Europe.
- PV fluctuations are attenuated on the DC side, and the overall PCS efficiency can always be maintained at the optimal power point, resulting in higher lifetime and efficiency.
- System simplification and decoupling: The PV system is connected to the power router through a DC/DC port, achieving independent decoupling in control logic.
- Solves STS-to-PCS connection, parallel operation, and reliability issues: this can be effectively achieved through a DC cabinet and an AC electrical prefabricated cabin solution.
- Meets fire-safety compliance requirements: safety regulations do not allow lithium batteries in indoor electrical distribution rooms of engineering buildings.
- Improves the success rate of smooth grid-connected/islanded transitions: compared with the AC solution, power-supply stability is higher.
- Improves overall power quality: Compared with direct inverter AC coupling, the DC/DC conversion process does not involve grid-frequency synchronization and can significantly reduce harmonics injected into the grid.
- Flexible multi-source access: Supports both AC and DC input and output, enables flexible integration of distributed PV, energy storage batteries, and EV chargers, and will make it easier to integrate DC fast chargers, support flexible-load capability, and implement V2G in the overall solution.

**Classification by topology:**

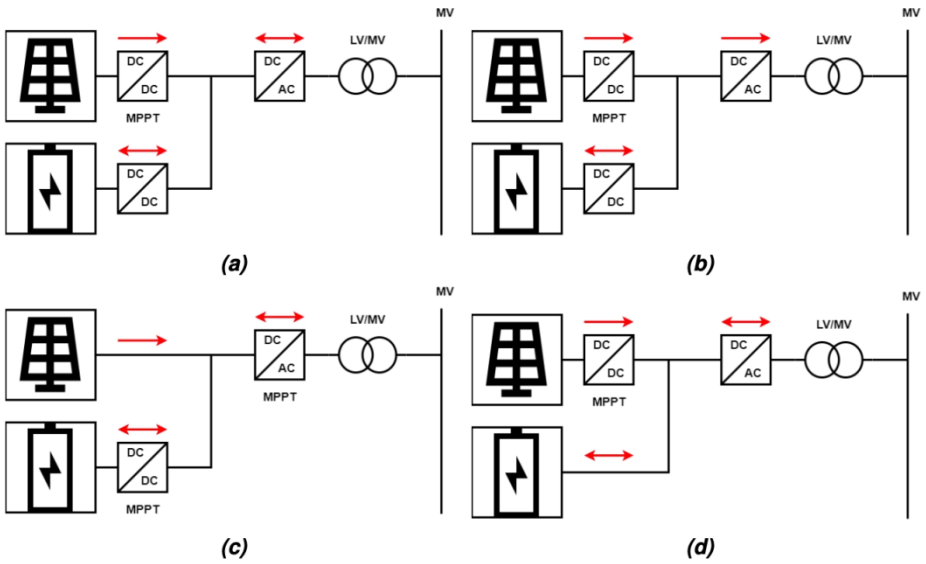


Image source: TECHNICAL AND COMMERCIAL COMPARISON OF AC- AND DC-COUPLED BATTERY ENERGY STORAGE SYSTEMS

| Evaluation metric | Loosely DC-coupled | Tightly DC-coupled | BESS-side DC-coupled |
|---|---|---|---|
| Primary energy | PV + bidirectional grid | PV only | PV + grid (physical isolation) |
| Grid arbitrage capability | Excellent (captures negative prices) | None (prevents grid charging) | High (depends on control software) |
| Subsystem sizing | High ILR/high BIR | Extreme ILR/medium-to-low BIR | Highly flexible/decoupled sizing |
| Capital expenditure (CapEx) | Moderate (shared hardware efficiency) | Lowest (minimum compliance/hardware requirements) | Highest level (requires discrete DC/DC circuits) |
| Regulatory and subsidy alignment | Moderate (complex REC auditing) | Excellent (natively compliant with ITC standards) | Moderate to excellent (software-defined) |
| DC-bus overvoltage risk | Moderate | Critical (requires sub-millisecond response) | Low (converter provides buffering) |
| PCS/BMS interdependence | High (dynamic load balancing) | Extreme case (BMS determines MPPT limits) | Low (hierarchical, decoupled control) |

## a. Loosely DC-coupled solution

This loosely DC-coupled architecture is the default standard for flexible modern hybrid systems after electricity market liberalization. In this topology, the PV array and energy storage system are co-located, share a central bidirectional inverter, and connect to the grid through a single point of common coupling (PCC). The main feature of a loosely coupled system is its bidirectional energy-routing capability: the battery can be charged either from the co-located PV array or from the external grid.

## b. Tightly DC-coupled solution

The tightly DC-coupled architecture is physically similar to a loosely coupled system: both connect the battery energy storage system (BESS) to the DC side of the PV inverter. However, a tightly coupled system is strictly constrained through hardware interlocks or permanent control software to ensure that the energy stored in the battery comes entirely from the co-located PV array. Grid charging is strictly prohibited.

Because the battery relies entirely on solar irradiance for charging, a tightly coupled system requires a very high inverter loading ratio. The PV array capacity must be sufficiently large, typically with an inverter loading ratio above 2.0, because strict charging restrictions create a phenomenon known as “loss of arbitrage value.” If the battery energy storage system (BESS) is depleted after nighttime discharge and the following day is cloudy, the battery will remain idle. The system is prone to energy underutilization and has poor cost-effectiveness.

At present, except under policy-driven factors, pure green-electricity requirements, and extremely constrained grid capacity, this mode is rarely adopted in commercial solutions.

## c. BESS-side DC-coupled solution

The BESS-side DC-coupled architecture represents a standard DC-coupled topology designed to introduce electrical isolation and modularity into the DC link. In this configuration, the solar PV array and the main DC/AC inverter share a main DC bus. However, the battery pack is not directly paralleled onto this high-voltage bus; instead, a dedicated bidirectional DC/DC converter is inserted between the energy storage system and the main DC link. This isolation mechanism facilitates the integration of different battery technologies. Operators can regulate the unique voltage profile of each battery through an independent DC/DC converter before merging them into the common PV bus, thereby safely paralleling lithium iron phosphate (LFP) battery packs with retired second-life EV battery packs and even sodium-ion energy storage modules.

Because the PV side has no MPPT solution, the overall PV sizing ratio and utilization rate are not high. It is generally upgraded to a loosely DC-coupled solution or a reverse (PV) DC-coupled solution.

## d. Reverse (PV) DC-coupled solution: the optimal solution for small commercial and industrial microgrids

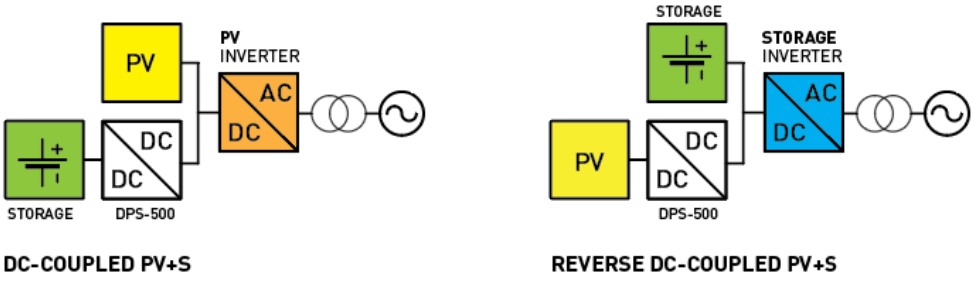


In a reverse DC-coupled topology, the battery energy storage system is directly connected to the main DC bus without an intermediate conversion stage. Although this approach eliminates the local DC-DC conversion stage for the battery and improves overall system efficiency, it also imposes strict constraints on the rated voltage of the battery pack. The rated voltage of the battery pack must precisely match the high-voltage requirements of the centralized DC bus and the main AC inverter.

This direct connection increases the system's sensitivity to bus-voltage instability during rapid charge-discharge cycling. When the system transitions sharply from full output (discharge) to large-capacity grid charging, the DC bus experiences severe voltage fluctuations. If the states of charge (SOC) of different battery packs are unbalanced, direct connection to the bus will exacerbate voltage deviations and cause local overcurrent. Operational analysis of reverse DC-coupled systems shows that significant voltage differences during charge-to-discharge transitions slightly reduce system operating efficiency. In addition, strict electrical isolation must be implemented in the architecture to ensure system safety. To achieve seamless integration, the battery or PV panels must be electrically isolated from the rest of the system. Innovative components such as bidirectional isolated energy storage DC-DC optimizers and dynamic-voltage DC-DC optimizers rely on electrical isolation to protect PV panels from large fault currents originating from centralized battery packs. This is a key requirement for building safe microgrids and avoiding catastrophic electrical failures.

**Relevant subsystem sizing notes:**

Diesel generator and load sizing ratio: 1.2 to 1.3:1. Operation should preferably be maintained at the optimal fuel-specific power point of 75% to 80%. If configured at 1:1, the SOC should be reserved as much as possible and the diesel generator should be started early based on forecasts. The system should also be capable of shedding non-critical loads to support subsequent battery charging.

Maximum PV MPPT DC/DC sizing ratio: 2:1. The standard configuration is 1.6:1, and full PV configuration can ensure maximum consumption of green electricity.

The battery should be configured according to the required support duration: the battery voltage in the DC cabinet must match the maximum voltage limit of the PV DC/DC MPPT module; otherwise, it cannot be used.

The BMS must support a three-tier architecture. The PCS must interface directly with the BSU (Battery Stack Control Unit) to ensure normal battery charging.

Load configuration requirements:

1. The loads are conventional loads and do not include impact loads. (If impact loads are present, such as motor starting, it is recommended to use a variable frequency drive (VFD) starting method with built-in ramping.)

2. If nonlinear loads are present (such as high-power charging piles), the EMS must be capable of ramp control during loading and unloading to ensure overall system stability.

3. If no VFD is provided, the total capacity of impact loads should be less than 30% of the system rated power.

4. Peak load apparent power < 0.8*system rated power

STS configuration requirement: the STS should satisfy >PCS maximum power + maximum load power

**Advantages of this solution:**

- The reverse DC-coupled solution supports a high PV configuration ratio of 2.0 or even 3.0 or higher, without requiring separate PV inverters and energy storage inverters, thereby simplifying system design and reducing the initial capital cost of equipment procurement.

- The integrated installation process and reduced maintenance requirements further reduce deployment and installation costs.

- Similarly, reverse DC coupling can integrate an existing AC-coupled energy storage system with a new PV system, thereby minimizing the need for costly system replacement.

- In addition, the efficiency improvements enabled by these coupling methods can deliver long-term cost savings by maximizing green energy consumption.

**Key stress points of this solution:**

- The distributed configurable hardware modules in the reverse DC-coupled solution impose a heavier burden on the monitoring system. The overall energy management system must rapidly coordinate bidirectional inverter setpoints, monitor the health status of directly connected batteries, and actively broadcast voltage and current commands to distributed DC-DC converters. Communication latency between the central controller and remote converters can increase control instability, especially when the overall system attempts to provide instantaneous grid services such as fast frequency response (FFR).

- The overall solution places high requirements on the DCDC MPPT modules. If the self-control of the MPPT modules and the PMS control mechanism are not properly coordinated, severe DC bus overvoltage may occur.

- Although the reverse DC-coupled solution reduces total equipment cost, it acts like a rigid conduit that constrains the simultaneous dispatch of multiple assets. In an AC-coupled system, if the interconnection protocol allows reverse power flow, a 1MW solar array and a 520KW battery system can instantaneously deliver 1520KW of power to the grid. In a reverse DC-coupled system, the output of both devices is limited by the rated power of the shared central inverter PCS, namely 520KW.

This shared constraint introduces complex opportunity costs under optimal market conditions. If wholesale electricity prices surge during peak solar irradiance periods (an extreme case), the operator must determine mathematically whether it is more profitable to export solar generation directly to the grid, discharge stored battery energy, or perform a hybrid dispatch that complies with the inverter maximum

output limit. During peak solar generation hours, battery discharge is fundamentally constrained by the inverter capacity ceiling.

In a DC-coupled configuration, the battery can only charge from the solar system, and can offer service to ERCOT only by injecting energy through the solar inverters.

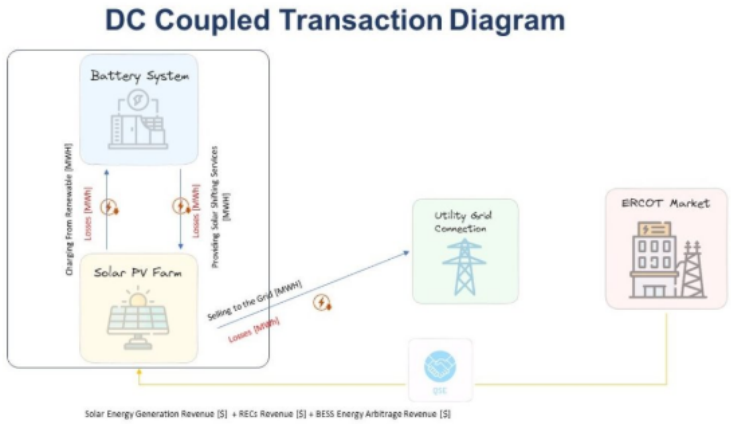


In a Reverse DC-coupled configuration, the solar energy is routed through the battery storage inverters meaning that the battery can charge from solar, and from the grid, and can offer Energy and Ancillary Services to ERCOT. In this configuration, the battery storage system can also charge from the co-located solar facility.

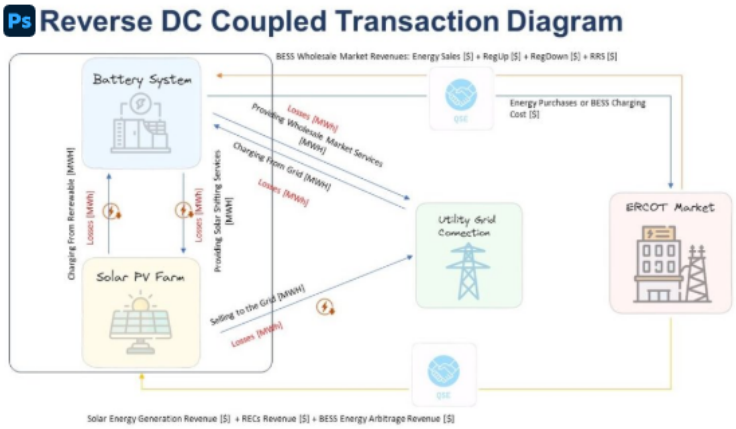


There are certain advantages and disadvantages to consider within these configurations related to their capabilities, costs, and control.

Form：https://acelerex.com/post/solar-storage-in-ercot---ac-vs-dc-coupling-connection-comparison

### Direct connection between PCS and BMS

The battery management system (BMS) should adopt a three-tier architecture consisting of the battery management unit (BMU), battery control unit (BCU), and battery service unit (BSU). The BMS provides functions including high-precision analog signal detection and reporting, fault alarms, data upload and storage, battery protection, parameter setting, passive balancing, battery SOC calibration, and information exchange with other equipment.

Through the battery module monitoring unit (BMU), battery string control unit (BCU), and battery stack control unit (BSU), the battery system can implement comprehensive battery information management, online SOC and SOH estimation, passive battery balancing management, fault diagnosis, and protection.

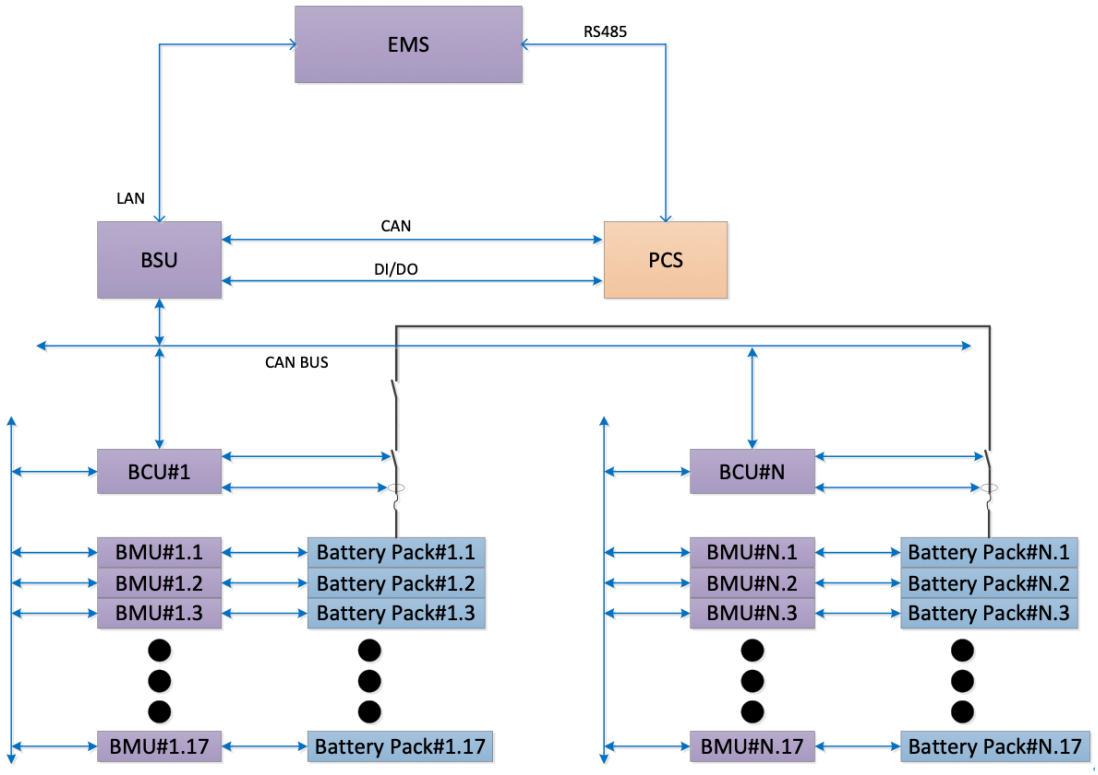


Communication architecture diagram of BMS

The third-level battery unit (BSU) is typically installed in the DC high-voltage box of the battery stack. It connects via CAN bus to the battery control units (BCUs) of all battery packs under the stack, collects all BCU data, including battery voltage, temperature, fault alarms, and other information, and analyzes these data to determine whether faults exist. Two communication methods are used between the BSU and the power conversion system (PCS): CAN bus and dry contacts. The CAN bus is used for routine information exchange, while dry contacts are used by the battery management system (BMS) to issue emergency shutdown commands to the main power management system (PMS) under emergency conditions.

### PV DC bus overvoltage issue

Because this solution over configures PV capacity, when the battery is nearly fully charged and nonlinear loads exist on the load side (such as unplugging a charging pile connector), DC bus overvoltage may occur under conditions such as the following:

- **Boost-mode configuration principle--open-circuit voltage at the PV installation extreme low temperature*number of PV modules in series<=minimum battery voltage (ZOE)**
- **Buck-mode configuration principle--maximum power operating voltage at the PV installation extreme high temperature>=maximum battery voltage**

1. **Load fluctuation stress**

   - Normal condition: at noon, PV generates 200kW. The load consumes 100kW, and the energy storage charges at full power of 100kW. The system is perfectly balanced, and the DC voltage remains stable at 750V.

   - Critical instant: a large motor in the factory suddenly stops, or a charging pile connector is

unplugged (100kW load rejection).

◦ Physical stress: PV is still outputting 200kW, but the charging capability of the energy storage has already reached its physical limit (100kW). The extra 100kW of pure surplus is instantaneously injected entirely into the DC bus capacitors of the inverter.

◦ Consequence: the capacitor voltage surges from 750V to above 900V or even 1000V within 10 milliseconds. To prevent the IGBT module from being directly punctured and destroyed by high voltage, the hardware protection circuit will immediately and uncompromisingly shut everything down (HW_OVP). The entire islanded system blacks out.

**2. MPPT operating condition (software-hardware time mismatch)**

The microgrid controller does not have droop control (f-P), causing PV curtailment to be too slow.

- Hidden pitfall: communication and the MGCC algorithm are too slow.
- Timeline: the DC capacitor can be charged to failure by 100kW in only 5~20 milliseconds. However, the full process in which the controller detects frequency/voltage abnormalities -> sends commands through the communication line -> the PV inverter exits maximum power point tracking (MPPT) and shifts the operating point takes at least 50~100 milliseconds even at its fastest.
- Conclusion: before PV has time to “brake,” the DC-side voltage has already exceeded its limit.

**3. BMS operating condition (battery fully charged/low-temperature charge rejection)**

◦ Assume the battery SoC reaches 95%, or the ambient temperature is too low in winter. To protect the cells, the BMS (battery management system) may suddenly limit the allowable charging power from 100kW to 10kW, or even directly open the DC contactor.

◦ In a 2:1 system, once this 100kW “buffer pool” closes, the large 200kW PV output will instantaneously drive the DC bus into overvoltage.

**Solution:**

Under an extreme ratio such as 2:1, relying only on software algorithms (EMS/microgrid controller) to suppress PV is absolutely insufficient. Physical measures must be used:

a. Dump resistor (Brake Chopper / chopper circuit): this is the most effective hardware line of defense. A high-power resistor and IGBT are connected in parallel on the DC bus. Once the DC voltage is detected to exceed 820V or 950V, the hardware circuit turns on within 1 microsecond and directly dissipates the surplus 100kW of energy as heat. This buys the critical 100 milliseconds needed for PV MPPT deramping.

b. Feed-forward control: the low-level DSP algorithm of the DCDC MPPT directly detects abrupt changes in AC current. Once it detects a sharp current reduction, without waiting for the frequency to rise, the low-level controller blocks part of the PWM pulses at the millisecond level to suppress energy injection and clamp the bus voltage.

4) The PV DCDC MPPT is directly paralleled with the battery and mainly operates in Mode A below (as seen by the PCS, it is similar to a battery).

**A. Improved strategy: adaptive droop control**

A conventional fixed droop coefficient can cause voltage sag or poor current-sharing accuracy. An adaptive scheme can optimize allocation: MDPI

- Consider line resistance compensation: for current-sharing deviations caused by unequal physical cable lengths, compensate line voltage drops through real-time calculation or communication.

- **Multi-mode switching control:**

  - Mode A (sufficient PV): PV outputs at full power (MPPT), while the battery absorbs surplus power or fills the deficit.

  - Mode B (battery fully charged): PV exits MPPT and switches to droop control to limit charging current.

**B. PV side (Boost): normally operates in MPPT mode and does not directly participate in droop allocation. However, when the battery is fully charged and the load is small, PV must switch from MPPT mode to constant-voltage/power-limiting mode to prevent excessive bus voltage.**

When the PV DCDC module operates in MPPT (maximum power point tracking) mode, if the battery reference voltage (*V_bat_ref*) fails, the system will typically face overvoltage or loss-of-control risks because it loses the closed-loop control reference at the output terminal.

Based on industrial standards and common control logic (such as HOLTEK MPPT algorithm applications), the recommended handling process is as follows:

**1. Trigger the protection mechanism (preferred action)**

- Stop PWM output: once an abnormal reference voltage signal is detected (such as a sampled value of 0, a maximum value, or a value outside the reasonable range), the controller should immediately block the PWM gate-drive signal and cut off energy transfer from the PV modules to the battery to prevent uncontrolled inductor current from damaging the module.

- Report fault status: the system should generate a “battery sampling abnormality” or “reference voltage loss” alarm and enter standby mode pending manual maintenance.

**2. Control-mode degradation (software remedy, not recommended due to high risk)**

If the hardware supports it and system continuity must be maintained, the control logic may attempt to switch as follows:

- Lock the duty cycle: lock the duty cycle calculated by the current MPPT algorithm at a small safe value and operate at extremely low power to prevent a rapid rise in output voltage.

- Switch to open-loop mode: ignore the MPPT logic and use a fixed constant voltage (for example, 0.7-0.8 times the open-circuit voltage of the PV array) for preliminary limiting. However, because feedback from the battery side is lost, this approach is high-risk and should be used only for emergency operation.

**3. Hardware redundancy switching**

- Switch to an auxiliary sampling channel: if redundant sampling is designed into the system, it should immediately switch to backup sensor data.

- Hardware overvoltage protection (OVP): even if the software reference fails, an independent hardware comparator circuit should forcibly shut down the system when the output voltage exceeds a safe threshold, such as the maximum allowable battery charging voltage.

**For the reverse DC-coupled solution, one-to-one cluster management is recommended.**

| Comparison dimension | Direct connection to the DC bus (centralized) | (one-to-one cluster management) |
|---|---|---|
| Energy yield | Lower. Affected by the “barrel effect,” inconsistencies among battery clusters accelerate capacity degradation of the overall battery bank. | Higher. Independent DC/DC control of charge and discharge for each cluster eliminates inconsistencies and increases effective capacity by approximately 5%-10%. |
| Parallel circulating current | High risk. Voltage differences between clusters can generate circulating currents, potentially causing contactor burnout or battery damage. | No circulating current. DC/DC conversion provides electrical isolation or active current limiting, completely eliminating circulating-current issues. |
| System design | Constrained. New and old batteries cannot be mixed, and the battery voltage must strictly match the PCS DC input range. | Flexible. Supports mixing new and old batteries and paralleling batteries from different manufacturers; the DC bus voltage can be increased to 950V to reduce losses. |
| Initial cost | Lower. The circuit is simple and requires no additional power conversion devices. | Low. Busbars and wiring complexity are increased. |
| Conversion efficiency | High single-stage efficiency. Electrical energy passes through only one PCS conversion stage. | Low loss. Only the PV DCDC MPPT module is involved. |
| Maintenance difficulty | High. A fault in one cluster may require the entire array to shut down, and locating the fault point is difficult. | Low. Supports online isolation and maintenance of a single cluster, enabling “single-cluster electrical maintenance.” |

**Control-layer description**

Layer 1: primary control layer (firmware level - microsecond-level resolution). This layer is located inside the chips of the PCS and DC-DC converters and relies on highly robust proportional-integral (PI) controllers and virtual impedance loops. The primary control layer is responsible for real-time PWM signal synthesis, internal current loops, and grid-connected VSG logic. It can provide the inertial response and instantaneous active/reactive power buffering required during load step changes, such as motor starting, without waiting for external network commands from the PLC.

Layer 2: secondary control (edge-controller level - millisecond-level resolution). This layer is deployed on a ruggedized local industrial PC or main PLC platform and, in distributed operating mode, is responsible for direct AGC and AVC dispatch logic. It continuously monitors AC frequency/voltage and DC bus stability. It receives the dynamic operating range calculated by Layer 3 and issues specific active power and reactive power setpoints (*P_ref*, *Q_ref*) to each battery pack (through the BMS) and PV converter to enforce strict SOC balancing and maintain precise microgrid parameters within regulatory limits. “PMS or MGCC”

Layer 3: tertiary control and predictive analytics (server/cloud layer - second- and minute-level resolution). This computing layer executes large-scale rolling power-envelope algorithms. Using machine learning models and historical persistent data, Layer 3 forecasts industrial loads and solar generation over the next 24 to 72 hours. It runs distributionally robust optimization algorithms to determine the most cost-effective unit commitment, ensuring that diesel generators are dispatched only when the forecast horizon indicates a mathematically determined forthcoming shortage of energy reserves. ()Layer 3 also calculates adaptive demand-charge constraints and dynamically adjusts module-level power limits (*P_min/P_max*) to prevent long-term thermal degradation and fully avoid cascading component failures.

**Core terminology**

- State of Charge (SOC): the ratio of the currently remaining usable energy of a battery energy storage system (BESS) to its rated total capacity. SOC is the most critical constraint for formulating microgrid charge/discharge strategies, implementing peak shaving and valley filling, and maintaining black start reserve energy. In optimization models, upper limits (such as 90%) and lower limits (such as 10% or 20%) must be strictly defined to prevent deep overcharge or overdischarge and thereby protect the electrochemical and physical structure of the battery.

- State of Health (SOH): the ratio of the battery's current maximum available capacity to its initial design capacity at manufacture, directly reflecting battery aging, cycle life degradation, and changes in internal resistance. In the IEC 61850-7-420 standard framework, SOH is monitored in real time as a key data object for evaluating equipment residual value and dispatch cost.

- Point of Common Coupling (PCC): the physical and electrical node at which the microgrid connects to the external main grid or distribution network. The PCC is not only the boundary for bidirectional energy exchange, but also the central hub for reverse-power-flow prevention logic, synchrocheck for grid-connected/islanded transition, and power-quality monitoring, such as voltage sags and harmonic distortion. According to IEEE 1547, control equipment at the PCC must have rapid fault detection and physical isolation capabilities.

- Grid-Connected Mode: the operating state in which the microgrid remains physically connected to and synchronized with the external main grid. In this mode, the main grid acts as an infinite bus, providing stiff voltage and frequency support for the microgrid. Distributed energy resources (DERs) inside the microgrid primarily adopt grid-following (GFL) PQ (active/reactive power) control strategies to maximize renewable energy output or execute economic dispatch commands.

- Islanded Mode: the operating state in which the microgrid disconnects at the PCC and independently supplies internal critical loads when the main grid experiences an outage, severe power-quality issue, or planned dispatch event. In this mode, a primary power source, typically a fast-response BESS or diesel generator, must switch to a grid-forming (GFM) voltage/frequency (V/f) control strategy to establish and maintain the voltage and frequency reference within the microgrid.

- Seamless Transition: an advanced technical process in which, during transitions between grid-connected and islanded modes, a microgrid uses advanced phase-locked loops (PLLs), high-frequency sampling, synchrocheck logic, and fast inverter control algorithms to constrain transient fluctuations in voltage magnitude, frequency, and phase within a very small range, ensuring that voltage-sensitive critical industrial or commercial loads do not experience outages or resets.

- Black Start: under the extreme condition in which the microgrid system experiences a complete blackout and is disconnected from the main grid, black start is a systematic self-healing process that does not rely on any external grid support. It starts internal micro-sources capable of self-starting, such as energy storage systems equipped with DC power supplies or diesel generator sets, gradually restores the internal AC voltage and frequency of the system, and restores power to transformers and loads within the microgrid according to a strict priority sequence.

**Explanation of DC cabinet matching**

For common configurations in which 260 series cells correspond to an 800VDC bus and 240 series cells correspond to a 750VDC bus, the corresponding 125kW/261kWh DC cabinet and 241Kwh DC cabinet typically have the following DC bus voltage parameters:

- **Maximum system voltage of PCS and DCDC MPPT: typically designed as 950Vdc (shutdown if exceeded)**

- The medium-voltage DC solution uses higher-capacity 314Ah cells, with two options for the number of cells in series, 240 and 260, corresponding to system capacities of 241kWh and 261kWh, respectively.
- Medium-voltage solution: 832V (composed of 5 1P52S Packs connected in series).
- Medium-voltage range: 715V ~ 923V or 702V ~ 936V

**(261kWh cabinet) uses 5*1P52S liquid-cooled Packs**

Technical parameters:

| **Configuration method** | **1P52S** | **Storage ambient temperature** | **-30℃~55℃** |
|---|---|---|---|
| Rated capacity | 300Ah | Thermal management method | Liquid cooling |
| Rated voltage | 166.4V | Fire protection system | Pack-level fire protection (perfluoro hex an one) |
| Voltage range | 145.6~187.2V | Protection rating | IP67 |
| Rated energy | 49.92kWh | Dimensions | 1128*800*240mm |
| Rated charge/discharge power | 0.5P | Weight | 336kg±2kg |
| Operating ambient temperature | -30℃~55℃ | Certification standards | GB/T36276、UL1973、UL9540A、IEC62619、IEC62477-1、UN38.3 |
| Number of 314 cells used | 52 cells | | |

**Basic parameters of the 314 cell:**

| Range | Specification |
|---|---|
| Typical capacity | 314 ampere-hours |
| Typical energy | 1004.8 watt-hours |
| Operating voltage | 2.5~3.65V，T>0°C<br>2.0~3.65V，T≤0°C |
| Impedance (1KHz) | 0.17±0.05mΩ, new battery (~30%SOC) |
| Transportation capability | 99±1Ah |
| Standard charging power | 0.5P，25±2°C |

| Range | Specification |
|---|---|
| Maximum continuous charging power | 0.5P |
| Standard charging voltage | Maximum battery voltage 3.65V |
| Standard discharge power | 0.5P，25±2°C |
| Maximum discharge power (continuous) | 0.5P |
| Discharge cutoff voltage | 2.5V，T>0°C<br>2.0V，T≤0°C |
| Residual capacity loss | ≤3.5% per month in the first month |
| Operating temperature | Charging temperature: 0~60℃; discharging temperature: -20~60℃ |
| Cell weight | 5.49±0.30 kilograms |
| Storage temperature | -35~60°C |
| Storage ambient humidity | ROH < 85%, non-condensing |
| Typical dimensions (width*height*thickness) | 174.26±0.8*204.41±0.8*71.65±0.8mm |
| Remaining SOC | ≥ 8% |
| Altitude | < 5000 meters |
| Cycle performance | 7000 cycles@70%SOH |

To prevent damage, modern battery management systems (BMSs) and hybrid inverter PCSs employ multiple protection measures:

## 3.3 Requirements for Products and Capabilities in Different Scenarios

### 3.4 Positioning Analysis of Hybrid Inverter-Integrated Units (60KW/110KWWH; 125KW/261KWH): Peripheral Nodes of Small C&I and Agricultural Microgrids

The 60KW or 125kW hybrid inverter-integrated energy storage system is clearly positioned as a core node unit for small commercial and industrial (C&I) applications and distributed microgrids. It achieves an effective economic and technical balance between power output and energy reserve, making it a preferred device for factory workshops, intensive farms, small cold-chain storage facilities, and decentralized new-energy vehicle charging stations. In terms of physical system design, this product category places strong emphasis on deployability in extremely constrained spaces. Taking the industry-

leading 125kW / 261kWh C&I all-in-one energy storage system as an example, its development concept focuses on "space optimization" and "high energy density."

Increasing the self-consumption rate of PV generation: factory and warehouse rooftops are often equipped with PV arrays at the hundreds-of-kilowatts scale. Because peak PV generation at noon often mismatches the load valley of some factories, large amounts of electricity are exported back to the grid at low or even zero prices. Through an efficient DC-coupled architecture, the 125kW system captures and stores surplus PV electricity and releases it during nighttime production peaks, eliminating PV grid-export waste and maximizing the value of clean energy.

1. Reducing demand-charge expenditures: for short-duration extremely high power demand caused by the startup of heavy stamping presses in factories or simultaneous connection of multiple new-energy vehicles in charging stations, the 125kW inverter injects active power into the bus instantaneously with millisecond-level response. Within the utility smart meter acquisition interval, such as 15 minutes, it precisely "flattens" the peaks of the power curve, thereby substantially reducing the high fixed demand-charge penalties faced by enterprises.
2. Providing 1 to 2 hours of backup power for critical loads: this metric has strategic importance for livestock farms. As discussed above, layer and broiler farms face rapid suffocation risks during power outages. A 125kW system equipped with a 261kWh battery provides full-load discharge for approximately 2 to 4 hours, which is sufficient to cover most instantaneous grid interruptions or short repair-related outages. It also provides robust energy support for continuous operation of environmental control equipment on farms, buying sufficient time for external rescue or diesel generator maintenance and startup, and aligns closely with the time-critical requirements of biosecurity for power continuity.
3. Diesel fuel savings in hybrid microgrids: in agricultural expansion areas with no grid access, the 125kW all-in-one unit often operates in parallel with small and medium-sized diesel generators. The system uses the battery's fast charge/discharge capability to handle all sudden and fluctuating loads, allowing the diesel generator to remain locked at its highest fuel-efficiency operating point, typically 75%-85% of rated power, with the cleanest emissions, while shutting the diesel engine down directly during low-load nighttime periods. This sharply reduces diesel fuel consumption.
4. Grid stabilization in weak-grid environments: at the ends of remote agricultural distribution networks with very long supply radii, severe voltage drops are prone to occur. The 125kW hybrid inverter-integrated unit incorporates a powerful dynamic reactive power compensation (SVG) algorithm that monitors terminal-node voltage in real time and supports the local voltage profile by absorbing or supplying reactive power through the bidirectional inverter, preventing precision IoT sensing equipment inside farms from collectively resetting or crashing due to low voltage.

### 3.5 Positioning Analysis of the 520kW PV-Storage-Diesel Integrated Unit: An Energy Fortress for Heavy-Load Parks and Mining Hubs

When the coverage of a microgrid expands from a single building to an entire industrial cluster, the system power base must transition from the hundred-kilowatt level to the megawatt level. The 520kW to 2MW hybrid battery energy storage system (BESS) is precisely positioned as the main power supply and regulation hub for industrial parks, large-scale warehousing and logistics bases, and medium-sized mining areas. In physical form, the 520kW-class system fully moves beyond the single-cabinet concept and transitions to standardized 10-foot or 20-foot high-strength ISO containerized packaging. This

packaging form not only enables rapid integral lifting and combined road/rail transport in harsh terrains such as mining areas, but also provides sufficient space for deploying complex industrial-grade liquid thermal management systems, perfluorohexanone automatic fire-extinguishing immersion systems, and explosion-proof exhaust pressure-relief devices. From a business-logic perspective, the 520KW PV-storage-diesel integrated unit is not merely a physical scale-up of the 125kW capacity; it also achieves a qualitative leap in system coordination:

1. Massive load buffering and energy recovery at the mining-area level: corresponding to the heavy-industry requirements analyzed in Section 3.3.1, the 520KW system has sufficiently deep energy storage, typically configured with a 0.5MWh to 1MWh battery array, and an extremely wide DC voltage operating range. It can calmly absorb and deliver megawatt-class short-duration impact regenerative energy released during downward braking of large beam-pumping-unit arrays or large mine hoists, and it has the strong overload starting-current output capability required to support staggered startup of multiple heavy crushers in mining areas.
2. Regional energy aggregation for large warehousing parks: modern large logistics parks often have hundreds of thousands of square meters of rooftop PV resources. A 520KW system, or even cascaded 2MW systems, acts as the “energy router” for the entire park. Through an upper-level energy management system, it centrally aggregates distributed PV generation, performs overall reactive and active power dispatch for park-level feeders, and fully smooths severe regional PV output fluctuations caused by fast-moving cloud cover, ensuring that the park grid appears to the external regional transmission network as a highly grid-friendly, dispatchable, and smooth load/source node.
3. “Master-slave” formation control for multiple heavy diesel generator sets: in traditional mining areas fully dependent on diesel generation, multiple diesel generators are typically operated in parallel while maintaining high spinning reserve to guard against sudden load increases. After a 520KW hybrid energy storage system is introduced, its advanced grid-forming inverter algorithm can be used to set the energy storage equipment as the “master voltage source” of the entire mining microgrid. At this point, heavy diesel generator sets that previously had to operate rigidly are relegated to “slave sources.” The energy storage system absorbs all transient frequency and voltage impacts, while the mining dispatch system can calmly decide which diesel generator sets to start or stop based on slow variations in average load. This completely breaks the technical constraint that diesel engines must operate inefficiently to handle impacts and substantially extends the engine overhaul interval.

**Summary:**

**The ZOE product matrix covers: 60kW~125KW hybrid inverter-integrated systems; 520KW ~ 2MW PV-storage-diesel integrated systems and their main target scenarios**

From a single plant, centralized farm, or distributed charging station to an entire heavy industrial park, centralized mining area, or logistics hub; physical form; IP55 outdoor deployment; microgrid role positioning; node-level peak shaving and valley filling; terminal weak-grid voltage support; critical-equipment UPS; regional energy control center; primary voltage/frequency reference source for the microgrid; core corresponding capabilities; meeting 1-2 hours of backup power for farm life-support systems; eliminating short-duration extremely high peaks at charging stations; absorbing massive regenerative energy from heavy mining machinery; coordinated dispatch of multiple heavy diesel generator arrays; thermal management and safety rating; forced air cooling or passive liquid-cooling design; high-density cabinet-level fire protection; industrial-grade deep liquid-cooling architecture; complete fire protection system

### 3.6 Ultra-Large-Scale Macro-Microgrids and Utility-Scale Solutions of 2MW and Above (not covered by the ZOE solution)

When the coverage boundary of a microgrid extends beyond the limits of a single enterprise or park to broad remote-island electrification retrofits, deep-sea ultra-large oil and gas production platforms, and ultra-large mining concessions spanning tens of kilometers, the scale of system construction inevitably enters the >2MW and even tens-of-megawatts utility-scale domain. At this macro scale, the energy storage and conversion system has fundamentally transformed: it is no longer merely an auxiliary regulation tool at the load end, but has become the core infrastructure governing the macro stability of the regional bulk power grid.

# 4. How to Plan and Design a Microgrid

| Component name | Key parameters | Recommended sizing relationship | Design logic and standards basis (Key Logic) |
|---|---|---|---|
| Energy storage system (ESS) | Power (kW) | 1:1 | IEEE 2030.9: must be capable of handling transient impacts such as motor starting and EV connection, while maintaining islanded voltage stiffness. |
| Energy storage battery | Capacity (kWh) | 0.5C(2X) | GB/T 51341: ensures the optimal life-rate range of 0.25C-0.33C; provides 3-4 hours of full-power support (corresponding in practice to 8-12 hours of autonomy), balancing CAPEX and diesel operating frequency. |
| PV modules | Power (kWp) | 1.6X~2.0X | IEC 62898-1: produces the full-day (24h) required energy within a limited solar window (4h); high over configuration reduces LPSP (loss of power supply probability). |
| PV MPPT | Power (kW) | 1.6X~2.0X | Efficiency-oriented: energy is valuable in off-grid systems; avoid over configuration clipping commonly seen in grid-connected systems and ensure maximum energy capture under weak irradiance and post-disaster recovery conditions (27). |
| Diesel generator | Power (kW) | 1.2:1 | Wet-stacking prevention: avoid low-load operation. Diesel generator power < energy storage power, forcing it to charge the battery simultaneously when operating and maintaining a >75% load factor. |
| DC bus | Voltage (V) | 800V DC<br>For 380VAC power levels, 750V is more suitable in China. | Energy-efficiency standard: matches mainstream EV fast-charging voltage platforms and reduces high-current transmission losses (21). |

# 5. Microgrid-Related Standards

## 5.1 Analysis of the IEEE 2030 Microgrid Standards

If the IEEE 1547 series define the “physical boundary” and “hardware baseline” of a microgrid, then the IEEE 2030 series establish its “nervous system” and “brain.” For future power systems that are inverter-based resource (IBR)-dominated, include massive numbers of communication nodes, and exhibit complex dynamic topologies, purely electrical specifications are far from sufficient. By comprehensively defining microgrid controller abstraction, standardized testing procedures, secure application-layer protocols, interoperability information models, and adaptive protection strategies, the IEEE 2030 series represent the current highest technical consensus in the microgrid field.

### 5.1.1 Microgrid controller specifications. IEEE Std 2030.7-2017

The microgrid control system (MGCS) is the central brain of the entire network. Given the diverse topologies, scales, ranging from single-building microgrids to complex systems covering large distribution networks, and asset portfolios in the market, without a unified abstraction of control logic, system integration will face exponentially increasing customized software costs. IEEE Std 2030.7-2017, “Specification of Microgrid Controllers,” provides a specification independent of specific platforms and underlying device components, abstracting the complex functions of an MGCS into two core functions: Transition and Dispatch.

The standard first theoretically models the steady-state and transient processes of a microgrid as a state machine, defining two steady-state operating modes (SS1: grid-connected steady state; SS2: islanded steady state) and four types of state transitions (T1 to T4). Transition Logic is the first safety line of defense of the microgrid controller and is responsible for ensuring smooth transitions between the two steady states while protecting critical loads during the transition:

1. Planned Islanding (T1): this refers to the process in which the system actively disconnects from the grid after receiving preset commands from dispatch personnel or an economic optimization program. In this scenario, the controller must achieve “seamless islanding”; that is, before opening the PCC breaker, the controller must dispatch internal micro-sources so that their output precisely matches internal loads and regulate power exchange at the PCC to near zero, ensuring no significant voltage or frequency fluctuation.
2. Unplanned Islanding (T2): this is the most technically challenging transition process. When the main grid experiences a sudden fault such as lightning, a short circuit, or another event causing an abrupt voltage/frequency drop, the controller must have low-latency islanding detection capability and rapidly issue a trip command to the grid-connected breaker to isolate the fault. At the instant of physical disconnection, a power deficit or surplus will inevitably exist within the microgrid. The controller must send low-latency control signals to internal power sources and energy storage nodes, causing their control modes to switch instantaneously from grid-following mode (Grid-following / PQ control) to grid-forming mode (Grid-forming / droop control or isochronous control), thereby rapidly establishing a local voltage and frequency reference.
3. Reconnection (T3): after monitoring that the main-grid fault has been cleared, the controller adjusts the internal microgrid voltage magnitude, frequency, and phase angle, and safely closes the grid-connection switch once both sides meet synchronization conditions.
4. Black Start (T4): when the entire microgrid loses power, the controller coordinates internal resources capable of self-starting, such as battery energy storage systems or diesel

generators, to restore bus voltage within the microgrid step by step, gradually connect critical loads, and ultimately restore the operating state of the entire system.

On the other hand, Dispatch Logic is responsible for optimally managing asset allocation within the microgrid under steady-state operation, whether grid-connected or islanded. In the grid-connected steady state, dispatch involves not only time- and price-signal-based economic optimization to reduce emissions and energy costs, but also response to main-grid signals for ancillary services, such as active power peak shaving or reactive voltage support. In the islanded steady state, the absolute priority of dispatch shifts from economics to maintaining system power balance and survivability. To ensure agility in responding to contingencies, the 2030.7 standard proposes an extremely important contingency mechanism: the Emergency Dispatch Order (EDO). When the controller operates in grid-connected mode, it continuously calculates and updates the EDO in the background based on the real-time source-load status of the current system. Once unplanned islanding (T2) occurs, because the response time available to the system is extremely short, often on the order of hundreds of milliseconds, the dispatch module does not need to recalculate, but immediately and unconditionally executes the latest generated EDO plan, such as rapidly shedding interruptible loads, thereby effectively preventing total microgrid collapse caused by frequency instability.

### 5.2.2 Microgrid controller testing IEEE Std 2030.8-2018

The theoretically rigorous design logic must be verified through strict and repeatable engineering test procedures. Because the physical generators, energy storage equipment, and critical loads involved in a microgrid are high-value assets with very low fault tolerance, directly testing extreme conditions on the physical system, such as deliberately creating unplanned islanding or extreme short-circuit faults, entails very high damage risk and economic cost. For this reason, IEEE developed IEEE Std 2030.8-2018, “Standard for the Testing of Microgrid Controllers,” as a companion engineering implementation guide to 2030.7, intended to provide standardized testbed specifications and quantitative evaluation metrics for control-system performance verification.

A core methodology of this standard is the strong recommendation to adopt the **Controller Hardware-in-the-Loop (C-HIL)** testing paradigm combined with a real-time digital simulator (RTDS). In this test framework, the physical hardware prototype of the microgrid controller is retained, while its external control interfaces are connected to a simulator running a high-fidelity electromagnetic transient (EMT) model of the microgrid. The controller receives simulated voltage, current, and breaker open/close status signals from the simulator and outputs control commands to the simulator based on its internal transition and dispatch algorithms. This fully closed-loop, non-destructive test environment allows engineers to perform exhaustive boundary-condition testing of the controller. The research team at Spain’s TECNALIA Smart Grid Technology Laboratory (SGTL) applied this standard in practical projects and demonstrated its high usefulness in verifying control functions and exposing communication latency and algorithm deadlocks.

At the level of specific assessment metrics, 2030.8 not only verifies whether the controller “can” complete an operation, but also quantifies the “quality” of completion. It uses IEEE 1547-2018 as the performance benchmark for underlying equipment and evaluates core functions along the following dimensions:

- Transient performance assessment: during simulated unplanned islanding transition (T2), the voltage sag depth, extreme frequency deviation, protection response time, and time required for voltage/frequency to restabilize within the normal range are recorded in real time to evaluate the robustness of the control system in emergency handling.

- Steady-state dispatch assessment: verifies, under steady-state conditions, the tracking accuracy, response delay, and algorithmic allocation rationality of underlying asset power output in response to setpoint changes when the controller receives external load changes or updated generation forecasts.

Although 2030.8 provides a complete testing framework, the Smart Electric Power Alliance (SEPA) offered a pragmatic recommendation in its industry briefing: given that the low-level behavior of distributed inverters has not yet been fully standardized, conditions are not yet mature for developing perfect control standards. Therefore, organizations conducting standard tests should prioritize “simplicity” and “broad applicability” rather than overly pursuing the inclusion of advanced but immature edge products in system requirements. This pragmatic engineering philosophy supports the rapid and safe commercialization of microgrid technologies.

### 5.2.6 Smart Energy Profile Application Protocol IEEE P2030.5 -2018 / 2023

As smart grids extend toward the edge of distribution networks, millions of smart inverters, battery energy storage systems, and electric-vehicle charging piles are being connected to the network. Enabling devices produced by different manufacturers to use the same language to communicate safely and efficiently with grid operators has become the largest bottleneck hindering decentralized energy development. IEEE 2030.5, formerly Smart Energy Profile 2.0 (SEP 2.0) initiated by the ZigBee Alliance, was established in this context as a universal application-layer protocol for modern smart-grid communication. In particular, after the California Public Utilities Commission (CPUC), through California’s interconnection Rule 21, mandated that all new distributed energy resources (DERs) default to the Common Smart Inverter Profile (CSIP) based on IEEE 2030.5, the protocol rose from an optional standard to a mandatory regulatory threshold determining whether equipment can enter core markets.

Flexible communication mechanism based on Internet architecture: departing from the highly customized, polling-based, closed architecture of traditional power-industry SCADA systems such as DNP3 or Modbus, IEEE 2030.5 adopts a RESTful API architecture fully consistent with the modern World Wide Web and operates over the HTTP/TCP/IP protocol suite. This choice means it can run seamlessly over any physical link supporting IP transport, including Ethernet, Wi-Fi, and cellular networks. The protocol adopts a client-server model: the utility DER management system (DERMS) or microgrid master controller acts as the server, creating, owning, and managing various “Resources,” such as demand response events, price signals, or inverter Volt-VAR curve settings; smart inverters or home energy management systems act as clients, using XML data format to actively discover, retrieve, or subscribe to these resources through GET requests, and returning their responses and operating status through POST or PUT. This mechanism allows underlying devices to determine data retrieval frequency based on their own network conditions, greatly reducing concurrency pressure on the central server. To simplify access for massive numbers of terminals, the protocol supports “zero-configuration discovery” of devices within the network based on mDNS (multicast DNS) or DNS-SD, enabling devices to automatically locate the server once connected to the network and reducing manual deployment difficulty.

Industrial-grade cybersecurity defense system: because microgrid and DER aggregation can materially affect power-flow patterns and stability in the bulk grid, malicious manipulation through cyberattacks could lead to catastrophic consequences. Therefore, IEEE 2030.5 treats cybersecurity as its core foundation and implements a defense-in-depth mechanism. In the 2018 version, the protocol mandates the use of Transport Layer Security (TLS 1.2) and specifies an advanced encryption cipher suite with forward secrecy (TLS_ECDHE_ECDSA_WITH_AES_128_CCM_8) for communication encryption. All communicating devices must undergo strong identity authentication through public key infrastructure (PKI)

and X.509 digital certificates, ensuring mutual trust between server and client. In addition, the system uses access control lists (ACLs) and PIN pre-registration mechanisms, enabling the server to grant client permissions at a fine-grained level, while unauthorized control commands are blocked directly at the application-protocol layer. At present, DER operators face substantial security compliance pressure, and existing device fleets in California and other regions are also required to gradually migrate and connect to this standard, a process that will comprehensively reshape the information-security landscape of distribution networks over the next several years.

Technical evolution in the 2023 version: embracing vehicle-to-grid (V2G). Technological development has not stopped; IEEE 2030.5-2023, released in 2023, introduced milestone updates, with its greatest highlight being deep support for complex distributed energy forms, especially electric vehicles (EVs) and vehicle-to-grid (V2G). Traditionally, EV charging networks, mainly using OCPP and ISO 15118 protocols, have primarily addressed “how to charge” and “how to bill.” However, when supporting reverse power flow from vehicles to the grid, namely V2G, they cannot provide complex grid-support functions required by IEEE 1547, such as reactive power control and frequency support. For this purpose, the new version of the 2030.5 protocol is seamlessly aligned with the SAE J3072 standard. Under the new architecture, electric vehicle supply equipment (EVSE) acts as a protocol relay, transmitting the grid’s complex IEEE 2030.5 dispatch commands and site-level dynamic output limits to the electric vehicle, while the vehicle’s built-in inverter system adaptively regulates charging and discharging based on these parameters. To address more advanced cyber threats, the 2023 version further strengthens security by mandating support for TLS 1.3. These upgrades make IEEE 2030.5 not only the cornerstone of microgrid communication, but also the ultimate common language connecting transportation networks and power networks.

### 5.2.4 Grid interoperability requirements IEEE Std 2030.4-2023

As the complexity of internal microgrid components increases and interactions between microgrid clusters and the bulk grid become more frequent, the absence of global architectural guidance can cause system development to become an “information silo.” IEEE Std 2030.4-2023, “Guide for Control and Automation Installations Applied to the Electric Power Infrastructure,” is intended precisely to provide a high-level abstraction-based system architecture design methodology for interoperability across the entire smart grid.

Smart Grid Interoperability Reference Model (SGIRM): the foundation of this guide is the Smart Grid Interoperability Reference Model (SGIRM) proposed in IEEE 2030-2011. The 2030.4 standard guides engineers in applying SGIRM to the practical development of microgrid controllers and distributed energy resource management systems (DERMS). To decompose the complex dimensions of power systems, SGIRM defines three core Integrated Architectural Perspectives (IAPs), each addressing a specific pain point in system integration:

1. Power Systems IAP: this is the most fundamental physical layer, focusing on the electrical connections, power-flow distribution characteristics, and system stability logic of physical assets such as generators, energy storage, transformers, and distribution lines. It addresses the physical flow of electrons.
2. Communications & IT IAP: this layer functions as the nervous network of the system and focuses on how massive data streams can be transmitted safely and with low latency among nodes. It covers the selection of physical-layer media, such as fiber optics and private wireless networks, transport protocol stacks, such as the IEEE 2030.5 protocol application discussed above, and the design of network architecture and routing strategies.

3. Business & Regulatory IAP: this is the key determinant of the commercial viability of a microgrid project. Through this perspective, the 2030.4 standard organically integrates electricity market transaction rules, such as spot-market arbitrage and virtual power plant participation mechanisms, regulatory policy constraints, and carbon-emissions compliance requirements into system design. The 2023 update substantially strengthened this section in particular, reflecting evolving electricity market mechanisms on both distribution and transmission sides and corporate consideration of environmental, social, and governance (ESG) factors.
4. Open architecture and avoidance of vendor lock-in: in practical projects, microgrid hardware and software systems are almost always assembled from multiple vendors, for example, an energy storage system from Company A, a PV inverter from Company B, and central control software from Company C. Reliance on closed proprietary protocols from each vendor not only creates redundant communication gateways and high system integration costs, but also places later system upgrades and expansion into a catastrophic “vendor lock-in” situation. Therefore, the 2030.4 standard strongly advocates and specifies the design principle of **Open Architecture**.

By adopting platform-independent interfaces with high modularity, extensibility, portability, and scalability in the design of control and automation systems, SGIRM not only enables plug-and-play integration and replacement of system components, such as sensors and controllers, but also ensures high reusability of control application software. This architecture substantially reduces the total deployment cost of a microgrid system over its full life cycle and lays the groundwork for seamless integration of future artificial intelligence (AI) forecasting models and complex multi-agent coordination algorithms. The complete requirements-determination methodology established by the guide helps stakeholders define the specific boundaries of computing capabilities, middleware, and network operating systems at the planning stage, providing indispensable methodological guidance for the digitalization of large-scale power infrastructure.

### 5.2.5 Microgrid protection. IEEE P2030.12-2023

Among all technical domains of microgrids, protection system design is the most challenging element and is directly related to personnel and asset safety. Switching between microgrid operating modes, namely grid-connected and islanded operation, together with the distinctive characteristics of inverter-based resources (IBR-dominated resources), creates a risk that conventional distribution-network relay protection philosophies may fail completely. IEEE P2030.12-2023, Guide for the Design of Microgrid Protection Systems, examines these challenges in depth and proposes advanced architectural strategies to address them.

The “low fault-current paradox” facing inverter-based microgrids Conventional power-system relay protection design, such as widely used 50/51 phase overcurrent relays, relies heavily on the short-circuit current supplied by synchronous generators at the instant of a fault, which can reach tens of times the rated operating current, to rapidly trip circuit breakers. Modern microgrids, however, integrate large amounts of PV and battery energy storage, which are connected to the grid through power semiconductor devices, namely inverters. Because semiconductor devices such as IGBTs have very limited thermal withstand capability, inverter internal control logic typically limits fault current within an extremely short time, on the order of milliseconds, to protect the device from damage, usually allowing only 1.1 to 1.5 times rated current as output.

This creates a critical safety paradox: when a microgrid operates in islanded mode after being disconnected from the main grid, if an internal short-circuit fault occurs, the limited fault current supplied

by the inverters often has a magnitude even lower than the starting current of some large motors. This means that conventional overcurrent relays based on current-magnitude thresholds may fail to detect the fault, allowing the fault arc to persist and potentially causing severe fire hazards or system-level equipment burnout.

To overcome this blind spot, the P2030.12 standard guides engineers toward more advanced fault-detection mechanisms. For example, voltage-controlled overcurrent protection (51VC) or voltage-restrained overcurrent protection (51VR) can be applied by combining severe bus-voltage sag with slight overcurrent characteristics to determine whether a fault has occurred. For faults involving ungrounded systems, one of the most difficult fault types in microgrids, the standard recommends negative-sequence overcurrent protection (46), because asymmetrical faults produce significant negative-sequence components. In addition, proper configuration of isolation-transformer grounding in the microgrid and the use of sensitive zero-sequence current threshold techniques have become standard practices for addressing this issue.

Adaptive protection systems (APS) for dynamic topologies In grid-connected mode, microgrid fault current is supplied by the strong main grid, which has very large short-circuit capacity; in islanded mode, the system relies entirely on the weak inverter short-circuit capacity. Because of this large disparity and the complex bidirectional power flows within a microgrid, any protection strategy based on fixed settings cannot simultaneously satisfy selectivity, speed, and sensitivity requirements under all operating states. For this reason, the P2030.12 standard establishes **adaptive protection systems (Adaptive Protection System, APS)** as the core development direction for microgrid relay protection.

The implementation of adaptive protection is mainly divided into two stages: offline analysis and online execution. In the offline analysis stage, engineers must enumerate all possible microgrid topologies and operating conditions, such as which circuit breakers are closed, whether the system is grid-connected or islanded, and which generators are online, and perform short-circuit current simulations to construct an “event table” (Event Table Creation) containing multiple relay protection setting groups.

For online execution, the standard discusses two main architectures in depth:

1. Centralized Adaptive Protection: A microgrid central controller (MCC) or dedicated protection computer acts as the central brain, continuously monitoring the status of all circuit breakers and distributed generators across the network through a high-speed fiber-optic network. When the operating topology or mode changes, the central brain queries the event table and immediately issues commands through the IEC 61850 protocol, using its high-speed, unacknowledged GOOSE messages, to intelligent electronic devices (IEDs/relays) distributed at each node, dynamically updating their protection setting groups or operating curves. This approach ensures that the protection coordination logic of the entire system remains optimal at all times. When a fault occurs, the central system can also coordinate the collection of local relay information, make the optimal decision to isolate the fault, and reconfigure network power supply as quickly as possible.
2. Decentralized APS & Directional Blocking: In some ring-type microgrid structures, when a fault occurs on a line, power flow may feed the fault point from both ends simultaneously. This requires IEDs not only to detect the fault but also to interact through communication-based logic, such as directional comparison blocking. This enables the system to isolate the smallest faulty section precisely while maximizing continuous power supply to critical loads in non-faulted areas. The medium-voltage microgrid on Hailuoto Island cited in the literature is a successful example of adaptive protection using communication-capable directional and

nondirectional overcurrent relays combined with a primary-secondary communication architecture.

It is worth noting that the P2030.12 guide also addresses the emerging field of DC microgrid protection. Because DC systems lack the “natural current zero crossing” inherent in AC systems during faults, fault arcs cannot extinguish automatically. This not only requires new solid-state DC circuit breakers or hybrid DC circuit breakers, but also requires protection algorithms to use ultrafast transient feature-based detection methods, such as current rate of change (di/dt) or current differential protection, to clear faults within a few milliseconds before the fault current rises to the device damage limit. Standardization in this field will be a key breakthrough for further improving microgrid safety and resilience.

## Summary

A systematic review of the underlying grid-interconnection standards for microgrids, including IEEE 1547, IEC 62898, and GB/T 33589, together with system-level control frameworks such as the IEEE 2030 series, clearly outlines the technical evolution of modern power infrastructure in response to the energy transition. This is not only a development path from simple interconnection to complex coordination, but also an industrial revolution driven by the deep integration of power engineering and information science.

Traditional physical interconnection standards, such as IEEE 1547, establish the basic electrical baseline for equipment entering the grid and define the foundational rules for physical interaction between microgrids and the main grid. However, in the face of exponentially growing decentralized nodes and stochastic renewable energy fluctuations, relying solely on rigid physical-layer constraints is no longer sufficient to maintain overall system stability. The IEEE 2030 series addresses this challenge by providing a complete “soft” methodology. IEEE 2030.7 and 2030.8, through abstract modeling and high-fidelity C-HIL validation, provide the “central brain” and rigorous logic that enable a microgrid to respond to fatal disturbances at the millisecond scale and maintain self-healing survivability. IEEE 2030.5 embeds modern Internet communication architecture and finance-grade encryption deeply into the protocol stack, creating a “common language” that enables countless heterogeneous devices to exchange commands and market prices securely and orderly. The IEEE 2030.4 reference model ensures that this complex evolution can continue without being constrained by a single vendor’s closed ecosystem. Finally, IEEE P2030.12 introduces adaptive and intelligent protection mechanisms to create a dynamically evolving “immune system” for this physically inertia-deficient and fragile system.

Looking ahead, the evolution of microgrid standards will deepen along two dimensions. First, they will extend from local microgrids toward wide-area coordinated control. As vehicle-to-grid (V2G) standards mature and protocols such as IEEE 2030.5 become widespread in new types of loads, electric vehicles will no longer be merely consumers; they will become highly mobile “mobile microgrids” with substantial energy storage potential. Coordinating such massive numbers of micro-nodes will require artificial intelligence algorithms based on edge computing to provide more flexible support at the protocol layer. Second, microgrids will be deeply integrated into, and contribute back to, bulk-power-system markets. In the future, microgrids will not only serve as safe havens during emergencies. Under normal conditions, they will operate as highly flexible virtual power plants (VPPs) or distributed energy resource management system (DERMS) nodes, seamlessly interfacing through standardized interfaces with wholesale electricity spot markets and carbon-emissions verification mechanisms.

# 6. Microgrids and Power Markets (VPP)

## 6.1 Blockchain-Based Peer-to-Peer (P2P) Energy Mutual-Aid Trading System

With the widespread adoption of distributed microsources such as rooftop PV, large numbers of prosumers, who both consume and produce electricity, are emerging within microgrids. In traditional centralized electricity markets, prosumers are forced to sell surplus electricity to monopoly utilities at very low prices through “net energy metering (NEM)” or “feed-in tariff (FiT)” mechanisms. To break this monopoly, blockchain-based decentralized peer-to-peer (P2P) energy trading networks are being widely integrated into community microgrids.

A P2P energy trading network is logically divided into a virtual layer and a physical layer. In the virtual layer, the microgrid abandons the traditional centralized trading server and instead uses distributed ledger technologies such as Ethereum. Smart meter data from prosumers are written to the blockchain in real time, and complex double-auction mechanisms are automatically executed through smart contracts. The underlying logical trading equation is highly automated: the system determines in real time the relationship between prosumer *i*’s PV output $P\_PV,i$ and its own load $P\_i$. When $P\_PV,i > P\_i$, the remaining tradable energy is labeled as $P\_sold = P\_PV,i - P\_i$. The smart contract automatically matches this *P_sold* according to bids from other consumers in the microgrid and triggers token settlement, without any manual intervention or third-party commission throughout the process.

However, such high-frequency and distributed decentralized trading inevitably affects the underlying physical microgrid. Frequent bidirectional power flows can significantly intensify system frequency oscillations and also make the system vulnerable to malicious cyberattacks such as eavesdropping and false data injection (FDI). To protect system boundary security, leading researchers have proposed an adaptive frequency-domain controller that integrates federated learning with local differential privacy (LDP). This approach allows each prosumer node participating in P2P trading to train models locally and upload only encrypted gradient data to a cloud server for aggregation. This mechanism fully prevents leakage of sensitive private data while giving the underlying controller strong disturbance-rejection and frequency-smoothing capabilities. More innovative approaches have proposed a “Proof of Prediction” mechanism and an end-to-end network-loss traceability algorithm to accurately quantify and compensate for physical losses during distributed energy transmission, enabling the entire P2P microgrid to maintain excellent supply-demand deviation performance under intense trading, with a peak-shaving rate of 29.6% and a deviation of only about 5%.

## 6.2 Aggregation: Top-Level Interactive Coordination of Virtual Power Plants (VPPs)

The capability of a single microgrid is ultimately limited by its physical capacity. When hundreds or thousands of microgrids, energy storage stations, and large numbers of distributed energy resources are aggregated, a large-scale entity capable of competing with conventional power plants emerges: the virtual power plant (Virtual Power Plant, VPP).

According to projections by the U.S. Department of Energy and the definition in IEEE 2030.14, a VPP has no physically centralized plant; instead, it aggregates geographically dispersed assets into a large

controllable entity through highly coordinated digital management and participates in capacity markets and ancillary service markets of the bulk power grid. Microgrids, as core constituent nodes of VPPs, have highly complex bidirectional interactive coordination strategies with VPPs.

When responding to grid-level frequency-drop events, the VPP macro-dispatch center sends secondary frequency-support commands to the microgrid clusters under its control through high-frequency communication links. At this point, the underlying PQ control strategy inside each microgrid shifts to a dynamic active-power allocation mode based on a secondary interpolation algorithm. It instantaneously calculates the maximum available power margin of current PV and energy storage resources and feeds this power as a boundary condition into the upper-layer mixed-integer linear programming (MILP) solver. Through this coordinated frequency control strategy, the VPP can extract all distributed energy resources within the microgrid cluster, including PV, wind power, and energy storage, within a very short time and deliver substantial aggregated active-power support to the main grid. Its short-term dynamic response capability can even exceed that of conventional thermal power units, whose response is constrained by rotor inertia. By balancing main-grid support and local autonomy (Energy Autarky), the VPP fully connects the chain from underlying microcontrollers to national electricity market transactions, elevating the microgrid from an isolated safe haven into a robust defense for overall energy security.

# 7. Description of the ZOE Microgrid Solution and Its Advantages

Organize the content for the sales team training PPT and COPY it here

# Appendix A: Equipment Selection Tables from the Supplied Outline

## Appendix Table A-1

| project | Comparative consideration of key indicators | ZOE Current Solution |
|---|---|---|
| System Architecture | Gaped solutions; Seamless solutions: AC bus solution; Hybrid solution; Full VSG solution | Hybrid solution: reverse DC-coupled |
| PCS | Weak grid support capabilities: three-phase balance, neutral node, grounding method; VSG capability; core components: third-generation SiC power chip (Infineon); overall efficiency; | It must support grid-connected, standby/off-grid operation, photovoltaic input (if applicable), battery charging and discharging, anti-islanding protection, and grid-compliant functions. |
| DC battery cabinet | | It is necessary to confirm the available capacity, battery chemistry, BMS limiting parameters, thermal management system, fire safety measures, and DC voltage operating range. |
| EMS/Controller | | Used to implement scheduling logic: time-of-use pricing arbitrage, demand control, photovoltaic priority strategy, diesel-powered coordinated control, and SOC (state of charge) protection. |
| Protective and protective devices | | AC circuit breakers, DC disconnect switches, fuses, surge protection devices (SPDs), emergency shutdown devices, insulation monitoring and grounding protection |
| Communication interface | | The BMS communicates with the PCS via CAN/RS485/Ethernet; and with the EMS via Modbus TCP, IEC 61850, 2030.5, or a vendor-specific protocol. |

## Appendix Table A-2

| Design Highlights | Require | ZOE Current Solution |
|---|---|---|
| AC voltage | Confirm the selection of a 400 V / 480 V / 690 V voltage level, or a medium voltage (MV) transformer interface scheme. | |

| Design Highlights | Require | ZOE Current Solution |
|---|---|---|
| Rated AC current | At 400 V, the current corresponding to a power output of 500 kW (at unity power factor) is approximately A; a margin should be allowed when selecting circuit breakers and cables. | |
| transformer | If connection to an 11 kV / 10 kV / 6.6 kV power grid is required, a transformer must be configured. | Optional transformers are available. |
| Short circuit capacity | The fault current contribution value of the inverter must be verified, and the coordination of the upstream protection device must be checked. | |
| grounding system | The selection of TN-S / TN-CS / TT / IT grounding schemes must be matched with the actual site conditions and the inverter's neutral point formation capability. | |
| harmonic | The total harmonic distortion (THDi) of the current, the potential resonance risk with the capacitor bank, and the short-circuit ratio (SCR) under weak grid conditions need to be checked. | |
| Power factor | Ensure adequate reactive power regulation capability; typically, a power factor range of ±0.8 or ±0.9 is required (depending on the inverter model). | |

## Appendix Table A-3

| field | Key points | |
|---|---|---|
| SOC range | The design should avoid covering the entire range of 0–100%; the actual usable range is typically 10–90%. | |
| Charge/discharge rate (C-rate) | 125 kW / 261 kWh ≈ 0.48C, which is a moderate rate for lithium iron phosphate (LFP) batteries and is beneficial to battery health. | |
| BMS Limitations | The PCS (Power Conversion System) must strictly comply with the instructions issued by the BMS regarding current, voltage, temperature, insulation status, and fault handling. | |
| Thermal Management | HVAC (Heating, Ventilation and Air Conditioning) systems must ensure that | |

| field | Key points | |
|---|---|---|
| | the battery operating temperature is maintained within the allowable range specified by the supplier. | |
| Battery degradation | The scheduling strategy should avoid unnecessary prolonged high SOC states, deep charge-discharge cycles, and high-temperature operating conditions. | |
| Black Boot | It needs to be confirmed whether the battery system and inverter combination has the ability to start from a complete shutdown and supply power to the local AC bus. | |

## Appendix Table A-4

| model | Control Logic | |
|---|---|---|
| Grid connection mode | Peak shaving and valley filling, self-consumption, time-of-use electricity arbitrage, and smooth photovoltaic output. | |
| Alternate mode | Detecting grid power failure, isolating the point of connection (PCC), and building a voltage/frequency source for the inverter. | |
| Offline mode | The energy storage inverter operates as a grid power source; the load power must be kept below the inverter's overload limit. | |
| Photovoltaic + Energy Storage | Photovoltaic power is prioritized for supplying electricity to loads, with the surplus used to charge batteries, and any remaining power is either connected to the grid or used for power limiting. | |
| diesel blend | Batteries are responsible for handling rapid transient load changes; diesel generators are responsible for handling prolonged energy shortages. | |
| weak grid | Enables voltage/reactive power (Volt/VAr) control, frequency/power (Frequency-Watt) control, ramp rate control, islanding protection, and | |

| model | Control Logic | |
|---|---|---|
| | low/high voltage/frequency ride-through functionality. | |

## Appendix Table A-5

| risk | Mitigation measures | |
|---|---|---|
| thermal runaway | Battery cabinet certification, gas/smoke/temperature detection, emergency ventilation | |
| DC fault | DC fuses, contactor coordination, insulation monitoring | |
| AC fault | Circuit breaker graded coordination, ground fault protection, and anti-islanding protection | |
| The fire spread | Safety distances, enclosure protection rating, fireproof partitions, and emergency response plans | |
| Overcharge/over-discharge | BMS hardware limits + EMS software limits | |
| Unauthorized access | Lockable cabinet, warning signs, remote monitoring network security | |

## Appendix Table A-6

| project | Require | |
|---|---|---|
| Installation location | Depending on the IP protection level and fire safety regulations, it can be placed on an outdoor base or in an indoor electrical room. | |
| Base | Concrete base; flood-resistant height required; reserved access channel for cable trench. | |
| Clearance requirements | Maintenance space and fire separation distances specified by the manufacturer must be maintained. | |
| ventilation | The system must meet the heat dissipation requirements of the HVAC system and handle abnormal gas emissions. | |

| project | Require | |
|---|---|---|
| Environmental conditions | The altitude, humidity, salinity, dust content, and seismic/wind load requirements need to be checked. | |
| noise | If the location is near office or residential areas, attention should be paid to the noise generated by the HVAC system and inverter fans. | |
| Equipment arrival | It is necessary to ensure that cranes/forklifts can enter the site smoothly in order to install the racks and carry out subsequent replacement work. | |
| | | |

## Appendix Table A-7

| stage | Specification parameters and key capabilities | Recommended Specifications |
|---|---|---|
| Factory test certificate | Cable wiring is correct, polarity is correct, insulation is correct, grounding is correct, and phase sequence is correct. | |
| Battery System | DC cabinet voltage matches the integrated unit; BMS communication, SOC calibration, and unit/module temperature system acquisition are normal. | |
| PCS | National power grid parameters, protection settings, charge/discharge testing | |
| EMS | Scheduling logic, SOC limits, alarm functions, remote monitoring | |
| Grid connection test | Anti-islanding, power limiting, power factor control, ramp rate control | |
| Backup test | Power failure simulation, switching time, load connection, black start | |
| Security Testing | Emergency stop, fire alarm interface, door interlock, fault stop | |

## Microgrid Applications and Design Considerations

1. Load and related application matching description: inductive loads with starting inrush current require reactive power compensation; nonlinear loads such as EV chargers; power-quality-sensitive loads such as IT equipment and medical instruments.
2. Be sure to verify the overload capability of the integrated unit, especially when the load includes motors, pumps, compressors, EV chargers, and similar equipment.
3. These are ordinary loads and do not include inrush loads. If inrush loads are present, such as motor starting, a variable frequency drive (VFD) starting method with built-in ramping is recommended.
4. If nonlinear loads are present, such as high-power chargers, the EMS must be able to perform OCPP-based control: ramp control for loading and unloading to ensure stable operation of the overall system.
5. If no variable frequency drive (VFD) is installed, the total capacity of inrush loads should be less than 30% of the system rated power.
6. Peak load apparent power < 0.8*system rated power
7. Confirm the neutral-point generation function in off-grid mode; not all integrated PCS units can establish a stable neutral-point reference.
8. The control logic of the energy management system (EMS) is as important as the hardware itself; improper core dispatch strategies can accelerate battery aging.
9. For off-grid operation, focus on VSG capability: in off-grid operation, VSG control mode provides excellent frequency and voltage stability and is suitable for applications requiring frequent grid-connected/islanded transitions.
10. Grid-code settings must match the requirements of the local utility and comply with local laws and regulations.

# Appendix B: Description of ZOE MG-EMS

A typical MG-EMS should have the following functions:

- Islanding detection capability; currently integrated into the STS equipment in the proposed solution.
- Rapid fault isolation capability; relay protection functions are currently implemented in the PMS.
- Capability for grid-connected and off-grid operation, enabling uninterrupted transitions between grid-connected and islanded operating modes;

Currently implemented through the STS equipment plus the PMS in the integrated PCS equipment.

- Energy balance within the microgrid; millisecond-level PMS plus EMS at the seconds level and above.
- Black start capability; implemented by the EMS in coordination with the PCS.
- Generation power forecasting and load power forecasting functions; implemented by the EMS.
- Economic operation of energy resources within the microgrid; implemented by the EMS.
- Communication support for optimized microgrid operation and remote monitoring of distributed energy resources; implemented by the EMS.

- Real-time monitoring of source-load information inside the microgrid and grid-connected/islanded switch status; implemented by the EMS.
- Support for nonlinear loads, such as chargers, with appropriate power ramping and power unloading control; implemented by the EMS.

## Main Function List of ZOE EMS+PMS:

| Functional Module | Physical Module | Description |
|---|---|---|
| Day-Ahead Power Forecasting Module | EMS | Based on the forecasting characteristics of user-side distributed PV and an offline parameter-optimization dataset, optimization algorithms are used to obtain optimal parameters for sample selection and forecasting algorithms, thereby completing day-ahead forecasting of PV output power. |
| Real-Time Power Forecasting Module | EMS | Based on the forecasting characteristics of user-side distributed PV and an offline parameter-optimization dataset, optimization algorithms are used to obtain optimal parameters for sample selection and forecasting algorithms, thereby completing real-time forecasting of PV output power. |
| Load Power Forecasting Module | EMS | Establish low-cost load forecasting models for various types of users to achieve low-cost and high-efficiency load power forecasting for the microgrid. |
| Energy Optimization Dispatch Module | EMS | Enables second-level system control, minute-level real-time optimized operation, and hour-level optimized dispatch and management for user-side smart microgrids. |
| Black Start Module | EMS | Enables automatic/manual startup of a user-side microgrid under collapse conditions, enhancing the microgrid's self-healing capability. |
| Islanding Detection Control Module | PCS | Enables islanding detection at the PCC of a user-side microgrid and reduces disturbance to microgrid power quality during the detection process. |
| Unified Synchronization of Multiple Devices | PMS | Synchronization capability during grid-connected/islanded transitions, ensuring consistency and reliability of synchronization capability. |
| Protection Control Module | PMS | Enables rapid and reliable fault clearing in the microgrid under islanded and grid-connected conditions. |
| Grid-Connected/Islanded Transition Module | STS | Implements safe and reliable seamless transition control in accordance with voltage and frequency requirements during user-side microgrid grid-connected/islanded transitions. |

| Functional Module | Physical Module | Description |
|---|---|---|
| Data Storage Module | EMS | Stores system historical data, initial configuration data, and related information. |
| Communication Module | EMS | Ensures data exchange among the control device, underlying equipment, and upper-level systems. |
| Human-Machine Interface | EMS | Provides human-machine interaction via a touch display screen. |

## Key EMS Indicators:

| Functional Module | Description |
|---|---|
| Day-Ahead PV Power Forecasting Module | The monthly average relative error shall not exceed 25%. Preferably, the error should be less than 10%. Forecast PV generation power values for 96 time points over the next 24 hours. |
| Real-Time PV Power Forecasting Module | The monthly average relative error shall not exceed 15%. Preferably, the error should be less than 6%. Rolling forecasts shall predict PV generation power values for 16 time points within the next 4 hours at each time point. |
| Load Power Forecasting Module | The forecast relative error shall not exceed 20%, and the real-time forecast relative error shall not exceed 15%. Forecast load power values for 96 time points over the next 24 hours; rolling forecasts shall predict load power values for 16 time points within the next 4 hours at each time point. |
| Energy Optimization Dispatch Module | Day-ahead optimization computation time <30 minutes; hourly optimization computation time <5 minutes. |
| Grid-Connected/Islanded Transition Module | Grid-connected/islanded transition time within 20ms. Preferably within 10ms. |

## Description of EMS Control Strategy

| Scenario No. | PV | Grid | Diesel Generator | Battery State of Charge | Load Power | Strategy Description |
|---|---|---|---|---|---|---|
| Power | A | | | | B | |

| Scenario No. | PV | Grid | Diesel Generator | Battery State of Charge | Load Power | Strategy Description |
|---|---|---|---|---|---|---|
| 1 | Available | Available | Unavailable | Not fully charged | Available | 1. When A>B, PV first supplies the load, and surplus power charges the battery; charging power variation and battery life shall be considered.<br>2. When A<B, all PV power supplies the load, and the (B-A) portion is drawn from the grid.<br>This scenario includes the case where load power is 0. |
| 2 | Available | Available | Unavailable | Fully charged | Available | 1. When A≥B, PV first supplies the load, and PV output power is limited according to load conditions to avoid reverse power flow;<br>2. When A<B, all PV power supplies the load, and the (B-A) portion is drawn from the grid.<br>This scenario includes the case where load power is 0. |
| 3 | Available | Unavailable | Unavailable | Fully charged | Available | 1. When A≥B, PV first supplies the load, and PV output power is limited according to load conditions to avoid reverse power flow.<br>2. When A<B, all PV power supplies the load, and the (B-A) portion is supplied by the battery. |
| 4 | Available | Unavailable | Unavailable | Not fully charged and no level-2 or higher undervoltage alarm | Available | 1. When A≥B, PV first supplies the load, and surplus power charges the battery. The charging power is the smaller of (A-B) and the PCS (BMS) power.<br>2. When A<B, all PV power supplies the load, and the (B-A) portion is supplied by the battery.<br>This scenario includes the case where PV power is 0. |

| Scenario No. | PV | Grid | Diesel Generator | Battery State of Charge | Load Power | Strategy Description |
|---|---|---|---|---|---|---|
| 5 | Available | Unavailable | Unavailable | Level-2 or higher undervoltage alarm present | Available | When A≥B<br>PV first supplies the load, and surplus power charges the battery. The charging power is the smaller of (A-B) and PCS power.<br>When A<B<br>1. Start the diesel generator, and the maximum diesel-generator power meets the load demand. Applicable to electrical diagram 1.<br>2. Stop supplying power to the load until the power-supply conditions are met. Applicable to electrical diagram 2.<br>This scenario includes the case where PV power is 0. |
| 6 | Available | Unavailable | Available | Not fully charged | Available | PV is prioritized for charging, and the diesel generator is prioritized for supplying the load. When diesel-generator charging is enabled, the remaining diesel-generator energy charges the battery; otherwise, battery charging is prohibited.<br>This scenario includes the case where PV power is 0. |
| 7 | Unavailable | Available | Unavailable | Not fully charged | Available | 1. If energy storage operates in backup-power mode, it is charged at full power under demand control and stops charging when the minimum backup energy level, configurable from |

| Scenario No. | PV | Grid | Diesel Generator | Battery State of Charge | Load Power | Strategy Description |
|---|---|---|---|---|---|---|
| | | | | | | 1% to 100%, is reached.<br>2. If energy storage operates in peak-shaving and valley-filling mode, it charges at the set power during the specified valley-price period and stops when fully charged. |

Notes:

1. After the diesel generator starts, whether the battery needs to be charged shall be determined by an enable switch. When enabled, the battery is charged; otherwise, battery charging is prohibited.
2. When the grid supplies power, battery charging power must follow the demand control strategy.
3. When the diesel generator supplies power, the maximum output power of the diesel generator must be considered during battery charging.

Charging power = generation power - load power, while also satisfying charging power ≤ the smaller of the STS single-circuit power and the PCS maximum power.

4. PV power is obtained from the MPPT equipment, grid power is read from the revenue meter, and load power is read from the load meter, with priority given to meter readings and then indirect calculation.
5. PCS maximum power and diesel-generator maximum output power are specified through settings.

# Appendix C: Description of ZOE MG-PMS Hardware + Software

Islanding detection control module: Classifies islanding conditions of the user-side microgrid into internal microsource islanding and whole-microgrid islanding. By combining islanding detection results configured in each distributed energy resource system with the open/closed status of related switches, it detects whether each control device is in the required state for off-grid operation;

Protection control module: Provides various types of combined protection for lines and buses, ensuring that each device in the system is protected under all operating modes;

Grid-connected/islanded transition module: Enables manual or automatic transitions, including planned grid-connected-to-islanded transition, planned islanded-to-grid-connected transition, unplanned grid-connected-to-islanded transition, and unplanned islanded-to-grid-connected transition; multi-device synchronization and GFL-mode grid-connection scheme.

## The PMS must have complete linkage capability with peripheral subsystems. Its control functions are as follows:

- Fuel generator set coordination (ATS and diesel generator): The PMS obtains automatic transfer switch (ATS) status through RS485 communication. In an emergency when utility power is lost and the energy storage battery SOC falls below an extremely low warning threshold, such as below 10%, the PMS autonomously determines the condition and outputs a dry-contact signal to start the standby diesel generator and connect it to the system network. It also coordinates with the PCS to adjust the operating mode, absorb diesel-generator energy, and charge the battery. After battery energy recovers, it smoothly shuts down the diesel generator. This function may also be implemented by the EMS.
- Load and circuit breaker management: Remote opening and closing control of miniature circuit breakers and contactors in the distribution system is implemented through digital output (DO) signals, including staged load shedding under undervoltage or low-frequency conditions. Auxiliary contact feedback from circuit breakers and grounding switches is collected through digital input (DI) signals to ensure that every topology reconfiguration command is physically executed. This function may also be implemented by the EMS.
- Environmental and auxiliary system monitoring: The system integrates closed-loop control of industrial air conditioners, fans, and dehumidifiers. The PMS not only collects humidity and temperature data through RS485 to adjust dehumidifier operating status, but also controls cabinet cooling fan start/stop directly through DO signals and monitors fan stall or shutdown fault alarms through DI signals, providing complete cooling-system fault protection linkage.
- Security and safety: Deep integration with the station-level fire alarm panel, emergency-stop button, and access control system is implemented through DI channels. Once a fire alarm or emergency stop (E-Stop) signal is received, the PMS triggers the highest-level station-wide software and hardware intertrip procedure within milliseconds, disconnecting all power-source outputs and blocking the phase-locked loop.
- Protection and fault recording: During protection execution and fault transition, the high-speed data buffer built into the PMS triggers the “fault recording” function, automatically freezing high-frequency voltage, current, and status-word curves for 30 seconds before and 30 seconds after the fault, totaling 60 seconds, to provide the most authentic field data for subsequent incident responsibility assessment and system improvement.

## Coordination with the DC/DC MPPT control module:

The microgrid is operating under heavy load in islanded mode, and the main load circuit breaker of a heavy industrial user trips unexpectedly. In an instant, tens or even hundreds of kilowatts of energy consumption disappear. Because the PV controller continues to execute MPPT logic, surplus power will be aggressively injected into the DC-link capacitors. If absorption relies only on battery DC/DC charging, absorption may fail because of limited battery current ramp rate or hard BMS charging boundary protection, causing DC overvoltage and damage to equipment across the network. In this scenario, the PMS demonstrates decisive coordination capability: within the first millisecond after detecting a sharp rise in AC bus voltage and a steep drop in current, the PMS sends mode-transition commands directly to all parallel PV DC/DC units through a high-speed bus. Within milliseconds, the PV system exits MPPT and is forced into controlled voltage regulation mode (CV Mode) to limit maximum output voltage and implement dynamic clipping. At the same time, the PCS rapidly lowers the AC-side voltage output amplitude. Only

through the instantaneous combined action of multiple devices can a fault that could otherwise cause a full-system outage be mitigated.

## Coordination with the battery BMS:

In a reverse DC-coupled scheme, the health status of the battery system is the survival baseline of the microgrid. In most conventional microgrid configurations, the battery management system (BMS) and the energy dispatch system are black boxes from different vendors, and information exchange between them has very high latency. If, during a sudden load increase, such as the instant a DC/DC MPPT unit goes offline due to a fault, the BMS detects that a cell has reached its discharge limit, it often opens the physical contactor immediately for self-protection (hard trip). This self-protection action instantaneously disconnects the largest support source for the DC bus, causing the entire system to collapse. The PCS must support the introduction of a deeply integrated “Soft Limit Logic” protection mechanism. The PCS continuously reads real-time state of charge (SOC), cell temperature, and maximum allowable charge/discharge current limits from the BMS. After calculating these dynamic boundary values, when it detects that battery charge/discharge C-rate limits are being approached, or when temperature rises due to continuous high-current discharge, it should immediately control PCS load power output and issue commands to coordinate with the PMS synchronously, forming an adaptive buffer between the software layer and the hardware dead zone and fully eliminating the safety hazard of hard BMS contactor disconnection.

## Core functions satisfied:

Complies with the six-level state-machine transition and dispatch logic of IEEE 2030.7

The PMS state machine includes two core mechanisms: the macro-scale “Dispatch” function and the microsecond/millisecond-scale “Transition” function. These mechanisms jointly manage transitions among the following operating states: logic embedded in the real-time system.

1. Steady-State Grid-Connected Operation (SS1): When the external bulk grid supplies power normally, the microgrid remains physically paralleled with the main grid. In this state, the dispatch function of the state machine activates long-term economic optimization strategies. The PV system operates at full MPPT generation, while the energy storage BMS and PCS perform slow energy throughput according to real-time price strategies or peak-shaving commands.

2. Steady-State Islanded Operation (SS2): When the microgrid is physically disconnected from the bulk grid and operates as an independent autonomous power system, the system enters SS2. In this state, economic dispatch becomes secondary, and power-supply security becomes the sole objective. The PMS activates rule-based energy allocation: the energy storage system is established as the absolute voltage support source of the system, PV is derated to match real-time load consumption, and uninterrupted supply to critical loads is closely monitored.

3. Transition State - Planned Islanding Transition (T2): This is a smooth grid-exit process initiated manually due to maintenance requirements or distribution-grid instructions. After receiving the request, the PMS does not immediately open the static transfer switch (STS). Instead, it first sends regulation commands to the PCS, causing it to gradually adjust active and reactive power output until the exchange power at the point of interconnection (POI) between the microgrid and the main grid dynamically approaches zero. Once power flow reaches zero, the STS opens without arcing at the zero-current crossing, and the system transitions seamlessly into SS2 without transient disturbance.

4. Transition State - Unplanned Islanding Transition (T1): This is the most challenging state. When sensors detect severe external faults such as a sharp grid-voltage drop or frequency collapse, the STS is forcibly opened in emergency mode, and the microgrid is forced into an “unintentional island.” At that moment, the internal energy balance of the microgrid is instantly disrupted. The PMS transition function immediately takes over globally, calls a millisecond-level response matrix, urgently triggers PCS mode switching from a PQ current source to a V/f voltage source, and issues PV power-limiting commands to forcibly stabilize the system within several AC cycles before handing control over to SS2 steady-state logic.

5. Transition State - Resynchronization and Grid Connection (T3): After the external grid fault is cleared and voltage and frequency return to normal, the system prepares for grid connection. The PMS activates the phase capture and phase-locked loop (PLL) modules inside the PCS and slowly regulates the frequency and phase on the islanded microgrid side. Through synchronization comparison, only when the voltage magnitude, frequency, and phase difference between the microgrid and the external grid simultaneously fall within allowable tolerance ranges (Phase Matching) does the PMS permit closure of the STS circuit breaker, enabling grid reconfiguration without inrush impact.

6. Transition State - Black Start (T4): If the microgrid experiences a total outage, the PMS activates a fully autonomous self-healing procedure. Using residual energy from a UPS or internal battery pack, it wakes the PMS main board and the energy storage DC/DC control unit, prioritizing soft pre-charging of the DC bus (DC Pre-charge). After the bus voltage reaches the operating threshold, the PCS self-starts to establish AC voltage, then sequentially wakes the PV system and connects critical loads in priority-based steps to restore microgrid operation.

## Core Data Indicators:

| KPI Evaluation Dimension | **System Performance Constraint Description and Evaluation Scenario** | **Mandatory Compliance Parameter Requirements** |
|---|---|---|
| Sensor End-to-End Latency | The time required for data to be collected from underlying Hall voltage/current sensors, pass through ADC analog-to-digital conversion, and fully arrive at the PMS controller input port through a high-speed communication bus. | **< 2 milliseconds** |
| Controller Computation Cycle | The time required for the logic core to execute one complete cycle, including parsing data frames, executing the droop compensation algorithm, computing the multi-device coordination matrix, traversing the state-machine anti-islanding protection logic, and generating control outputs. | **< 1 millisecond** |
| Command Issuance and Execution Latency | The time from issuance of a control command at the PMS network port, transmission through the Ethernet bus to underlying actuators such as the PCS and DC/DC converters, and parsing and writing into the corresponding control registers. | **< 5 milliseconds** |

| KPI Evaluation Dimension | **System Performance Constraint Description and Evaluation Scenario** | **Mandatory Compliance Parameter Requirements** |
|---|---|---|
| Total Microgrid Closed-Loop Response | The total end-to-end time from occurrence of an external disturbance event to substantive converter hardware adjustment of PWM duty cycle and output of corrective power. | **< 20 milliseconds** |
| V-DC Bus Steady-State Ripple | The percentage of rated voltage represented by voltage ripple on the DC common bus when the microgrid is in pure DC islanded steady state under fixed load and stable irradiance. | **< 2%** |
| V-DC Transient Recovery Indicator | The maximum time required for DC bus voltage to converge from severe fluctuation back to the nominal stable voltage range after the largest power step within rated capacity, such as sudden utility disconnection or a major load trip. | **< 100 milliseconds** |
| Under steady-state off-grid conditions | Frequency control accuracy must remain within ±0.05 Hz, and voltage deviation must remain within ±1% of the nominal setpoint; off-grid power quality. | **Frequency: ±0.05 Hz Voltage: ±1%** |

## Basic PMS Function List

| **Function Description** |
|---|
| The PMS control completes system logic functions, including complete secondary control logic. |
| The PMS controls the STS according to utility status to implement automatic grid-connected/islanded transition; |
| The PMS communicates with the MPPT module through RS485 and controls PV start/stop and PV power according to load demand and energy storage charge/discharge requirements; |
| The PMS communicates with the ATS through RS485 and controls diesel-generator start/stop according to battery state of charge and utility status; |
| The PMS controls PCS operating mode according to utility and diesel-generator status and controls PCS power according to charge/discharge requirements; |
| Communicates with the EMS, receives EMS start/stop commands, and uploads integrated real-time status information for the PCS, STS, PV, and diesel generator to the EMS; |
| The PMS provides remote upgrade functionality for the PCS; |
| The PMS communicates with the system cabinet display screen through RS485, executes display-screen setting commands, and uploads implementation information to the display screen; |

| Function Description |
| --- |
| The PMS controls system fan operation through DO signals and detects fan status through DI signals; |
| The PMS controls circuit breakers through DO signals and detects circuit breaker status through DI signals; |
| The PMS controls system indicator lights through DO signals; |
| The PMS detects access control, fire protection signals, emergency-stop signals, fan status, grounding-switch feedback, and related signals through DI signals, implementing fault logic processing for fire protection faults, emergency-stop faults, circuit breaker faults, fan faults, access control faults, and similar events, thereby realizing system protection functions; |
| The PMS controls system relays through DO signals; |
| The PMS communicates with the dehumidifier, meters, and leakage-current detection equipment through RS485 to obtain real-time information; |
| Related protection functions: |

*This report is provided with research support from ZOE Energy Storage Research Institute. As a leading innovator in the digital energy sector, ZOE Energy Storage is dedicated to the development of high-security lithium battery energy storage systems and AI-powered energy management platforms. With over 2GWh of energy storage projects deployed globally, we provide the technological foundation for smart grid transformation.*